UNIVERSIDADE DE SÃO PAULO
INSTITUTO DE FÍSICA DE SÃO CARLOS

André Cidrim Santos

Quantum turbulence and multicharged vortices in trapped atomic superfluids

São Carlos
2017

André Cidrim Santos

Quantum turbulence and multicharged vortices in trapped atomic superfluids

Thesis presented to the Graduate Program in Physics at the Instituto de Física de São Carlos, Universidade de São Paulo to obtain the degree of Doctor of Science.

Concentration area: Basic Physics

Supervisor: Prof. Dr. Vanderlei Salvador Bagnato

Corrected version
(Original version available on the Program Unit)

São Carlos
2017

Cataloguing data revised by the Library and Information Service
of the IFSC, with information provided by the author

Santos, André Cidrim
Quantum turbulence and multicharged vortices in trapped atomic superfluids / André Cidrim Santos; advisor Vanderlei Salvador Bagnato - revised version -- São Carlos 2017.
109 p.

Thesis (Doctorate - Graduate Program in Física Básica) - - Instituto de Física de São Carlos, Universidade de São Paulo - Brasil , 2017.

1. Bose-Einstein condensate. 2. Quantum turbulence. 3. Atomic superfluids. 4. Quantized vortices. I. Bagnato, Vanderlei Salvador, advisor. II. Title.

I dedicate this thesis to
Auzier, Gilce, Adriana, and Lílian.

ACKNOWLEDGEMENTS

Although this thesis compiles part of my work from the past four years, this PhD cannot be reduced to just one short period. It is a result of my history and, as a consequence, I owe so many people the joy of completing this scientific journey.

I must start by thanking my supervisor Prof. Vanderlei Salvador Bagnato, not only for sharing his physics knowledge and his amazing intuition for problem solving throughout the years, but also for boosting my motivation every time I needed. I particularly thank him for showing me through examples, and not only words, how to promote and appreciate our Brazilian science (even if the odds are against us sometimes).

I thank Prof. Francisco Ednilson for teaching me more than just physics during these years and for giving me the most valuable advices. Also from our theoretical group, I thank Marios Tsatsos, Mônica Caracanhas, Alexander Novikov, Rafael Poliseli, and Diogo Lima, who have helped me feel part of a special bunch. I must acknowledge the other theoretician colleagues Tiago Santiago, Carlos Máximo, and Prof. Romain Bachelard for sharing offices, experiences, and laughs. Particularly Tiago for giving me shelter and sharing his own apartment with me during the first couple of years. I also thank my dear friends Diego Carvajal and Abasalt Bahrami for the great times together in São Carlos.

Being a theoretician among experimentalists, I have had the great opportunity of participating in valuable discussions with those who see physics happening in real time in the lab, teaching me the fun to go beyond the (sometimes boring) computer simulations. For that I thank Pedro Tavares, Patrícia Castilho, Rodrigo Shiozaki, Amilson Fritsch, Freddy Jackson, Edwin Pedrozo, Emmanuel Mercado, and Arnol Orozco.

From my exchange year in Newcastle, I am immensely indebted to Prof. Carlo Barenghi for his supervision and advices. I am thankful to him for teaching me so much about physics since the very first day we had a meeting. Above all, I admire Carlo for being one the most humane persons I have ever met.

Still in Newcastle I had the pleasure to be part and co-founder of the Superfluid Mafia, featuring Paolo Comaron, Luca Galantucci, Fabrizio Larcher, George Stagg, and Donatello Gallucci. I must also thank Nick Loughlin for turning me into an avid music-theory nerd.

In the more personal context, I have to thank my dear long time friends. They are many and I am sure I will unfortunately forget some names, though not on purpose. Geographically, I will start by thanking my amazing friends from Lafaiete, Luís Fernando Tavares and André Marinho, with whom I always share great (and often nostalgic) times every time we meet again. From Belo Horizonte, I have to acknowledge the immortal team André Diniz, Diego Barraza, Edson Filho, and Anderson Ferraz, and also the girls from the [a.s.] originals Laís Aguiar, Débora Hugo, Clarisse Simões, and Amanda Modesto.

From undergrad times, I thank Raphael Casseb, who became as close to me as a brother.

My special thanks to my fiancée Lílian Menezes for her endless support and for teaching me so much about life. With you I understood the meaning of love and friendship altogether. Of course, from her I have earned a second family, Maria, José, Lidiane, and Lidemarques, with whom I have shared great moments in Aracaju.

Finally, for supporting my early interest in science and for giving me the best upbringing I could ever ask for, I thank my amazing parents, Auzier and Gilce, and my dear sister Adriana. There is not enough ways to thank your constant support and your love. Thank you so much for giving me a sense of belonging when times were tough.

I acknowledge CNPq and Capes for financial support.

"Não sou nada.
Nunca serei nada.
Não posso querer ser nada.
À parte isso, tenho em mim todos os sonhos do mundo."
Álvaro de Campos (Fernando Pessoa)

ABSTRACT

SANTOS, A. C. **Quantum turbulence and multicharged vortices in trapped atomic superfluids**. 2017. 109p. Tese (Doutorado em Ciências) - Instituto de Física de São Carlos, Universidade de São Paulo, São Carlos, 2017.

In this thesis, we numerically investigate quantum turbulence in trapped atomic Bose-Einstein condensates (BECs). We first discuss the appropriate qualitative characterization of turbulence in these systems, showing the limitation of analogies with classical hydrodynamics and turbulence in large superfluid Helium experiments. Due to their lack of available length scales, our investigated systems can only fit the ultraquantum (or Vinen) type of quantum turbulence. Secondly, we propose experimentally feasible schemes for more controlled investigations of turbulence making use of dynamical instability of multicharged vortices as an onset for complex vortex dynamics. In two dimensions, our suggested scheme allows control over vortex polarization in the harmonically trapped system. This setup is then used to study how turbulence decays in such a scenario, through the phenomenological modeling of a vortex-number rate equation. As a consequence, we were able to identify that vortex annihilation in these trapped systems happens through a four-vortex process. For three dimensions, we have first provided a study on the decay of a quadruply-charged vortex, also in a harmonically trapped BEC. Having this setting as a comparison point, we propose a quasi-isotropic turbulent system, starting from a phase-imprinted initial state of two doubly-charged, anti-parallel vortices. The vortex turbulence arisen from such configuration was shown to agree with the Vinen turbulent regime, after we characterized specific features of its decay, such as the energy spectrum $[E(k) \sim k^{-1}]$ and the time evolution of the vortex-line density $[L(t) \sim t^{-1}]$. Although these features have been frequently verified in the context of superfluid Helium turbulence, here this identification was for the first time done for realistic, trapped atomic BECs.

Keywords: Bose–Einstein condensate. Quantum turbulence. Atomic superfluids. Quantized vortices.

RESUMO

SANTOS, A. C. **Turbulência quântica e vórtices multicarregados em superfluidos atômicos aprisionados**. 2017. 109p. Tese (Doutorado em Ciências) - Instituto de Física de São Carlos, Universidade de São Paulo, São Carlos, 2017.

Nesta tese, investigamos numericamente a turbulência quântica em condensados de Bose-Einstein (BECs) aprisionados. Discutimos, inicialmente, a caracterização qualitativa apropriada para estes sistemas, mostrando a limitação de analogias tipicamente feitas com hidrodinâmica clássica e turbulência em grandes sistemas com Hélio superfluido. Devido às suas limitadas escalas espaciais, os sistemas investigados somente podem exibir o tipo de turbulência conhecida como ultra-quântica (ou de Vinen). Em seguida, propomos sistemas experimentalmente factíveis que permitem investigações mais controladas da turbulência, fazendo uso da instabilidade dinâmica de vórtices multi-carregados como ponto de partida para geração de dinâmicas complexas. Em duas dimensões, nossa proposta permite controle sobre a polarização de vórtices em sistemas aprisionados em potencial harmônico. Este arranjo é então utilizado no estudo do decaimento da turbulência nesse contexto, através de um modelo fenomenológico para equação que descreve a taxa de variação do número de vórtices. Como consequência, pudemos verificar que a aniquilação de vórtices dá-se através de um processo que envolve quatro vórtices. Em três dimensões, apresentamos um estudo do decaimento de um vórtice de carga topológica quatro, também em potencial harmônico. Mantendo em mente esse sistema a título de comparação, propomos um cenário turbulento, quase-isotrópico, partindo de um estado inicial formado por dois vórtices duplamente carregados, mas orientados anti-paralelamente. Verificamos que a turbulência decorrente desse arranjo coincide com a regime de Vinen analisando características do seu decaimento, especificamente obtendo o espectro de energia $[E(k) \sim k^{-1}]$ e evolução temporal da densidade de linhas de vórtices $[L(t) \sim t^{-1}]$. Apesar de que essas características são comumente encontradas no contexto de Hélio superfluido, apresentamos pela primeira vez essa identificação no cenário realístico de BEC aprisionados.

Palavras-chave: Condensado de Bose-Einstein. Turbulência quântica. Superfluidos atômicos. Vórtices quantizados.

LIST OF FIGURES

CONTENTS

1 INTRODUCTION

During the past decade, atomic superfluids have received considerable attention from the scientific community. The remarkable property of certain cold atoms to exhibit the phenomenon of Bose-Einstein condensation (BEC) made possible the manipulation of quantum properties in a macroscopic level with unprecedented controllability. In these systems, atomic physicists were capable, for instance, to realize Schrödinger's cat-like states, study coherence in matter-wave interference experiments, and even induce complex far-from-equilibrium dynamics such as quantum turbulence (QT).

The term turbulence was originally applied to a quantum mechanics context by Feynman[1] when discussing the interesting consequences of low-temperature conditions to liquid helium. When sufficiently cooled down, these liquids flow without viscosity, defining the remarkable emergence of superfluid properties such as quantized vorticity. The actual research on QT was initiated by the first observations of quantized vortices interacting chaotically in experiments using superfluid liquid helium.[2,3] After decades of development, the field of QT witnessed exciting breakthrough with the verification of classical-like turbulence statistics (Kolmogorov scaling in the energy spectrum) in these low-temperature systems,[4] motivating discussions on the origin and possible explanations for such quantum-classical correspondence. More recently, investigations on the subject have intensified due to the advent of BEC in ultra-cold gases and the growing interest in using this phenomenon to explore far-from-equilibrium physics.

In contrast with superfluid helium experiments, trapped BEC systems are still considerably smaller. Despite this, QT can also be studied in atomic BECs;[5–10] their relatively small size limits the study of scaling laws but offers opportunities to study minimal processes that also take place in larger systems (e.g. vortex interactions, vortex reconnections, vortex clustering) with greater experimental controllability and more direct visualization than in liquid helium. Added to this experimental advantage, atomic BECs have a fairly well-established theoretical framework, with their dynamics being successfully described by mean-field approaches (Gross-Pitaevskii model) or by simplified beyond mean-field models.

Given their both experimental and theoretical advantages, our aim is to explore general aspects of QT in atomic superfluids. The current thesis focus on theoretical studies with the numerical simulation of these systems, proposing new ways to generate and characterize the emerging complicated dynamics. In summary, our idea here is to explore multicharged vortex instability in condensates to allow for highly energetic and, later in evolution, chaotic states. The practical objective is to provide experimentally reproducible protocols to achieve turbulence in laboratory, which is still a challenge nowadays. With a more fundamental perspective we also discuss on how to better define the quantum

turbulence in finite systems, as turns out to be the case of real-life experiments with BECs.

1.1 Thesis outline

This thesis can be divided into two main parts. The first, comprises a theoretical overview of Bose-Einstein condensates and superfluidity, in Chap. 2, followed by a discussion on how these phenomena are connected with the topic of quantum turbulence, in Chap. 3. The second part collects our results in two chapters. Chap. 4 discusses our investigations on the decay of a giant vortex and the generation of polarized, two-dimensional quantum turbulence. Chap. 5 presents a scheme to create quantum turbulence in trapped, three-dimensional atomic superfluids making use of multicharged vortices, and provides an interpretation for the phenomenon, drawing comparisons with a well-known regime of quantum turbulence (the so-called Vinen turbulence) in superfluid helium. Each result's chapter closes with remarks on connections between our numerical studies and real-life experiments, and also with prospects. Finally, Chap. 6 is dedicated to our overview and conclusions. Few appendices are included at the end of this thesis, where we provide a more detailed description of some numerical procedures applied in our investigations.

This thesis discusses, and in some cases expands, the results published in the following papers:

- *Quantum turbulence in trapped atomic Bose–Einstein condensates.*

  M.C. Tsatsos, P.E. Tavares PE, A. Cidrim, A. R. Fritsch, M. A. Caracanhas, F. E. A. dos Santos, C. F. Barenghi, and V. S. Bagnato. Physics Reports 622:1-52 (2016)

- *Controlled polarization of two-dimensional quantum turbulence in atomic Bose-Einstein condensates.*

  A. Cidrim, F. E. A. dos Santos, L. Galantucci, V. S. Bagnato, and C. F. Barenghi. Physical Review A 93, 033651 (2016)

- *Vinen turbulence via the decay of multicharged vortices in trapped atomic Bose-Einstein condensates.*

  A. Cidrim, A. C. White, A. J. Allen, V. S. Bagnato, and C. F. Barenghi. Physical Review A 96, 023617 (2017)

- *Twisted unwinding of multi-charged quantum vortex and generation of turbulence in atomic Bose-Einstein condensates.*

  G. D. Telles, P. E. S. Tavares, A. R. Fritsch, A. Cidrim, V. S. Bagnato, A. C. White, A. J. Allen, and C. F. Barenghi. arXiv preprint arXiv:1505.00616 (2016).

2 BOSE-EINSTEIN CONDENSATION AND SUPERFLUIDITY

In this chapter we introduce fundamental concepts of Bose-Einstein condensation and superfluidity. More than a review chapter, we intent to prepare the ground for connecting these interrelated quantum phenomena to well-known ideas in classical turbulence, by viewing dynamics in the light of a nonlinear Schrödinger equation (the Gross-Pitaevskii equation) and its hydrodynamical form.

This thesis, in particular, aims at exploring the instability of multicharged vortices as a starting point to generate turbulent states. For this reason we also present a discussion on their stability in trapped atomic condensates (Sec. 2.7).

2.1 Non-interacting BEC

In this thesis we will be interested in describing a particular many-body quantum phenomenon that allows us to interpret certain macroscopic quantum effects in the framework of fluid dynamics. As a general remark, we should start by introducing the concept of a *quantum fluid*: a many-particle quantum system in which indistinguishability of particles gives rise to intriguing quantum-statistical effects (such as superfluidity, as we shall see later).

Nonetheless, in order for statistics to come into play in a many-particle system, one must first guarantee that quantum mechanical effects among the particles are significant. A simple argument that assures this condition begins with the quantum mechanical postulate of matter's wave-like behavior. We know from deBroglie that a particle with momentum p has an intrinsic wavelength $\lambda \sim h/p$ associated with it, where h is Planck's constant. As is the case of any wave-like phenomena, quantum mechanics should play an important part when the mean spatial separation d among these particles is comparable to their intrinsic spatial extension λ. In other words, we should have $\lambda \gtrsim d$, which in terms of momentum becomes $h/p \gtrsim d$. For the sake of argument, let us say that these many particles are homogeneously distributed in space according to a density ρ, allowing us to say that $d \sim \rho^{-1/3}$ (this is particularly valid for typical real-life experiments with ultracold gases). When in thermal equilibrium at a temperature T, the particles acquire an average momentum $p \sim \sqrt{m k_{\mathrm{B}} T}$. Therefore, substituting the above relations we are left with the condition

$$\frac{h^2 \rho^{2/3}}{m} \gtrsim k_{\mathrm{B}} T. \tag{2.1}$$

This simple relation gives us a qualitative idea of why massive particles, such as alkali atoms (as opposed to electrons), need to be cooled down to very low temperatures (sometimes of the order of few nK) in order to exhibit clear quantum mechanical effects. The smaller the ratio in the left hand side of (2.1), the smaller the temperature to satisfy the requirement.

2.1.1 Quantum statistics

Elementary particles in nature (e.g. electrons and photons) can either be fermions or bosons, depending on whether their intrinsic angular momentum (spin degree of freedom) is a half-odd-integer or integer multiple of $\hbar$, respectively. This is a well-known consequence of the *spin-statistics theorem*.[11] When a system composed of many elementary particles roughly satisfies condition (2.1), quantum effects are thus relevant and this spin property is determinant to the physics that arises from a many-body, quantum-mechanical system.

As opposed to classical mechanics, in quantum physics these elementary particles are *indistinguishable*. Let us assume that we know the many-body wave function $\Psi(\mathbf{r}_1, .., \mathbf{r}_N)$, which represents a system of N elementary particles of the same kind (either fermions or bosons), where $\mathbf{r}_i$ comprises the coordinates (including relevant quantum numbers such as spin) of particle i. According to quantum mechanics, if two particles i and j of this system undergo a collision process, for instance, there is no labeling that can tell an observer which particle is i or j after the process. In essence, this implies that the system's wavefunction must be invariant to the particle coordinate exchange, hence

$$|\Psi(\mathbf{r}_1, ..., \mathbf{r}_i, ..., \mathbf{r}_j, ..., \mathbf{r}_N)|^2 = |\Psi(\mathbf{r}_1, ..., \mathbf{r}_j, ..., \mathbf{r}_i, ..., \mathbf{r}_N)|^2 . \tag{2.2}$$

Mathematically, this holds true if the exchange of i and j adds a global phase $e^{i\alpha}$ to the wavefunction Ψ. At this point, it becomes relevant whether we are dealing with fermions or bosons. The acquired phase for particle coordinate exchange is intrinsically associated with the spin degree of freedom, and the global phase is

$$e^{i\alpha} = \begin{cases} -1, & \text{for fermions,} \\ +1, & \text{for bosons.} \end{cases} \tag{2.3}$$

The above phase is the connection with quantum statistics and responsible for the fundamental difference of how the probability amplitudes of indistinguishable fermions and bosons interfere with themselves, finally dictating the rules of which way particles are distributed over quantized states. This gives rise to the famous Pauli exclusion principle for fermions, which forbids half-integers spin particles to occupy the same particle state.

An interesting point is that all the above discussion can be extended to non-elementary particles. In fact, in terms of energetics, complex particles (composed of several elementary particles combined) can effectively behave as either fermions or bosons, therefore obeying spin-statistics as well. This happens for the simple fact that probability amplitudes for some state transitions are practically null, due to unrealistically, highly-energetic processes involved. Consider, for instance, two atoms of a same atomic species, therefore composed of the same nucleons. Rigorously, in order to correctly define their state, a full quantum mechanical description should in principle contemplate the possibility of nucleons from the two different atoms to be individually exchanged (e.g. a proton of one atom swaps place with a proton of the other atom). However, the energy for this to happen

is exceptionally higher than a typical energy scale for an atomic center-of-mass swapping, for example. Consequently, if one is not dealing with extreme cases of relativistically energetic particle collisions, transitions such as these are in practice impossible, and have virtually zero amplitude. This is the case of typical experiments with ultracold alkali Bose gases, which will be the focus of our thesis.

2.1.2 Bose gas in the Grand-canonical ensemble

We can now make use of the above statistical distinction of particles imposed by quantum statistics to understand the thermodynamics of a quantum gas. Let us focus on the case of Bose gas of free particles.

One possible and commonly used formalism to study thermodynamical properties of a noninteracting (ideal) Bose gas is the *Grand-canonical ensemble*, where the number of particles is allowed to fluctuate.[12] Associated with this ensemble is its bosonic partition function, defined as

$$\ln \mathcal{Z}(T, V, \mu) = -\sum_i \ln\left[1 - e^{-\beta(\epsilon_i - \mu)}\right], \tag{2.4}$$

with volume V, temperature T, chemical potential μ, and as usual $\beta \equiv 1/k_B T$ with k_B the Boltzmann constant. The ϵ_i represent energies for one-particle states (orbitals) i. From (2.4) we can for instance obtain the average number of particles occupying each state as in

$$\langle n_i \rangle = -\frac{1}{\beta}\frac{\partial}{\partial \epsilon_i} \ln \mathcal{Z} = \frac{1}{e^{\beta(\epsilon_i - \mu)} - 1}. \tag{2.5}$$

In order to (2.5) make physical sense (i.e. positive or null occupation number), we see that the chemical potential must satisfy the condition $\mu < 0$. The total number of particles N is then given by

$$N = \sum_i \langle n_i \rangle = \sum_i \frac{1}{e^{\beta(\epsilon_i - \mu)} - 1}, \tag{2.6}$$

which can provide an equation of state $\mu = \mu(T, N)$ for the system.

From Eq. (2.6) we can perform an interesting limit, namely $\mu \to 0^-$, from which we see that the lowest energy state will tend to accumulate all particles on its level. This happens for a critical temperature T_c approximately given by the left side of (2.1), which characterizes a phase transition. In this limit, Eq. (2.6) needs to be written in the form

$$N = N_0 + \int_0^\infty d\epsilon \frac{g(\epsilon)}{e^{\beta\epsilon} - 1}, \tag{2.7}$$

where N_0 is the number of particles occupying the ground state (with energy $\epsilon_0 = 0$). The sum was substituted by an integral over energy, with the help of a weight function $g(\epsilon)$ that characterizes the density of states. This function is a particularity of the physical system under investigation and imposes interesting dimensional constraints for the convergence of (2.7). For instance, it diverges for any finite temperature in the case of free-particles

(homogeneous system) in one and two dimensions. Nevertheless, this is not true anymore for certain trapped systems, which can heal this dimensional restriction.

In fact, the above limit leads to the *Bose-Einstein condensation* (BEC) in Bose gases: a macroscopic occupation of the same quantum level by the majority of particles in a system. This quantum-mechanical phenomenon of the condensation is purely due to the statistical nature of particles, which implies the impossibility of its occurrence for particles behaving as fermions, owing to Pauli's exclusion principle. In order to undergo condensation, fermionic systems must somehow participate in a collective phenomenon to generate effective symmetric wavefunctions. This is the case of Cooper-pairing formation that explains the superconductivity of innumerable fermionic systems.[11]

2.2 Interactions taken into account

Pioneered by Bose and Einstein,[13] the above seminal discussion predicting the condensation does not take into account the effects of interactions. One of these effects is to prevent that all particles occupy the condensate level (even for ultra-low temperatures), promoting some of them to higher energy levels (condensate depletion). However, this should not lead one to an erroneous intuition that their effect is to completely hinder condensation. On the contrary, it was later realized that the presence of interparticle interaction can actually assist in the formation of the BEC[14] and is essential for explaining the existence of super-phenomena such as superfluidity. Another interesting aspect of the non-ideal Bose gas is that the more energetic particles are, in general, spatially overlapped with the condensate. This reflects the fact that condensation happens in momentum space, where phase separation can be distinguished, as shown in Fig. 1 in a real experimental depiction of the phenomenon (particularly in the case $T < T_C$, in which the zero-momentum state reveals a density peak alongside a surrounding distribution of non-condensed atoms).

The full description of particle interactions is generally a hard problem to tackle and approximations are commonly employed. In the case of BEC in alkali gases, a mean-field approach, where only contact interactions are considered and quantum fluctuations are neglected, has successfully described a myriad of experiments, even in a simplified $T = 0$ description. This mean-field model takes the form of a nonlinear Schrödinger equation for the macroscopic wavefunction ψ that describes the condensate, whose general properties we shall discuss next.

2.2.1 Gross-Pitaevskii model

Accounting for particles interactions starts from basic energetic assumptions. According to scattering theory,[16] low-energy, many-body systems collide mainly via s-wave processes. An effective two-body contact interaction can then be used to model these interactions through a pseudo-potential in the form of a Dirac delta $\delta(|\mathbf{r} - \mathbf{r}'|)$, where $\mathbf{r}$

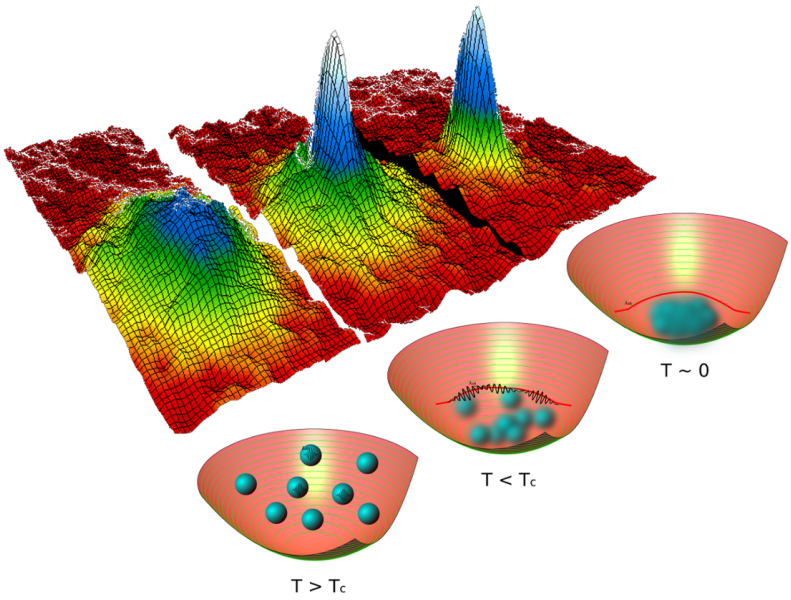

Figure 1 – Transition to a BEC state as the temperature is lowered. The upper row of images show momenta distributions taken in the JILA experiments. The lower row displays schematically the distribution of particles in the trap and the condensation to the lowest particle state.
Source: TSATSOS et al.[15]

and $\mathbf{r}'$ represent spatial coordinates. This is a remarkably precise approximation for the case of very dilute Bose gases at ultralow temperatures, whose s-wave scattering length a_s characterizes the strength of the (nonlinear) interaction, measured by the parameter $g = 4\pi a_s \hbar^2/m$. This allows for a many-body representation of the Hamiltonian for N-interacting bosons simply given by

$$H = \sum_{i=1}^{N} \left[\frac{\mathbf{p}_i^2}{2m} + V(\mathbf{r}_i) \right] + g \sum_{i<j} \delta(\mathbf{r}_i - \mathbf{r}_j), \tag{2.8}$$

where $\mathbf{p}_i$ is the momentum for particle i of mass m at position $\mathbf{r}_i$, subjected to an arbitrary external potential $V(\mathbf{r})$.

From the second-quantization formalism, we know that the creation and annihilation bosonic field operators $\hat{\psi}^\dagger(\mathbf{r})$ and $\hat{\psi}(\mathbf{r})$ obey the commutation relations

$$\left[\hat{\psi}(\mathbf{r}), \hat{\psi}^\dagger(\mathbf{r}') \right] = \delta(\mathbf{r} - \mathbf{r}'), \tag{2.9}$$

and

$$\left[\hat{\psi}(\mathbf{r}), \hat{\psi}(\mathbf{r}') \right] = 0. \tag{2.10}$$

Using this fact, the second-quantized version of the Hamiltonian (2.8) can be expressed as

$$H = \int d\mathbf{r} \left\{ \hat{\psi}^\dagger(\mathbf{r}) \left[-\frac{\hbar^2}{2m} \nabla^2 + V(\mathbf{r}) \right] \hat{\psi}(\mathbf{r}) + \frac{g}{2} \hat{\psi}^\dagger(\mathbf{r}) \hat{\psi}^\dagger(\mathbf{r}) \hat{\psi}(\mathbf{r}) \hat{\psi}(\mathbf{r}) \right\}. \tag{2.11}$$

The Hamiltonian (2.11) accounts for a fairly general scenario, where quantum fluctuations are present. The full bosonic field $\hat{\psi}(\mathbf{r})$ can be expressed in the form of a mean-field $\psi(\mathbf{r}) \equiv \left\langle \hat{\psi}(\mathbf{r}) \right\rangle$ over which fluctuations $\delta\hat{\psi}(\mathbf{r})$ exist, therefore

$$\hat{\psi}(\mathbf{r}) = \psi(\mathbf{r}) + \delta\hat{\psi}(\mathbf{r}). \tag{2.12}$$

In the so-called mean-field approximation these quantum fluctuations are neglected, and the substitution of $\hat{\psi}(\mathbf{r})$ by the c-number $\psi(\mathbf{r})$ in (2.11) yields the following energy functional

$$E[\psi] = \int d\mathbf{r} \frac{\hbar^2}{2m} |\nabla\psi|^2 + V(\mathbf{r}) |\psi|^2 + \frac{g}{2} |\psi|^4 . \tag{2.13}$$

In the mean-field description, $\psi(\mathbf{r}, t)$ is the macroscopic wavefunction at instant t. It serves as the order parameter for the BEC (as will be discussed in the next subsection), whose normalization provides the macroscopic number N of particles occupying the specific Bose-condensed one-particle state. Associated with this description, we can write the following Lagrangian[17]

$$L[\psi] = \int i\frac{\hbar}{2} \left(\psi^* \frac{\partial\psi}{\partial t} - \psi \frac{\partial\psi^*}{\partial t} \right) d\mathbf{r} - E[\psi]. \tag{2.14}$$

The minimization of (2.14) with respect to ψ (or equivalently ψ^*) leads to the celebrated Gross-Pitaevskii equation[18,19] (GPE)

$$i\hbar \frac{\partial\psi(\mathbf{r}, t)}{\partial t} = \left(-\frac{\hbar^2}{2m}\nabla^2 + V(\mathbf{r}) + g|\psi(\mathbf{r}, t)|^2 \right) \psi(\mathbf{r}, t), \tag{2.15}$$

which describes the dynamics of the condensate at $T = 0$. This equation is simply a Schrödinger equation, when considering the usual linear (kinetic and potential V) operators, but with the addition of a nonlinear contribution $\propto |\psi(\mathbf{r})|^2$ coming from the two-body contact interaction.

The GPE assumes its time-independent form when one substitutes $\psi(\mathbf{r}, t) = \psi(\mathbf{r})e^{-i\mu t/\hbar}$ in (2.15), which then reduces to the eigenvalue problem

$$\mu\psi(\mathbf{r}) = \left(-\frac{\hbar^2}{2m}\nabla^2 + V(\mathbf{r}) + g|\psi(\mathbf{r})|^2 \right) \psi(\mathbf{r}), \tag{2.16}$$

with the eigenvalue μ being the chemical potential and its associated eigenfunction $\psi(\mathbf{r})$ the stationary solution.

Due to its nonlinear nature, equation (2.16) is typically hard to be solved analytically. However, a particularly interesting limit is when interactions are strong enough that the wavefunction varies slow and smoothly in space. In this case, spatial derivatives (therefore, kinetic terms) can be neglected, and a simple stationary state assumes a density profile $\rho(\mathbf{r}) \equiv |\psi(\mathbf{r})|^2$ which is straightforwardly given by

$$\rho(\mathbf{r}) = \frac{\mu - V(\mathbf{r})}{g}, \tag{2.17}$$

for values of $\mu > V(\mathbf{r})$ and null elsewhere. This is known as the *Thomas-Fermi approximation*, which is fairly accurate in many real-life experiments with alkali gases and thus useful for providing an estimate for the system's spatial extensions. From this assumption we conclude that the density acquires the inverted format of the external potential V. For the particular case of a harmonically trapped system, with $V(\mathbf{r}) = \frac{m}{2}(\omega_x^2 x^2 + \omega_y^2 y^2 + \omega_z^2 z^2)$ and trapping frequencies ω_i, we obtain an inverted-parabola solution in each Cartesian direction i. The system's extension can thus be defined as the largest distance $R_{\mathrm{TF},i}$ along the Cartesian axis i where $V = \mu$,

$$R_{\mathrm{TF},i} = \sqrt{\frac{2\mu}{m\omega_i^2}}, \tag{2.18}$$

which are known as the Thomas-Fermi radii.

An important scale intrinsic to the GP model is the *healing length* ξ, defined as the extension over which kinetic energy becomes comparable to, and equals, the interaction energy. Thus,

$$\frac{\hbar^2}{2m}|\nabla\psi|^2 \sim g|\psi|^4 \Rightarrow \frac{\hbar^2}{2m}\frac{|\psi|^2}{\xi^2} \equiv g|\psi|^4. \tag{2.19}$$

For a homogeneous system, we know that the wavefunction assumes a constant background density value of $\rho_0 \equiv |\psi_0|^2$. In this case,

$$\xi = \frac{\hbar}{\sqrt{2mg\rho_0}}. \tag{2.20}$$

If a system is inhomogeneous, the above definition of the healing length becomes arbitrary, since the condensate's density varies locally. For this reason, in harmonically trapped systems, for instance, it is common to define $\rho_0 \equiv |\psi(x = 0, y = 0, z = 0)|^2$. The healing length has the physical meaning of the typical scale over which a condensate that is locally perturbed requires to "heal" from the perturbation and recover its density bulk value ρ_0. This scaling is particularly important to estimate the dimensions of highly nonlinear structures such as solitons and vortices.

Using suitable trapping potentials, atomic BECs can be easily shaped. In these settings, a particular dimension i can be so tightly confined (large confining frequency ω_i) that the dynamics along it is practically frozen (to the smallest width possible, given by the Heisenberg's uncertainty principle), and excitations in that direction are energetically costly (since $\hbar\omega_i \gg \mu$). It is possible then to achieve, for instance, a two-dimensional (2D) limit. In particular, assuming again that the system is harmonically trapped in all directions, the frequency ω_z of the trap in the z-direction can be chosen to be much larger than the radial frequencies ω_x and ω_y. Consequently, the wave function can be factorized in $\psi(x, y, z) = \psi_r(x, y)\psi_z(z)$. The fact that the system is so tightly confined in z also means that ψ_z is approximately the ground state of a 1D harmonic trap in that direction, which justifies assuming its Gaussian form $\psi_z(z) = e^{-z^2/2a_z^2}/(2a_z^2)^{1/4}$, where $a_z \equiv \sqrt{\hbar/m\omega_z}$.

Therefore, integrating out the z-dependent terms and fixing normalization, the GPE (2.15) reduces to its 2D version

$$i\hbar\frac{\partial\psi_r(x,y,t)}{\partial t} = \left(-\frac{\hbar^2}{2m}\nabla^2 + V(x,y) + g_{2\mathrm{D}}|\psi_r(x,y,t)|^2\right)\psi_r(x,y,t), \tag{2.21}$$

where $g_{2\mathrm{D}} \equiv g/\sqrt{2\pi a_z^2}$ is the effective interaction parameter.

2.3 Bose-Einstein condensation and definitions

Although the BEC phenomenon might be qualitatively understood following the statistical discussion in Sec. 2.1, it should be generalized for the inclusion of interactions. A precise definition, however, can be challenging (and sometimes still matter of debate in the literature[11]). For completeness, we present below the most commonly used criteria to define a BEC, which are applicable for realistic interacting systems.

The reduced density matrix – Let us assume the *a priori* knowledge of a many-body wave function $\Psi_i(\mathbf{r}_1, ..., \mathbf{r}_N, t)$ which describes a particular pure state i of a Bose gas with N particles at instant t and satisfies, naturally, the condition in (2.3) for bosons. A set $\{i\}$ of such pure states allows a general, mixed state of the Bose gas to be described by a *reduced single-particle density matrix* as in

$$\rho(\mathbf{r},\mathbf{r}',t) \equiv N\sum_i p_i \int d\mathbf{r}_2 ... \int d\mathbf{r}_N \Psi_i^*(\mathbf{r},\mathbf{r}_2,...,\mathbf{r}_N,t)\Psi_i(\mathbf{r}',\mathbf{r}_2,...,\mathbf{r}_N,t), \tag{2.22}$$

where p_i is the (classical) probability weight associated with a particular pure state i and the integrals represent partial traces over coordinates $\mathbf{r}_2$ to $\mathbf{r}_N$. Alternatively, this can also be written in terms of field operators from the expectation value

$$\rho(\mathbf{r},\mathbf{r}',t) \equiv \left\langle \hat{\psi}^\dagger(\mathbf{r},\mathbf{t})\hat{\psi}(\mathbf{r}',\mathbf{t})\right\rangle. \tag{2.23}$$

We can always find a set of single-particle states $\{\phi_i\}$ which diagonalizes $\rho(\mathbf{r},\mathbf{r}',t)$, with corresponding occupation-number eigenvalues $n_i(t)$. Therefore, in that complete orthogonal basis, one can write

$$\rho(\mathbf{r},\mathbf{r}',t) = \sum_i n_i(t)\phi_i^*(\mathbf{r},t)\phi_i(\mathbf{r}',t). \tag{2.24}$$

There are two possible definitions of the BEC which follow from properties of the reduced density matrix. Namely,

- (I) "Penrose-Onsager" criterion: this definition consists of analyzing the behavior of the eigenvalues $n_i(t)$ of $\rho(\mathbf{r},\mathbf{r}',t)$ extracted from (2.24). If one of these eigenvalues is of the order of N, say n_j, we can assure that the corresponding single-particle state ϕ_j is macroscopically occupied, therefore the system described by $\rho(\mathbf{r},\mathbf{r}',t)$ exhibits a simple BEC in that component. If more than one eigenvalues are of the order of

N, a more complex possibility arises, defining a fragmented BEC (i.e. coexistence of more than one Bose-condensed components). In this thesis we will be concerned with the case of a simple BEC and should adopt this definition, being it more appropriate for trapped systems.

- (II) "Yang" or "off-diagonal long-range order" criterion: postulates that ρ, in the appropriate long-range limit, can be written as

$$\lim_{|\mathbf{r}-\mathbf{r}'|\to\infty} \rho(\mathbf{r},\mathbf{r}',t) = f^*(\mathbf{r},t)f(\mathbf{r}',t) + \tilde{\rho}(\mathbf{r},\mathbf{r}',t). \tag{2.25}$$

If this limit is finite, with $\tilde{\rho} \to 0$, the function f indicates that the system exhibits BEC and $\psi(\mathbf{r},t) \equiv f(\mathbf{r},t)$ can be identified as the system's order parameter. However, this limit is not well defined for trapped systems, and the previous criterion is somehow more general.[11]

Finally, there is a third definition derived from the concept of *symmetry breaking*.

- (III) "Spontaneous symmetry breaking": this definition requires that the $U(1)$ gauge symmmetry (system's invariance to a global phase change, therefore related to particle number conservation) must be broken to allow for the existence of a BEC. This means that the expectation value of the field operator,

$$\psi(\mathbf{r},t) \equiv \left\langle \hat{\psi}(\mathbf{r},t) \right\rangle, \tag{2.26}$$

should be nonzero by spontaneous symmetry breaking and represents the system's order parameter. Some criticism on this definition lies on the fact that fragmented BECs are not well described by the spontaneous symmetry breaking, which would make it less general than the "Penrose-Onsager" definition.[11]

2.4 Hydrodynamic formulation

Once we assume that the mean-field approximation is an adequate description to the condensate (as is the case of most experiments with ultracold alkali gases), we can write the associated macroscopic wave function as simply being

$$\psi(\mathbf{r},t) = \sqrt{\rho(\mathbf{r},t)}e^{iS(\mathbf{r},t)}, \tag{2.27}$$

which describes a classical field ψ with amplitude $\sqrt{\rho}$ and phase S. This is known as the *Madelung transformation* for the macroscopic wavefunction.[20] We can choose to conveniently normalize $\int |\psi|^2 d\mathbf{r} = 1$.

Inserting (2.27) in the GPE [Eq. (2.15)] and separating real and imaginary parts we are left with

$$\frac{\partial \rho}{\partial t} = -\frac{\hbar}{m}\nabla \cdot (\rho \nabla S) \tag{2.28}$$

and

$$-\hbar\frac{\partial S}{\partial t} = -\frac{\hbar^2}{2m\sqrt{\rho}}\nabla^2\sqrt{\rho} + \frac{\hbar^2}{2m}\left|\nabla S\right|^2 + V(\mathbf{r}) + g\rho. \tag{2.29}$$

We know from quantum mechanics that, associated with this wavefunction, there is a probability current

$$\mathbf{j} = \frac{\hbar}{2mi}(\psi^*\nabla\psi - \psi\nabla\psi^*) = \frac{\hbar}{m}\rho\nabla S. \tag{2.30}$$

Since this flux can also be written as $\mathbf{j} = \rho\mathbf{v}$, we identify straightaway the velocity field

$$\mathbf{v} = \frac{\hbar}{m}\nabla S. \tag{2.31}$$

Taking the gradient of (2.29) and substituting the above definitions in both (2.28) and (2.29), we arrive at the *hydrodynamic equations* for the BEC[17]

$$\frac{\partial\rho}{\partial t} + \nabla\cdot\mathbf{j} = 0 \tag{2.32}$$

and

$$\frac{\partial\mathbf{v}}{\partial t} = -\frac{1}{m\rho}\nabla\left(\frac{\rho^2 g}{2}\right) - \nabla\left(\frac{v^2}{2}\right) + \frac{1}{m}\nabla\left(\frac{\hbar^2}{2m\sqrt{\rho}}\nabla^2\sqrt{\rho}\right) - \frac{1}{m}\nabla V, \tag{2.33}$$

with $v \equiv |\mathbf{v}|$. Eq.(2.32) is just the continuity equation, the same that one finds for the linear Schrödinger equation. This implies that the inclusion of contact interactions in the GP model does not affect the conservation of the probability $|\psi|^2$. Eq.(2.33) is the quantum version of the Euler equation, which we shall discuss in more detail in the next chapter. The important aspect of this description is that the GPE has now a hydrodynamic interpretation that allows comparing the BEC with a perfect classical fluid and which elucidates remarkable properties of quantum fluids.

2.5 Elementary excitations, superfluidity, and vortices

2.5.1 Superfluidity

The so-called *super-phenomena*, superfluidity and superconductivity, are startling consequences of the macroscopic manifestation of quantum mechanics. Below a certain critical temperature, fluids may flow without viscosity in the former case and currents flow with no resistance in the latter. Analogous in their fundamental mechanism, these phenomena are intimately linked to the occurrence of Bose-Einstein condensation,[20] a necessary but not sufficient condition for their manifestation.[21] Interactions play essential role as they change (as we shall see next) the dispersion relation of a simplistic Bose gas of noninteracting particles to that of a much richer system, allowing for elementary, collective excitations. In a nutshell, super-phenomena occur when there is a condensed system that requires a finite amount of energy to be paid in order to generate collective excitations. For an obstacle which moves in a BEC, for instance, this condition sets a

velocity criterion, first derived by Landau[22] from simple energy-momentum conservation arguments. Landau's criterion states that below a critical velocity

$$v_c = \min\left[\frac{\epsilon(p)}{p}\right] \tag{2.34}$$

scattering of an elementary excitation of energy $\epsilon(p)$ and momentum p is absent and flow past the obstacle can be regarded as dissipationless. This criterion can thus be used to define superfluidity and also its breakdown. To exemplify this, let us first find the energy spectrum for the case of a homogeneous BEC.

2.5.2 Energy dispersion for a homogeneous BEC

For a homogeneous BEC, let us consider the macroscopic wavefunction $\psi(\mathbf{r},t) = \sqrt{\rho_0}e^{-\frac{i\mu}{\hbar}t}$, where $\mu = g\rho_0$ is the chemical potential. One can also assume that perturbations over this background may be accounted for writing

$$\psi(\mathbf{r},t) = \sqrt{\rho_0}e^{-\frac{i\mu}{\hbar}t} + \delta\psi(\mathbf{r},t). \tag{2.35}$$

We are interested in very weak perturbations, which justifies substituting this Ansatz in Eq. (2.15) and keeping only linear terms in $\delta\psi$. This yields

$$i\hbar\frac{\partial\delta\psi}{\partial t} = -\frac{\hbar^2}{2m}\nabla^2\delta\psi + g\left(2\left|\psi\right|^2\delta\psi + \psi^2\delta\psi^*\right). \tag{2.36}$$

At this point we assume that the interesting solutions for us are periodic in time (additionally to the global phase $e^{\frac{-i\mu t}{\hbar}}$, already present in the background solution), with the form

$$\delta\psi(\mathbf{r},t) = u(\mathbf{r})e^{-i\omega t} + v^*(\mathbf{r})e^{i\omega t}. \tag{2.37}$$

This is known as the *Bogoliubov transformation*, a powerful canonical transformation (here cast in a simplified form) which helps linearizing quadratic Hamiltonians. This leads us to the coupled equations,

$$-\frac{\hbar^2}{2m}\nabla^2 u(\mathbf{r}) + \mu\left[u(\mathbf{r}) - v(\mathbf{r})\right] = \hbar\omega u(\mathbf{r}), \tag{2.38}$$

$$-\frac{\hbar^2}{2m}\nabla^2 v(\mathbf{r}) + \mu\left[v(\mathbf{r}) - u(\mathbf{r})\right] = -\hbar\omega v(\mathbf{r}), \tag{2.39}$$

known as the *Bogoliubov-de Gennes equations*.

We can use the fact that we are dealing with a homogeneous system, and therefore solutions should satisfy translational invariance. For this reason, we can assume that $u(\mathbf{r})$ and $v(\mathbf{r})$ are plane waves, thus proportional to $e^{i\mathbf{k}\cdot\mathbf{r}}$. With this, the above equations become

$$\left(\frac{\hbar^2k^2}{2m} + \mu - \hbar\omega\right)u_k - \mu v_k = 0, \tag{2.40}$$

$$\left(\frac{\hbar^2k^2}{2m} + \mu + \hbar\omega\right)v_k - \mu u_k = 0, \tag{2.41}$$

or explicitly written as the eigen-problem

$$\mathcal{O}\begin{pmatrix} u_k \\ v_k \end{pmatrix} = \hbar\omega \begin{pmatrix} u_k \\ v_k \end{pmatrix}, \tag{2.42}$$

where the operator

$$\mathcal{O} \equiv \begin{pmatrix} E & \mu \\ -\mu & -E \end{pmatrix}, \tag{2.43}$$

with $E = \frac{\hbar^2 k^2}{2m} + \mu$. The coefficients u_k and v_k are assumed to satisfy the normalization condition

$$|u_k|^2 - |v_k|^2 = 1, \tag{2.44}$$

which imposes that the associated excitations satisfy bosonic commutation relations and also implies that ω is always real.[23,24]

Equation (2.42) has solution if

$$\det\left[\mathcal{O} - \hbar\omega\right] = E^2 - \mu^2 = 0 \implies (\hbar\omega)^2 = \frac{\hbar^2 k^2}{2m}\left(\frac{\hbar^2 k^2}{2m} + 2\mu\right). \tag{2.45}$$

Considering only positive eigen-frequencies ω (thus positive energies) we are left then with the Bogoliubov spectrum for the homogeneous interacting BEC, given by

$$\epsilon(p) = \hbar\omega = \sqrt{\epsilon^0(p)\left[\epsilon^0(p) + 2\mu\right]}, \tag{2.46}$$

where momentum $p = \hbar k$ and $\epsilon^0(p) \equiv \frac{p^2}{2m}$ is the free-particle dispersion relation.

2.5.3 Superfluidity breakdown

Notice from (2.46) that for a noninteracting system $\epsilon(p) = \epsilon^0(p)$ (since $\mu = g\rho_0 = 0$), implying zero critical velocity, according to equation (2.34). This means that the ideal Bose-gas, even when condensed, does not exhibit superfluidity in Landau's sense. However, this is different for interacting homogeneous systems. In these cases, the energy dispersion relation (2.46) for low momenta is linear, i.e. $\epsilon(p) \approx \sqrt{2\mu\epsilon^0(p)} = cp$, therefore (2.34) gives us a finite $v_c = c$, where $c \equiv \sqrt{\mu/m}$ is the velocity of sound in the system. This linear dispersion is related to quasi-particles known as *phonons*, which are long-wavelength density excitations (sound waves). For larger momentum we see that the spectrum follows the free-particle dispersion. Clearly, the type of excitations (quasi-particles) appearing will depend on the specific energy dispersion $\epsilon(p)$. For superfluid helium (^{4}He – a system where interactions are considerably strong and thus not quantitatively well described by the GPE) for instance, additionally to this linear low-momenta dispersion, there is a local minimum in $\epsilon(p)$ associated with *rotons*, which are subsonic, short-wavelength elementary excitations. If one interprets the superfluid as a background for these excitations, one has some of the ingredients for understanding the system in a two-fluid (or two-component) model,[1,25] which proved to be very successful in explaining features of superfluid helium.

Landau's criterion implies that, once elementary excitations are produced, the flow starts to be dissipative, and quasi-particles are scattered to the non-condensed part of the fluid (*superfluidity breakdown*). However, the analysis based solely on the above mentioned dispersion curves has proven to overestimate the critical velocity for breakdown in real experiments. Feynman was the first to suggest that the presence of other types of (nonlinear) excitations is responsible for the flow's drag instead[1] – the *quantized vortices*. These vortices can be excited even when the fluid's bulk velocity past an obstacle is subsonic. The geometry of the obstacle (its shape and penetrability) alongside boundary conditions imply that flow can be supersonic locally, thus allowing for vortex shedding in pairs. With the possibility of creating true 2D flows with atomic BECs (and their unprecedented controllability when compared to superfluid helium experiments), theoretical predictions for the subsonic breakdown of superfluidity based on the generation of vortices[26–29] have been confirmed in recent experiments with alkali superfluids[30] ($v_c \approx 0.40c$). In similar context, the effects of rough boundary layers in liquid helium containers has recently gained attention. The presence of irregularities on a surface where the superfluid flows gives rise to abundant and complex tangling of vortices on the container's surface, illustrating the importance of quantized vortices to understand many aspects of superfluidity.[31]

2.6 Quantized vortices

The fact that velocity field (2.31) is given by the gradient of a scalar field S * has important consequences on the types of motion that can occur in a condensate, particularly the irrotational property of the flow,

$$\nabla \times \mathbf{v} = 0. \tag{2.47}$$

Note that the above result holds true when the field ψ has continuous first and second derivatives. However, this is no longer valid if there is a line along which $\mathbf{v}$ diverges.

As an example, let us assume an axially symmetric system which can be described by the macroscopic wave-function in the form

$$\psi(\mathbf{r}) = \psi(r, z, \phi) = f(r, z)e^{iS(\phi)}, \tag{2.48}$$

where $\mathbf{r} = (r, \phi, z)$ are cylindrical coordinates. $f(r, z)$ is some prescribed real function and S is assumed to depend only on the coordinate ϕ. Then, we see from this Ansatz then, that

$$\mathbf{v} = \frac{\hbar}{m}\nabla S = \frac{\hbar}{m}\frac{1}{r}\frac{\partial S}{\partial \phi}\hat{z}. \tag{2.49}$$

* Although it is common to assume the validity of the last equality in (2.31), this is not formally correct. The scalar field S represents a phase, it is therefore a multivalued field. The discontinuities (branch-cuts in Riemann surfaces) in its definition requires an appropriate chain rule which modifies (2.31), as recently discussed for the specific context of BECs.[32] This has consequences for the hydrodynamic formulation arising from the Gross-Pitaevskii equation.

Therefore, unless $S(\phi)$ is a constant, the velocity field presents a singularity on the axis at $r = 0$, and thus (2.47) cannot be true everywhere.

In fact, as a general result, the single valuedness of a macroscopic wavefunction describing the condensate implies that, around a closed loop C, the line integral

$$\oint_C \nabla S \cdot d\mathbf{l} = 2\pi\kappa, \tag{2.50}$$

with κ being an integer. In the absence of divergences in $\mathbf{v}$, $\kappa = 0$, regardless of the chosen closed path C. Nevertheless, if there is a divergent line and C encloses one of its points, $\kappa \neq 0$. As a consequence, the hydrodynamic measure of *circulation*,

$$\Gamma = \oint_C \mathbf{v} \cdot d\mathbf{l} = 2\pi\kappa\frac{\hbar}{m}, \tag{2.51}$$

can only assume integer multiples κ of a quantum of circulation h/m.[1,33] These lines of divergence are topological defects known as *quantized vortices*, with associated topological charge κ. If $|\kappa| = 1$, the vortex is singly-quantized. If $|\kappa| > 1$, the vortex is said to be multicharged.

Formally, we can rewrite (2.47) to account for a quantized vortex, where vorticity $\omega = \nabla \times \mathbf{v}$ becomes a (two-dimensional) delta function,[17]

$$\nabla \times \mathbf{v} = \kappa\frac{h}{m}\delta^{(2)}(\mathbf{r} - \boldsymbol{\ell}_0)\hat{\boldsymbol{\omega}}, \tag{2.52}$$

where $\boldsymbol{\ell}_0$ describes a line in space which contains the singular points and $\hat{\boldsymbol{\omega}}$ is the unit vector parallel to this line. (In the example above, $\boldsymbol{\ell}_0 = \mathbf{z}$ and $\hat{\boldsymbol{\omega}} = \hat{z}$.)

The fact that $\mathbf{v}$ diverges at some points implies that the wavefunction must also go to zero at exactly the same points, that is, inside the vortex core. In other words, both real and imaginary parts of ψ go to zero at $r = 0$ yielding a zero density at the singularity $r = 0$. Therefore, the fact that the velocity diverges as $r \to 0$ is not physically inconsistent: there are no atoms in the vortex core which move with infinite speed. The vortex line is a hole in the superfluid, that therefore renders its bulk a multiply-connected space. A quantum vortex, being a local node of the density, can also be thought to have an opening of the order of the healing length ξ.

Mathematically, the flow pattern of a quantum vortex line has the characteristics of its classical counterpart, as can be found in elementary fluid dynamics textbooks: a node at $r = 0$ and a velocity field around it which decays as $r \to \infty$ away from the axis.

2.7 Stability of multicharged vortices

As we see from the discussion above, the quantized vortex is a topological excitation of a BEC. It is a node in the wavefunction, which increments the energy of a vortex-free condensate for two reasons: firstly, because it deforms the BEC density, adding kinetic energy coming from spatial derivatives and also extra nonlinear contribution from

interactions; secondly, due to the phase profile of the vortex, giving rise to a centrifugal term $E_c \propto \kappa^2/r^2$ [see (2.49)]. Therefore, if we naively assume that the first corrections (due to density variations) are small compared to the second (centrifugal kinetic energy), we see that, for a given charge κ, it is energetically favorable for the system to contain κ singly-charged vortices rather than one multicharged vortex. This roughly justifies the energetic instability of multicharged vortices, which typically prefer splitting into singly-quantized vortices.

This naive argument, however, holds true only for homogeneous and some particular trapped systems. Interestingly, steeper-than-harmonic potentials (such as quartic[34] and hard-walled cylindrical potentials) support multicharged vortices as energetically favorable solutions (as opposed to an array of singly-charged vortices with same net circulation), becoming genuine ground states of the trapped system.[35] For harmonically trapped systems, a multicharged vortex is always unstable against the splitting. Nevertheless, these states can appear during rapid rotations of harmonic traps (with additional perturbation of repulsive laser beams to enforce the appearance of a large vortex core[†])[37] or if phase-imprinted.[38] Despite their instability in harmonic traps, they can be long-lived structures with interesting splitting dynamics, which can thus be studied in real-life experiments.

Similarly to the analysis shown in Sec. 2.5.2, we can study the behavior of linear perturbations over a stationary solution of the GPE, but in this case instead of (2.35),

$$\psi(\mathbf{r},t) = \psi_\kappa(\mathbf{r})e^{-\frac{i\mu}{\hbar}t} + \delta\psi(\mathbf{r},t). \tag{2.53}$$

The state $\psi_\kappa(\mathbf{r})$ represents a BEC with a multicharged vortex of charge κ, which is the stationary solution of the time-independent GPE.[35,40]

It is convenient that, instead of (2.37), we look for solutions of the type

$$\delta\psi(\mathbf{r},t) = \sum_q \left[u_q(\mathbf{r})e^{-i\omega_q t} + v_q^*(\mathbf{r})e^{i\omega_q^* t}\right], \tag{2.54}$$

which are also canonical Bogoliubov transformations, although in a linear combination of specific modes q. Note that in this Ansatz we allow the eigenfrequencies to be complex numbers. This means that if a particular solution with mode q has complex eigenfrequency with positive imaginary part, for instance, we can say that the system is *dynamically unstable*. The reason is that, as time evolves, this mode (in fact, a pair of modes with same characteristic frequency) will present a divergent amplitude [see (2.54)], exponentially escaping from the linear approximation we have initially stated. Physically, this means that the multicharged vortex splits into singly-charged vortices.

[†] The trapping frequency ω_r of harmonic trap acts as a rotation speed limit, above which centrifugal forces overcome the confinement and imprisoned atoms start to escape. This above-ω_r rotation destroys condensation,[36] preventing the creation of multicharged vortices. That is the reason why an extra perturbation is required.

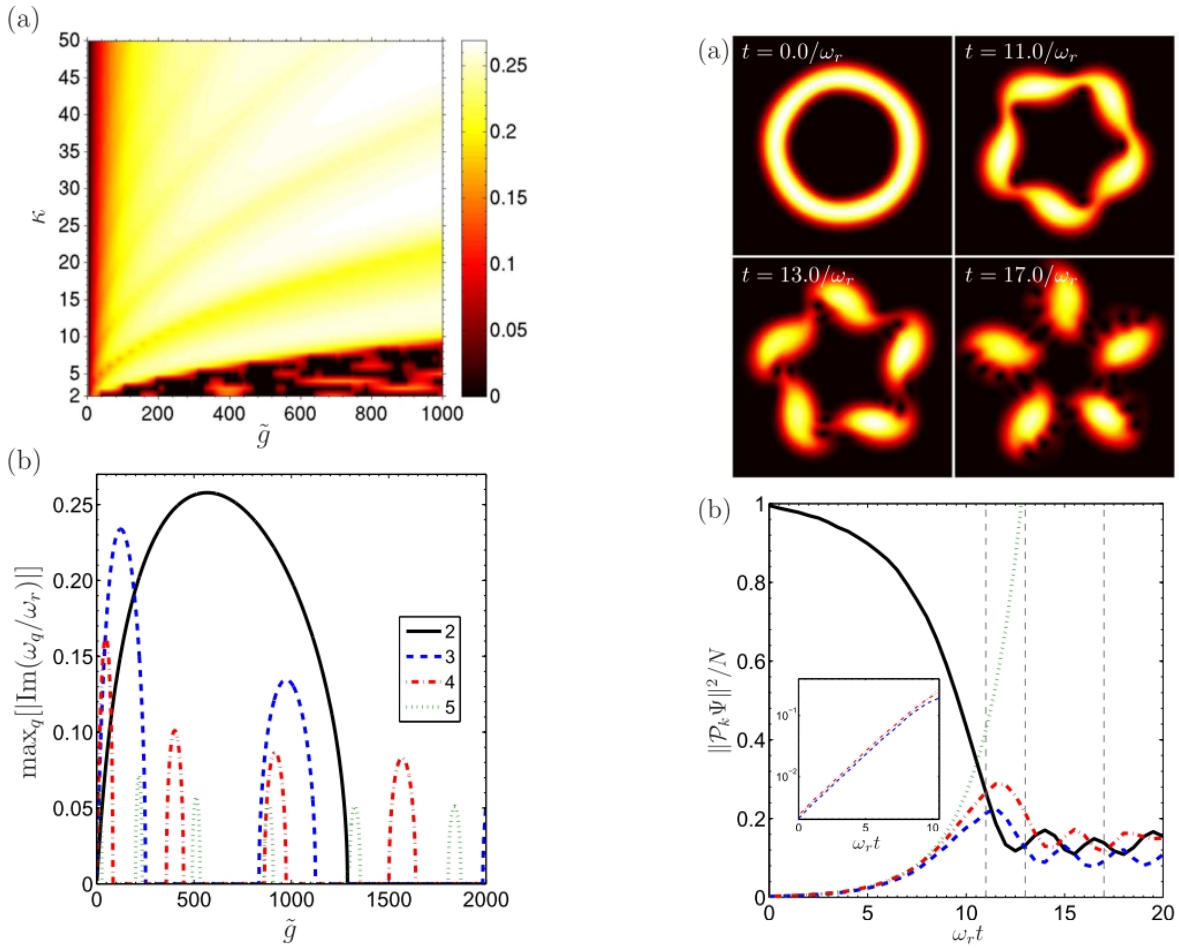

Figure 2 – Left:(a) Regions of stability in the $\kappa\times$ interaction $\tilde{g}$; (b) most unstable modes for a vortex with charge $\kappa = 10 \times \tilde{g}$. We can notice small regions of dynamical stability for the interaction strength $1400 \leq \tilde{g} \leq 2000$. Right: (a) Evolution of the giant vortex of charge $\kappa = 30$ decay, with normalized interparticle interaction $\tilde{g} = 200$. A perturbation of $l_q = 5$ with amplitude $\eta_m = 0.05$ was introduced. The symmetry of this unstable mode, as can be seen in (a), is followed by fragmenting the condensate in five vortex-free clouds. (b) The solid, dashed and dash-dotted curves correspond to $\kappa = 30$, 35 and 25, respectively. The dotted green curve corresponds to the exponential time divergence $e^{2\mathrm{Im}\{\omega_q\}t}$ found solving the Bogoliubov equations.
Source: KUOPANPORTTI et al.[39]

For a harmonically trapped system in a quasi-2D geometry, a cylindrically symmetric state of a muticharged vortex can be expressed as

$$\psi_\kappa(\mathbf{r}) = \sqrt{\rho(r)}e^{i\kappa\phi}, \tag{2.55}$$

where $\rho(r, z)$ is the particle density of the condensate. For this specific problem, the Bogoliubov amplitudes can be written as

$$\begin{aligned} u_q(\mathbf{r}) &= u_q(r)e^{i(l_q+\kappa)\phi}, \\ v_q(\mathbf{r}) &= u_q(r)e^{i(l_q-\kappa)\phi}. \end{aligned} \tag{2.56}$$

The value l_q represents the angular momentum (and therefore the l_q-fold symmetry) of a particular excited mode q.

By numerically solving the associated Bogoliubov-de Gennes equations for the stationary state (2.55) and perturbations of the type (2.56), Kuopanportti et al.[39] have computed an stability map for different values of κ ($2 \leq \kappa \leq 50$) and (dimensionless) interaction parameter $\tilde{g}$ ($0 \leq \tilde{g} \leq 1000$), based on the imaginary part of the unstable modes (see Fig. 2). After performing GPE simulations and comparing with the Bogoliubov analysis, they find that symmetry of the decay (including the shape of the multicharged vortex core oscillation) is imposed by the angular momentum l_q of the unstable leading mode (as can be seen in the example displayed in the right part of Fig. 2). For this interaction range, they show that vortices with charge $\kappa \leq 20$ tend to decay with quadrupole ($l_q = 2$) excitations. (As we will see in following chapters, the quadrupole turned out to be the leading decay mode in most of our numerical investigations, for our range of parameters).

Following the same line, Kuopanportti et al.[40] also showed that, in the Thomas-Fermi approximation (where kinetic energy is negligible compared to the interaction strength), the radius of a multicharged vortex core grows with $\approx \sqrt{\kappa}$. Moreover, it was verified that the dynamical instability of a vortex state increases only slowly with its charge, thus suggesting a slow decrease of the splitting time of a giant vortex with the increase of its charge. This is consistent with the view that, although dynamically unstable, such multicharged vortices are long-lived, coherent structures.[37]

2.8 Finite temperature effects

The condensate is typically surrounded by particles in excited states. As already mentioned, interactions play a role in this depletion phenomenon, but so do finite-temperature effects.

There is an extensive review on the various existing finite-temperature models by Proukakis and Jackson[41] which cover the main theories applied in the context of atomic BECs. Since our focus on this thesis is not, in principle, to deeply explore finite temperature effects, we will restrict ourselves to justify a fairly simplified phenomenological approach, which we adopt in Chap. 4.

In summary, in the phenomenological description, finite temperature effects are considered by making the substitution $t \to (1 - i\gamma)t$ in the GPE. The non norm-conserving dynamics that such a theory describes is considered to account for thermal effects and energy or particle loss of the superfluid towards the thermal cloud. This simple model was initially considered without any microscopic justification. The motivation came later with stochastic approach to dissipation, which shows that the γ term relates to temperature T as in

$$\gamma = i\frac{\hbar}{4k_{\mathrm{B}}T}\sum^{K}(\mathbf{r},t) \approx 12\frac{ma}{\pi\hbar^3}k_{\mathrm{B}}T. \tag{2.57}$$

$\sum^K(\mathbf{r}, t)$ is the so-called Keldysh self-energy, which represents incoherent collisions between condensate and excited atoms.[41] From Eq. (2.57) we can choose values for γ that agrees with experimental measurements of temperature, allowing us to model more realistic scenarios than a simple zero-temperature GPE.

3 TURBULENCE REVIEW

In this chapter, we define what is nowadays known as the field of quantum turbulence (QT). In order to do that, one should start from essentials of turbulence theory in classical fluids, then extrapolate the concepts to quantum liquids. Therefore, after briefly presenting the main concepts of classical turbulence (CT) in Sec. 3.1, we proceed to define and identify the different types of QT in Sec. 3.2. In this thesis we will be mostly interested in quantized vortex turbulence, which will be discussed in Sec. 3.5. Another type of turbulence present in compressible quantum liquids is due to nonlinear interactions of waves which, although not being our main focus, will be shortly discussed in Sec. 3.9.

Most of the content presented in this chapter can be found in our review paper.[15] For brevity, we focus here on the theoretical aspects of QT and omit the experimental details, which are not directly related to the current thesis.

3.1 Classical turbulence

Turbulence is widely accepted as a complicated problem involving the nonregular motion of fluids. Its complexity can be seen as long-standing puzzles in several disciplines such as mathematics, physics, engineering, and even life-sciences. It is remarkable that, although turbulent fluids are typically too complicated to be well-described using analytical tools, some general patterns arise from their flow, making possible the observation of universal properties shared by fluids that are in principle very different from each other.

The first, main feature that allowed a conceptual definition of turbulence is the presence of intertwined eddies in a turbulent fluid. Whilst this feature may seem sensible, it opposes to a common naive view of classical turbulence as being an unstructured mess, which does not exhibit any patterns. This feature has found a strong mathematical support in the nonlinear behavior of fluids described by differential equations such as the famous classical Euler equation for an inviscid (non-viscous) fluid

$$\frac{\partial \mathbf{v}}{\partial t} + (\mathbf{v}\cdot\nabla)\mathbf{v} = -\frac{1}{\rho}\nabla p, \tag{3.1}$$

where $\mathbf{v}$ is the fluid's velocity field, p the pressure, and ρ the density. This particular nonlinear term $(\mathbf{v}\cdot\nabla)\mathbf{v}$ arises simply from Newton's second law, i.e. from the force (per unit volume) acting on a moving fluid parcel, where the fluid is treated as a continuum. The interaction of eddies in the flow are result of this nonlinear behavior.

The Euler equation is considered to be the skeleton of an appropriate description of real turbulent fluids. In fact, real fluids are viscous, and more suitably described by the Navier-Stokes (NS) equation,

$$\frac{\partial \mathbf{v}}{\partial t} + (\mathbf{v}\cdot\nabla)\mathbf{v} = -\frac{1}{\rho}\nabla p + \nu\nabla^2\mathbf{v} + \mathbf{g}, \tag{3.2}$$

with

$$\nabla \cdot \mathbf{v} = 0, \tag{3.3}$$

valid for an incompressible fluid (i.e. of constant density). By comparison, the NS equation (3.2) is clearly a generalization of the Euler equation (3.1), where an extra term proportional to the kinematic viscosity of the fluid (the ratio of viscosity and density) ν is included alongside a term $\mathbf{g}$ which represents external forces. This mathematical description is remarkably powerful and accounts for several phenomena, including realistic turbulent scenarios. One particular aspect that it captures is the transition from laminar to turbulent flows in a pipe (see Fig. 3), which was rigorously described for the first time in experiments in the late 19th century by the British physicist Osborne Reynolds. He understood that the onset of turbulence is intimately related to the interplay of viscous and inertial forces. Observing his own experiments, Reynolds noticed that turbulence was achieved for large values of a dimensionless velocity parameter

$$Re = \frac{vD}{\nu}, \tag{3.4}$$

nowadays known as the Reynolds number. This number can be regarded as an approximate ratio of inertial and viscous forces in the system, where v is the average velocity of the fluid in the pipe and D its diameter. Reynolds observed that when Re was a small number, meaning that viscous forces were dominant, the resulting flow was smooth and laminar. On the other hand, if Re was large, the well-behaved, laminar flow would eventually become unstable and a large number of interacting eddies of various sizes would start to appear in the system, characterizing turbulence. The Reynolds number captures an intrinsic instability of fluids dynamics described by the NS equation, and it is extensively applied to several practical examples. Therefore Reynolds' observations shed light on the importance of viscosity for classical turbulence, and can be considered as a another main qualitative feature of turbulent flows.

A third feature was conceptualized by the seminal work of Lewis Richardson in the 1920s,[43] when the important concept of energy cascade was introduced. At the time, Richardson knew that turbulence could be defined as a state of irregular, spatially and temporally disordered flow, involving a large number of degrees of freedom which are simultaneously excited and interact in a nonlinear fashion, as described by the NS equation. But he also realized that in order to describe this state of motion, one would need to look at its statistical properties. Richardson understood that in the simplest possible case of turbulence away from boundaries (i.e. a case which is much simpler than Reynolds' experiment) a statistical steady state requires a constant input of energy at large length scales and, at the same rate, the dissipation of energy by viscous forces at the small length scales. At intermediate length scales, in a so called *inertial range*, the transfer of energy from large to small eddies is independent of viscosity. This picture implies a *self-similar*

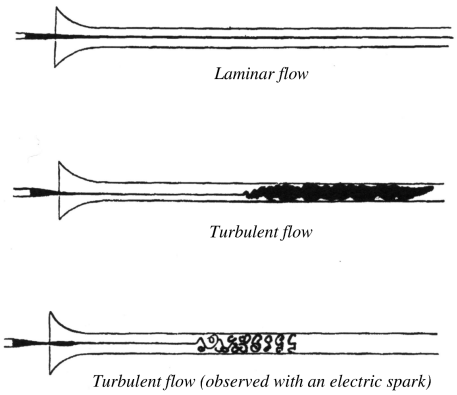

Figure 3 – Osborne Reynolds' original drawing of the observation on the different types of flow of water through a pipe. Reynolds quantified the different emergent flows of water by using the celebrated eponymous number Re.
Source: REYNOLDS.[42]

behavior of the eddies in the inertial range (larger eddies, breaking into smaller, identical eddies). This transfer is called the *energy cascade*.

Two decades later, the mathematician Andrei Kolmogorov[44] relied on Richardson's cascade picture and provided the first mathematically formal results known in turbulence. Kolmogorov was capable to analyse the turbulent flow patterns in terms of spectral properties and self-similarity, highlighting the importance of scaling laws in such systems. He assumed an idealized flow, where the fluid was supposed to be in a statistically homogeneous and isotropic steady-state (as also assumed by Richardson). In this hypothetical scenario, energy is injected in the system in a typical large scale D and flows to the smallest scales of the order of $\eta = (\nu^3/\varepsilon)^{1/4}$ (known as the Kolmogorov length scale, which represents the effective size of small eddies), where it is dissipated into heat. Within these two scales, the energy dissipation rate ε is assumed constant. Kolmogorov's idea was to connect these scales through this later assumption, which can be easily done with simple dimensional analysis. Recalling the quantities composing the Reynolds number Re (3.4), energy must be $\sim u^2$ and is injected in the form of large eddies in a scale D. A typical time-scale $\tau = D/u$ can be then associated with their dynamics. Therefore, the energy flux $\varepsilon \sim u^2/\tau = u^3/D$. Finally, substituting this last relation in the definition of η one must have that

$$\frac{D}{\eta} \approx Re^{3/4}, \tag{3.5}$$

which means that the Reynolds number can be interpreted as the available space for turbulence to develop, i.e. the size of the inertial range. Following these dimensional arguments, Kolmogorov suggested that a turbulent state has universal properties inside this range. One remarkable property in particular is that the distribution of kinetic energy over length scales is the same for all flows and does not depend on the fluid's specific nature. This means that inside the inertial range the microscopic particularity of a certain

system (i.e. how it dissipates energy in small scales) does not matter, which is translated in a well-defined power-law, shown in the following discussion.

Kolmogorov's work draws attention to the advantage of representing energy on spectral basis, where length scales r are associated with the inverse wavenumbers $k = |\mathbf{k}| = 2\pi/r$, and $\mathbf{k}$ is the three dimensional wavevector. Due to the statistical nature of turbulence it is convenient to define the three-dimensional Fourier transform of the averaged kinetic energy distribution as in

$$E^{(3D)}(\mathbf{k}) = \frac{1}{2(2\pi)^3}\int d\mathbf{r}\,\langle \mathbf{v}(\mathbf{x})\cdot\mathbf{v}(\mathbf{x}+\mathbf{r})\rangle\, e^{i\mathbf{k}\cdot\mathbf{r}}, \tag{3.6}$$

$$E_{\text{tot}} = \int d\mathbf{k} E^{(3D)}(\mathbf{k}) = \frac{1}{2}\langle \mathbf{v}(\mathbf{x})\cdot\mathbf{v}(\mathbf{x})\rangle, \tag{3.7}$$

where $\langle\cdots\rangle$ stands for the statistical average and E_{tot} for the total kinetic energy. If statistical isotropy of the velocity field $\mathbf{v}$ is assumed, $E^{(3D)}$ in fact depends only on the magnitude $k = |\mathbf{k}|$, then becoming a one-dimensional distribution through

$$E^{(1D)}(k) = 4\pi k^2 E^{(3D)}(k), \tag{3.8}$$

$$E_{\text{tot}} = \int_0^\infty dk\, E^{(1D)}(k). \tag{3.9}$$

Using this spectral representation and dimensional arguments, Kolmogorov showed that inside the inertial range, the kinetic energy spectrum of a turbulent flows scales as in

$$E(k) \equiv E^{(1D)}(k) = C\varepsilon^{2/3}k^{-5/3}, \tag{3.10}$$

where C is a dimensionless constant of order one. This is possibly the most celebrated result in classical turbulence and is known as Kolmogorov's law. In summary, it states that in homogeneous isotropic turbulence most of the energy is contained in the largest eddies (small k) and smaller eddies of size $r = 2\pi/k$ contain proportionally less energy. The direction of kinetic energy flow in k-space (from small to large k) defines a direct energy cascade.

All the above arguments apply to 3D flow. However, dimensionality plays an important role in turbulence, and dynamics in 2D (e.g. in soap films,[45] planetary atmospheres) differs dramatically from 3D. For instance, in 1967, Robert Kraichnan showed that in 2D turbulent flows kinetic energy does not cascade down from small to large k (as in 3D), but is rather in the opposite direction.[46–49] The same scaling $k^{-5/3}$ as for the direct cascade however is found [Eq. (3.10)]. This *inverse energy cascade* (IEC) is accompanied by a direct (forward) cascade of a second inviscid quadratic invariant – the enstrophy,

$$\mathcal{E} \equiv \int dS\,(\nabla\times\mathbf{v})^2, \tag{3.11}$$

which can be interpreted as a measure of vorticity variance, defined by the surface S integral on the xy plane - which makes the energy spectrum scale with k^{-3} for large momenta.

Lastly, another distinction which should be made when studying turbulence is its nature regarding forcing. Forced systems can exhibit the so-called *stationary turbulence* that requires a constant injection of energy and also removal of it at the same rate by dissipative mechanisms. However, in nature, a stationary turbulent system is destined to decay at a certain point, when the system is ceased to be forced. Although this frames a very distinct out-of-equilibrium scenario known as *decaying turbulence*, there are transient periods where similarities can be drawn with the idealized, stationary case.

3.2 Quantum turbulence is born

More than acknowledging the importance of the classical problem of turbulence,[50] Feynman was the first to propose the idea of a turbulent flow in superfluid helium in 1955,[1] suggesting that quantized vortices could interact and form a chaotic tangling. This concept influenced the low-temperature physics community of the time and developments by Hall and Vinen with liquid ^{4}He[51,52] eventualy led to the first experiments in the field of QT, pioneered by Vinen[53] in 1957. In those early experiments, the introduction of heat flux to a helium container induced mutual friction of the normal and superfluid parts (in the context of Landau's two-fluid model - see Sec. 2.5), forming a disordered configuration of vortex lines. Later on, the type of disordered state created by this *counter-flow* mechanism would be identified as *Vinen* or *ultraquantum* turbulence, as will be discussed in the following sections.

Feynman's initial concept is applicable to any quantum fluid (i.e. which exhibits the phenomenon of superfluidity), since it only depends on the properties of quantized vorticity. Therefore, the progress in understanding QT in liquid helium (^{4}He and ^{3}He) experiments[2,54] heavily motivated the extension of the field to other quantum liquids, such as atomic BECs. It was only in 2009 that the first experimental evidence[6] of quantum turbulence in trapped, dilute atomic Bose-Einstein condensates (BECs) was observed.

Although the definition of QT given by Feynman provides a qualitative picture of the problem, for a long period since the first experiments in the 60s, the term was loosely applied without proper definitions to specific cases. The more rigorous definitions came along with investigations that started to compare quantum turbulence with ordinary (classical) turbulence. The similarities and differences between both caused the field to branch out into several contexts, as shown in the schematic Fig. 4. A first distinction which should be made is regarding the structures taking part in the turbulent dynamics, whether vortices or waves. If one is dealing with vortices (as in Feynman's idea), the QT is said to be *hydrodynamic* (except for the case we are interested in waves over vortex lines, hence the Kelvin waves arrow in Fig. 4 – see Sec. 3.9). Depending on how quantized vortices orient themselves in the superfluid, either an average large-scale or a simple statistically random flow can be created, defining the particular cases of *quasi-classical* (Kolmogorov) or *ultraquantum* (Vinen) type of turbulence, respectively. However, similarly to classical

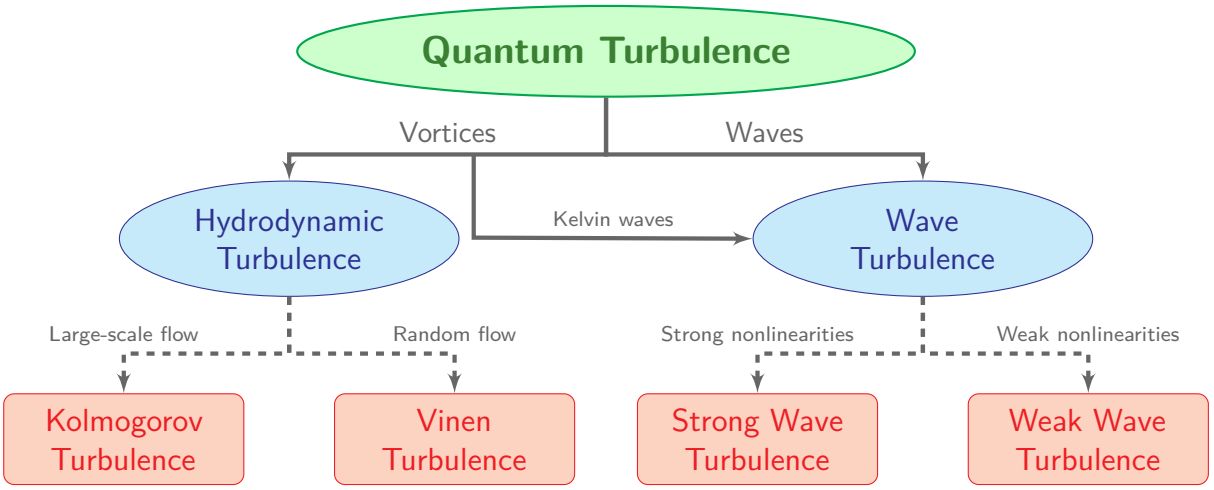

Figure 4 – The quantum turbulence branching scheme.
Source: By the author.

fluids, a quantum fluid can be compressible in nature (i.e. its density is not homogeneous) and the existing density waves can exhibit turbulent behavior through their nonlinear interactions (either strong or weak), characterizing the quantum version of *wave turbulence*. We present below a more detailed definition for each of these types of QT displayed in the scheme of Fig. 4.

At this point, we should further motivate the study of quantum turbulence, acknowledging it to be more than a mere scientific curiosity of the phenomenon's own complexity. The quantized nature of vortices in particular makes QT a "simplified" version of its classical counterpart, where vorticity is continuous. Vortices are clearly defined and simpler to detect in the former case:[55] they are zero-density lines of the quantum fluid, around which the quantum mechanical phase wraps by multiples of 2π. For this reason, many researchers have been attracted to the subject in the past decade, hoping that it may eventually help us develop analogies to better understand some unclear aspects of CT.

Even though the field of QT was born from the physics behind superfluidity in helium, in this thesis we are interested in the turbulence arising from ultracold quantum gases. While smaller systems (of the order of few μm) when compared to huge containers of liquid helium (of the order of meters), these atomic condensates are ideal testbeds for fundamental aspects of QT. In contrast to helium experiments, with atomic BECs virtually all parameters can be varied by large amounts by tuning the number of atoms, the confining trap, and the strength of the interactions. It should also be pointed out that our main interest will be the hydrodynamic (vortex) turbulence in BECs. Nevertheless, the relevance of wave turbulence to experiments with ultracold quantum gases will be briefly discussed throughout the text.

Since these atomic superfluids are successfully described by the mean-field Gross-Pitaevskii equation under many different contexts, we present next a theoretical connection

between this quantum model and what was previously discussed as being general aspects of CT.

3.3 Theoretical connection for BECs

Motivated by our discussion on classical turbulence in Sec. 3.1, we can ask ourselves: why should turbulence be expected in quantum fluids? The reason is not only associated with the presence of vortices in such systems. For the particular case of atomic BECs, it is intimately related to the dynamical equation that successfully governs their dynamics, the Gross-Pitaevskii equation (GPE). Although a crude approximation for superfluid helium, the mean-field theory for alkali BECs, instead, can be very accurate. Following the discussion on Subsection 2.2.1, we have seen that the GPE can be recast in the so-called hydrodynamical form (2.33), making use of the Madelung's transformation (2.27). Again, by identifying the velocity field of the superfluid with the gradient of the macroscopic wavefunction's phase S as in (2.31), we obtain*

$$\frac{\partial \mathbf{v}}{\partial t} = -\frac{1}{m\rho}\nabla p - \nabla\left(\frac{v^2}{2}\right) + \frac{1}{m}\nabla\left(\frac{\hbar^2}{2m\sqrt{\rho}}\nabla^2\sqrt{\rho}\right) - \frac{1}{m}\nabla V_{\text{trap}}, \tag{3.12}$$

where the fluid's density $\rho = |\psi|^2$ and a pressure-like term $p = \rho^2 g/2$ is conveniently defined.[17] The only term that depends on $\hbar$ in (3.12) is known as the *quantum pressure*, which has kinetic origin. In fact, it corresponds to the *zero-point* quantum mechanical motion and, since it depends on derivatives of the density, it is relevant only when the density of the fluid varies abruptly in space (for instance, close to vortex lines), being negligible otherwise.

One should notice the resemblance of this dynamical equation to that of a classical incompressible fluid described by the Euler equation (3.1). As a matter of fact, by making $\hbar \to 0$ the above equation becomes identical to the Euler equation for a classical irrotational fluid ($\nabla \times \mathbf{v} = 0$), which is the dissipation-free ($\nu = 0$) form the of the NS equation (3.2), with the identification of external forces $\mathbf{g}$ with the trapping potential force ∇V_{trap}. This resemblance indicates that the same nonlinearities present in the Euler equation (which we identified to be the skeleton of CT problems) are also present in quantum fluids that follow the GPE dynamics, therefore it being reasonable to expect turbulent behavior arising in such systems.

In reality, atomic BECs (and other quantum fluids) are not composed entirely of a condensed fraction, and thermal atoms are constantly interacting with it. Although these thermal effects can be sometimes negligible, for a more realistic description, a phenomenological dissipation can be modeled by including an imaginary term in the

* As already mentioned (see the footnote in Sec. 2.6), an often overlooked matter is that the chain rule for a multivalued field must be appropriately redefined,[32] otherwise a hydrodynamic formulation given by (3.12) is thus incomplete: it does not describe any vortex dynamics.

GPE,[56] making its time evolution complex substituting $t \to (i-\gamma)t$ (see Sec. 2.8). This is a simplified way to account for thermal effects from non-condensed atoms and the resulting damping. With this modification, the hydrodynamical form of the GPE (for an incompressible quantum fluid) corresponds then to a *quantum Navier-Stokes* equation

$$\frac{\partial \mathbf{v}}{\partial t} = -\frac{1}{m\rho}\nabla p - \nabla\left(\frac{v^2}{2}\right) + \frac{1}{m}\nabla\left(\frac{\hbar^2}{2m\sqrt{\rho}}\nabla^2\sqrt{\rho}\right) - \frac{1}{m}\nabla V_{\text{trap}} - \nu_q\nabla^2\mathbf{v}, \tag{3.13}$$

where $\nu_q \equiv \hbar\gamma/2m$[57] is the analogous (quantum) kinematic viscosity.

3.4 Energies of a BEC in momentum space

Associated with the GPE, we can write down the following total energy functional [Eq. (2.13)]

$$E = \int d^3r \left(\frac{\hbar^2}{2m}\left|\nabla\psi(\mathbf{r},t)\right|^2 + V_{\text{trap}}\left|\psi(\mathbf{r},t)\right|^2 + \frac{g}{2}\left|\psi(\mathbf{r},t)\right|^4\right), \tag{3.14}$$

which, after once again identifying the superfluid's density as ρ and velocity as $\mathbf{v}$, can be separated as a sum of different contributions as in $E = E_{\text{K}} + E_{\text{V}} + E_{\text{I}} + E_{\text{Q}}$. In this sum kinetic E_{K}, potential E_{V}, interaction E_{I}, and quantum E_{Q} parts[57,58] are determined according to

$$E_{\text{K}} = \frac{m}{2}\int d^3r\rho(\mathbf{r},t)\left|\mathbf{v}(\mathbf{r},t)\right|^2, \tag{3.15}$$

$$E_{\text{V}} = \int d^3r\rho(\mathbf{r},t)V_{\text{trap}}(\mathbf{r},t), \tag{3.16}$$

$$E_{\text{I}} = \frac{g}{2}\int d^3r\rho(\mathbf{r},t)^2, \tag{3.17}$$

$$E_{\text{Q}} = \frac{\hbar^2}{2m}\int d^3r\left|\nabla\sqrt{\rho(\mathbf{r},t)}\right|^2. \tag{3.18}$$

Here it is again clear that the energy owing to the zero-point motion E_{Q} goes to zero in the classical limit.

In our brief discussion of CT we have assumed that the classical fluid satisfied the incompressibility condition, Eq.(3.3). However, real fluids are typically compressible, and their velocity field can be separated into an incompressible (or solenoidal) part $\mathbf{v}_{\text{i}}$, with $\nabla\cdot\mathbf{v}_{\text{i}} = 0$, and an irrotational, compressible part $\mathbf{v}_{\text{c}}$, with $\nabla\times\mathbf{v}_{\text{c}} = 0$. (In fact, this can be performed to any vector field via Helmholtz decomposition.[59]) A similar separation can also be applied to a generic compressible superfluid system. It is convenient first to define the so-called *density-weighted velocity field*

$$\mathbf{w}(\mathbf{r},t) = \sqrt{\rho(\mathbf{r},t)}\mathbf{v}(\mathbf{r},t). \tag{3.19}$$

This field heals singularities in $\mathbf{v}$ caused by vortices for instance (the superfluid density goes to zero exactly at the point where the velocity field diverges) and allows for an analogy with the classical fluid velocity. Separating then $\mathbf{w}$ in its solenoidal $\nabla\cdot\mathbf{w}_{\text{i}}(\mathbf{r},t) = 0$ and

irrotational $\nabla \times \mathbf{w}_{\rm c}(\mathbf{r},t) = 0$ parts (see Appendix D), allows the kinetic energy $E_{\rm K}$ to be split in its compressible and incompressible parts[57]

$$E_{\rm K}^{\rm (i)} = \frac{m}{2}\int d^3r\,|\mathbf{w}_{\rm i}(\mathbf{r},t)|^2\,, \tag{3.20}$$

$$E_{\rm K}^{\rm (c)} = \frac{m}{2}\int d^3r\,|\mathbf{w}_{\rm c}(\mathbf{r},t)|^2\,, \tag{3.21}$$

$$E_{\rm K} = E_{\rm K}^{\rm (i)} + E_{\rm K}^{\rm (c)}, \tag{3.22}$$

which also have a simple representation in Fourier space

$$E_{\rm K}^{\rm (i,c)} = \frac{m}{2}\int d^3k\,|\tilde{\mathbf{w}}_{\rm i,c}(\mathbf{k},t)|^2\,, \tag{3.23}$$

$$\tilde{\mathbf{w}}_{\rm i,c}(\mathbf{k},t) = \frac{1}{(2\pi)^{3/2}}\int d^3k\,e^{i\mathbf{k}\cdot\mathbf{r}}\mathbf{w}_{\rm i,c}(\mathbf{r},t). \tag{3.24}$$

In classical turbulence, this kinetic energy separation means that the Richardson picture of big eddies decaying into smaller eddies should be looked for in the field with non-vanishing vorticity, i.e. the incompressible part of the velocity field. For the same reason, when dealing with vortex turbulence (our main interest in this thesis) we will be looking at the behavior of the incompressible velocity field.

It is crucial to highlight that even in a strict $T = 0$ description, i.e. in the absence of thermal atoms, where dynamics is simply determined by the standard GPE (2.15), vortex turbulence finds an effective dissipative mechanism through *vortex reconnections* (see Sec. 3.8). This means that, although the system is superfluid (and inviscid by its quantum nature), if one looks only to the rotation kinetic energy due to vortices, this can be lost in time and transformed into other forms of kinetic energy (related to waves), as will be further detailed.

3.5 Vortex (or hydrodynamic) turbulence

As anticipated before, when the manifestation of turbulence is hydrodynamic in nature in the sense that it requires a nontrivial velocity field (i.e. with singularities), containing quantized vortices, we call it vortex or hydrodynamic quantum turbulence. Analogously to the classical case, a one-dimensional (incompressible kinetic) energy distribution can also be defined for isotropically distributed $\tilde{\mathbf{w}}_{\rm i}(\mathbf{k},t)$ as in

$$E_{\rm i}\,(k,t) = \frac{m}{2}4\pi k^2\left\langle|\tilde{\mathbf{w}}_{\rm i}(\mathbf{k},t)|^2\right\rangle, \tag{3.25}$$

where the average $< ... >$ is performed over a shell of radius k in the 3D Fourier space. (For the sake of simplicity, note that we have dropped the index K used before to identify the kinetic energy.) Since the dynamics and interactions of quantum vortices are strongly nonlinear problems, analytical approaches are very restricted and almost all the literature on this subject relies mainly on numerical simulations to provide the spectral behavior of (3.25). The emergence of power laws in this quantity reveals relevant statistical signatures

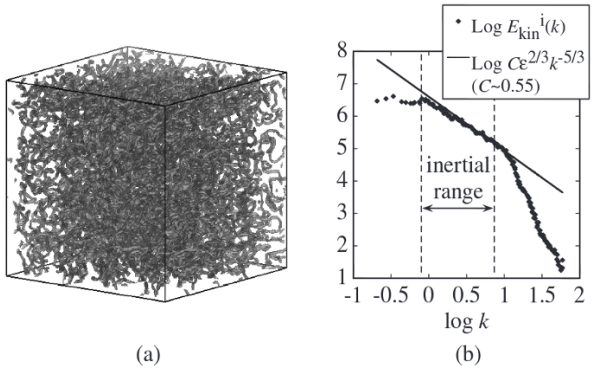

Figure 5 – (a) A typical vortex tangle. (b) Spectrum of the kinetic energy $E_{\rm kin}(k,t)$ as a function of the wavenumber k for a quantum turbulent gas. The plotted points are for an ensemble average of 50 randomly selected states. The solid line is the Kolmogorov $-5/3$ scaling.
Source: TSUBOTA.[60]

(as observed by Kolmogorov for the case of CT) that assists us in the definition of different types of QT.

Another quantity, whose temporal behavior is used to characterize the type of hydrodynamic turbulence, is the length of vortex lines L (vortex length per unit volume). This can be interpreted as a practical measure of the intensity of quantum turbulence, and is typically used in the context of decaying turbulence. From the knowledge of L, one estimates that the typical distance between the vortex lines is $\ell \approx L^{-1/2}$.

3.5.1 Kolmogorov (or quasiclassical) turbulence

High-accuracy numerical simulations of the GPE for initial states with random phase profile[61] (decaying vortex turbulence) were performed showing the existence of a Kolmogorov-like $k^{-5/3}$ power-law for $E_{\rm i}(k)$. This classical-like scaling suggests thus some similarity between the turbulent dynamics of $\mathbf{w}_{\rm i}(\mathbf{r},t)$ and the velocity field in incompressible Navier-Stokes equation, defining the *Kolmogorov* or *quasiclassical quantum turbulence*. In summary, its energy spectrum follows

$$E_{\rm i} \propto k^{-5/3}, \quad \text{for} \quad k \lesssim k_\ell \tag{3.26}$$

$$E_{\rm i} \propto k^{-3}, \quad \text{for} \quad k \gtrsim \xi^{-1}, \tag{3.27}$$

with ξ being the healing length and $k_\ell \equiv 2\pi/\ell$.

In analogy to CT, the first power-law (3.26) should indicate the existence of energy cascade from large to small length scales. This interpretation requires self-similarity throughout a long range of scales, which is believed to be provided by the process of *vortex bundling*. Large bundles transfer energy to smaller ones, in a process which goes down to the scale of single vortices. Further numerical investigations[62] determined that if the energy spectrum of the turbulent system obeys the Kolmogorov $k^{-5/3}$ scaling, the vortex tangle contains transient regions where the vortex lines are oriented in the same direction (vortex

bundles); the large scale flows generated by such parallel lines concentrate the energy in the small k region of the energy spectrum. Fig. 6 clarifies that such vortex bundles also contain many random vortex lines; in other words, the spatial polarization is only partial. However, although Kolmogorov energy spectra have been observed experimentally in superfluid helium,[4] there is yet no direct experimental observations of these vortex bundles.

The second scaling (3.27) arises from the universal characteristic of the velocity field profile of a vortex in a superfluid, therefore representing solely the internal structure of the quantized vortex core. It is also independent of dimensionality, thus the spectra for 2D systems with quantized vortices behave likewise for $k \gtrsim \xi^{-1}$, as we will discuss below.

Associated with this quasiclassical regime of turbulence is the temporal evolution of the total vortex length L which follows[62] $L \sim t^{-3/2}$.

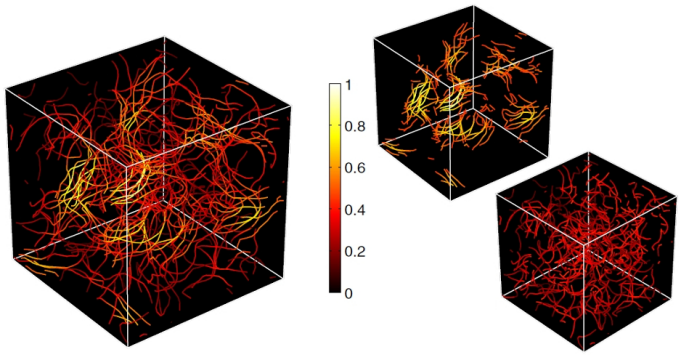

Figure 6 – Left panel: tangle of vortex lines computed in a periodic domain to model superfuid helium, analyzed in terms of the local vorticity. The vortex lines are locally colored according to the magnitude of the local 'coarse-grained' vorticity. Yellow (lighter color) corresponds to large vorticity ($\boldsymbol{\omega} > 1.4\omega_{rms}$), red (darker color) to small vorticity ($\boldsymbol{\omega} < 1.4\omega_{rms}$); in other words, the yellow lines are vortices which are part of a bundle of vortices which are all locally parallel to each other. Right panel: yellow and red lines plotted separately.
Source: BAGGALEY et al.[62]

This quasiclassical behavior in the low temperature limit is surprising, but can be understood if we recognize that the energy transfer responsible for the cascade arises from the key nonlinearity of the Euler equation, the $(\mathbf{v} \cdot \nabla)\mathbf{v}$ term (which reduces to ∇v^2 given the incompressible condition $\nabla \times \mathbf{v} = 0$). This result confirms the view that quantum turbulence contains the fundamental mathematical skeleton of classical turbulence.

3.5.2 Vinen (or ultraquantum) turbulence

Under other conditions, a different kind of turbulence called *ultraquantum* or *Vinen turbulence* has also been found both experimentally[63] and numerically,[64] characterized by random tangles of vortices without large-scale, energy-containing flow structures. In this case the energy spectrum does not build up for small k region. This randomness in the

orientation of quantized vortices (absence of bundling) makes the spectrum follow a k^{-1} power-law.[65] In summary then, the spectral features for the Vinen turbulence are

$$E_{\mathrm{i}} \propto k^{-1}, \quad \text{for} \quad k < \xi^{-1}, \tag{3.28}$$

$$E_{\mathrm{i}} \propto k^{-3}, \quad \text{for} \quad k \gtrsim \xi^{-1}. \tag{3.29}$$

When decaying, the Vinen turbulence is expected to follow the $L \sim t^{-1}$ temporal scaling for the total vortex length. This is the asymptotic behavior of the Vinen's equation, a phenomenological model which states

$$\frac{dL}{dt} = \alpha L^{3/2} - \beta L^2, \tag{3.30}$$

where α and β can be temperature dependent coefficients.[66]

3.6 The effect of reduced dimensionality

In contrast with their classical analogue, where assuming two-dimensionality is an approximation, quantum fluids can achieve a true two-dimensional limit (see end of Sec. 2.2.1). The quantized nature of quantum vorticity together with this lowering of dimensionality implies that the properties of the vortex line are no longer relevant for dynamics. The one-dimensional (line) vortex now becomes an almost zero-dimensional (point) vortex in the plane, with well defined positive or negative circulation charges whether vortex or anti-vortex, respectively. In the context of hydrodynamic turbulence, these point-like (instead of line-like) vortices interact with each other following complicated dynamics dictated by the 2D GPE (2.21), where tangling and reconnections are now replaced by vortex-antivortex annihilation processes. In these events, two vortex cores can coalesce and annihilate [Fig. 7(a)], evolve into a solitary wave [Fig. 7(b)] and eventually disappear as atoms fill up the empty space [Fig. 7(c)]. In Sec. 3.1 we mentioned that 2D classical turbulence (2DCT) is very different from the 3D case and presents interesting features, such as the inverse energy and enstrophy cascades. In the quantum scenario the contrast is also present and the search for similar startling characteristics in quantum fluids has been intense.

Our previous definitions of Kolmogorov and Vinen regimes of vortex turbulence for 3D systems are also suitable for 2D, provided that one adjusts the concept of vortex bundling to that of *vortex clustering* as being the process which introduces large-scale flow. This clustering happens when, under appropriate forcing in small scales, it becomes energetically favorable for vortices of the same sign of circulation to gather, forming clustered structures which may vary in size. This effect was predicted for idealized 2D classical turbulent systems by the *vortex gas* theory of Onsager (in which classical vortices were modeled as points) and was recently applied to quantum fluids.[67] An interesting interpretation of such theory is that clustering represents a phase transition for a certain

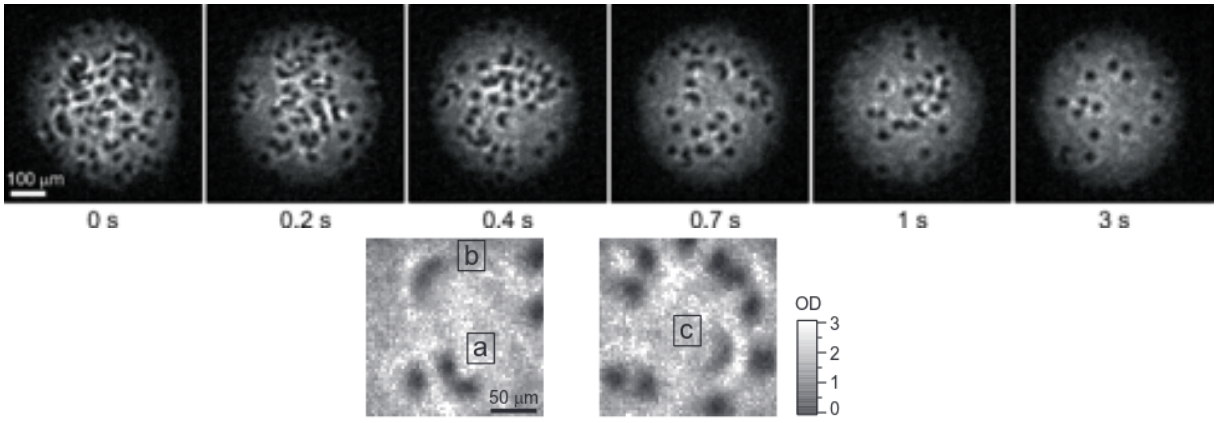

Figure 7 – Vortex annihilation as a mechanism of turbulence relaxation. In a recent experiment[10] a large number of vortices has been created in an oblate condensate of 10^6 sodium atoms by rapidly sweeping a transverse laser across the gas. Upper panel: Sequence of absorption images where the number of vortices is seen to decrease in time according to Eq. (3.31). Lower panel: detail of vortex-antivortex annihilation that assists the relaxation of the turbulent gas.
Source: KWON et al.[10]

distribution of vortices associated with a negative-temperature state (see Fig. 8). An effective temperature T can be defined in terms of the entropy $S \equiv E/T$ of a particular vortex configuration with (incompressible kinetic) energy E. As opposed to an arrangement where vortex dipoles (pairs composed of a vortex plus an anti-vortex close together) are formed and annihilations are highly probable (see left region of the schematic plot in Fig. 8), the clustering, also known as Onsager condensation, tends to suppress annihilations. The effective temperature of such configuration is negative and is the key signature of an inverse energy cascade in turbulent systems, since clustering processes represent transfer of incompressible energy from small to larger scales.

3.6.1 Kolmogorov turbulence in 2D

Several numerical studies on 2D homogeneous superfluids[57,68,69] have explored the emergence of the quasiclassical regime, where the incompressible kinetic energy spectrum was shown to follow the same features as in 3D, namely Eqs. (3.26) and (3.27). A typical spectrum is qualitatively illustrated in Fig. 9 for a system forced in small scales $k_{\mathrm{F}} \sim \xi^{-1}$. The first power-law (3.26) is clearly the Kolmogorov scaling for large spatial scales in the system, which is here associated with an inverse energy cascade (IEC) through vortex clustering. The universal scaling (3.27) in this 2D context raises a puzzle, however: as discussed for 2DCT, enstrophy [Eq. (3.11)] exhibits a direct cascade which accompanies the IEC and also, in that case, scales as k^{-3}. But in order to reveal a cascade, a physical quantity (being it energy or enstrophy) should be inviscid (conserved) for a particular inertial range. Nevertheless, in superfluids, the quantized nature of circulation makes enstrophy to be proportional to the total number of vortices[57,70] and hence the possibility

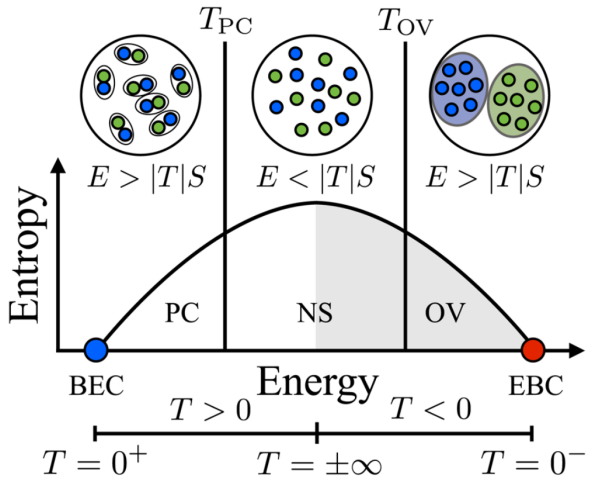

Figure 8 – Negative-temperature and Onsager condensation. The scheme shows the behavior of entropy for a point vortex model as a function of temperature. As temperature decreases and reaches negative values, the system passes through a phase-transition where vortex clustering, a coherent Onsager vortex (OV) state, becomes favorable against vortex dipoles and unbound vortices. For $T = 0^+$ a zero-entropy Bose-Einstein condensate (BEC) is present. Its negative temperature counterpart ($T = 0^-$) is an Einstein-Bose condensate (EBC). At $T = \pm\infty$ entropy is a maximum and the vortex distribution is said to be in a entropy dominated normal state (NS). The vortex binding-unbinding phase transition separates this normal state from the pair collapse (PC) state at positive temperature.
Source: SIMULA et al.[67]

of vortex-antivortex annihilations may force enstrophy not to be an inviscid quantity in quantum fluids. For this reason, both the conservation and even the meaning of enstrophy in such systems are still open debates in the field.[68,71] Furthermore, the direct enstrophy cascade in superfluids may exist, but might also be disguised by the identical scaling behavior due to the vortex core properties coexisting in the same range of k-space.

3.6.2 Vinen turbulence in 2D

Again, the spectrum for the Vinen turbulence regime in 2D coincides with the 3D counterpart of random flow, following then (3.28) and (3.29).

Recent experimental and numerical[10,30,72,73] efforts have been focusing on understanding the decay of Vinen turbulence in 2D (and also aiming at an eventual extension to the Kolmogorov regime, still unexplored). One of them,[10] in particular, performed experiments with a sodium gas confined in a quasi-2D trap that was brought to a turbulent state by sweeping a repulsive laser beam of Gaussian shape through its center. After producing ~ 60 vortices, the repulsive laser beam was turned off. The number of vortices N as function of time was observed to decay non-exponentially. A phenomenological description [analogous to the 3D Vinen's equation (3.30)] was thus proposed by means of

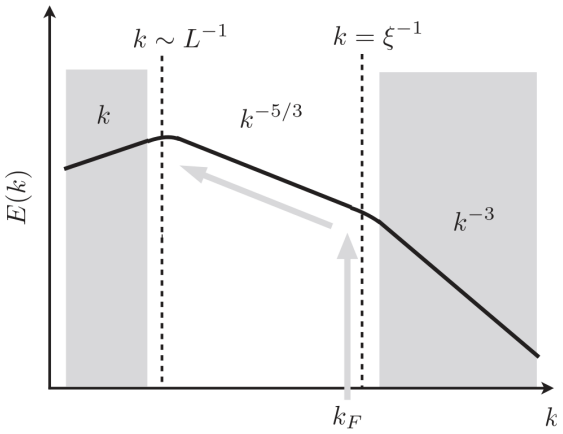

Figure 9 – Qualitative picture of the incompressible kinetic energy spectra for a 2D system. The k^{-3} part of the spectrum appears due to the structure of the vortex core while the k region pertains to distances larger than the largest intervortex distance L and has no net vorticity. The nonshaded region is the inertial range where Kolmogorov scaling $k^{-5/3}$ manifests and k_F is forcing scale, where energy is injected.
Source: BRADLEY et al.[57]

a rate equation given by

$$\frac{dN}{dt} = -\Gamma_1 N - \Gamma_2 N^2, \tag{3.31}$$

with Γ_1 and Γ_2 real, positive parameters, attributed to one-body and two-body losses. The decrease in the number of the vortices is seen in the first panel of Fig. 7. The crescent shapes (see lower panel of Fig. 7) observed in the experiments are visualizations of vortex-antivortex collisions, culminating in annihilations; such processes give rise to the two-body term in Eq. (3.31). This rate equation was in principle regarded to be universal. However, we anticipate that one of our focus on this thesis was not only to investigate this claim, but also to suggest modifications to (3.31) as detailed in Chapter 4.

3.7 Vortex turbulence in trapped BECs

Now that we have defined the different regimes of quantum vortex turbulence, we need to realistically face the question of what kind of vortex turbulence we are witnessing in nowadays trapped systems.

To answer this classification problem, we must look at the ratio L/ξ, which quantifies the available space for turbulence development. L is the typical largest scale of the system (e.g. size of a helium container or extension of the trap for an atomic superfluid) and ξ is the healing length, which sets the approximate size of the vortex core. A large value of L/ξ enables the occurrence of self-similarity throughout several scales, increasing thus the inertial range. For a quantum system to exhibit quasiclassical spectral characteristics (Kolmogorov scaling), a relatively large ratio is necessary and the quantity $\log(L/\xi)$ roughly tells us how many decades are available between ξ and L for this to happen. In that sense,

systems with small ratio present few decades [$\log(L/\xi) \approx 1$ or 2]. This is an intrinsic spatial limitation that may hinder the formation of large-scale, self-similar structures. Experiments involving superfluid He show $\log(L/\xi) \approx 4$ and this number justifies why both quasiclassical and ultraquantum limits could be easily observed.[4] In contrast, current experiments with atomic BECs display 1 to 2 decades and the observation of complicated vortex tangle dynamics in such relatively small-ratio systems[6] typically shows evidence of Vinen (ultraquantum) turbulence. In fact, this regime has been extensively explored in the context of superfluid helium and only recently has it been truly investigated in the context of the GPE and atomic BECs.[74,75] In Chap. 5 we describe our contribution to the identification of this regime in realistic, numerically simulated trapped BECs.

3.8 Effective dissipation in waves

As already mentioned above, although quantum fluids are by definition inviscid, there can be an effective viscosity, even in an idealized $T = 0$ model. Although total energy is conserved (in the absence of thermal excitations), incompressible kinetic energy E_i can be converted to compressible E_c. As discussed before, the former is mainly associated with vortex dynamics, and the diminishing of E_i in favor of E_c can be seen as vortex energy dissipation. Physically, this happens through wave-like density excitations (e.g. phonons) interacting with (or even being generated by) vortices.[76] Oscillating vortices can create phonons which, by energy conservation, reduce their (incompressible) kinetic energy from the scale of the vortex-core size to larger system-wide scales.[77] Similar phonon emissions can happen in processes of vortex reconnections (when vortex lines overlap in space) or vortex-line wave excitations (Kelvin waves) propagating on a vortex.[78] This energy coupling can be bidirectional and even oscillations between compressible and incompressible energies are possible.[58] This emergent effective dissipation mechanism – present in conservative systems as well – is not to be confused with the dissipation caused by the presence of thermal particles (see Sec. 2.8).

3.9 Wave turbulence in BECs

As we have anticipated, in addition to the hydrodynamic turbulence, waves can interact nonlinearly in a BEC and eventually give rise to wave turbulence (WT). Structures analogous to eddies in hydrodynamic turbulence are created and energy cascades thus appear with power-laws in the energy spectrum.[79] When the nonlinearities are weak, analytic investigations[80,81] are possible and nearly all the properties associated with the stationary turbulent states can be obtained from the knowledge of wave dispersion relations, where lowest order nonlinear terms are taken into account. Although this regime is very approximate if compared with real-life experiments, it provides qualitative insights into more complex nonlinear dynamics.

WT typically coexists in an experiment with the hydrodynamic quantum turbulence. In a sense it is "more classical" than the turbulence associated with vortices, but it is intimately related to the excitation spectrum of a BEC.

Notice that we have qualitatively made a distinction between quantized vortex turbulence and wave turbulence (see Figure 4). In reality, vortex lines can exhibit a sort of wave turbulence coming from *Kelvin waves*, which are vibrations over the vortex extension that can appear from large (comparable to intervortex distances $k \sim k_\ell$) to scales much smaller than the hydrodynamic scales ($k \gtrsim 1/\xi$).

Since it is not the central subject in this thesis, WT theory is only briefly reviewed here to support prospective results to be presented in Sec. 5.3. We also focus our attention in the so-called weak-wave turbulence (WWT) regime, which can offer analytical results on scalings. For a complete discussion on the matter (including strong-wave turbulence) see Nazarenko's review book on the subject.[80]

3.9.1 Phonon turbulence

In the last chapter (see Sec 2.5.2) we have seen that sound waves, or phonons, are small amplitude excitations $\delta\psi(\mathbf{r},t)$ over the background macroscopic wavefunction $\psi(\mathbf{r},t)$. We have assumed there that this wavefunction for the homogeneous BEC could be written as $\psi(\mathbf{r},t) = \left[\sqrt{\rho_0} + \delta\psi(\mathbf{r},t)\right] e^{-\frac{i\mu}{\hbar}t}$ (with $\mu = g\rho_0$ being the chemical potential) and we have restricted ourselves to linear perturbations. Now, however, we are interested in analyzing small nonlinearities, thus we will keep second-order terms in $\delta\psi$ when substituting ψ in Eq. (2.15). In this way we get

$$i\hbar\frac{\partial\delta\psi}{\partial t} = -\frac{\hbar^2}{2m}\nabla^2\delta\psi + g\rho_0\left(\delta\psi + \delta\psi^*\right) + g\sqrt{\rho_0}\left(2\delta\psi^*\delta\psi + \delta\psi^2\right), \tag{3.32}$$

instead of (2.36). In Fourier representation, the above equation becomes

$$\begin{aligned} i\hbar\frac{d\delta\psi\left(\mathbf{k}\right)}{dt} &= \frac{\hbar^2k^2}{2m}\delta\psi\left(\mathbf{k}\right) + g\rho_0\left[\delta\psi\left(\mathbf{k}\right) + \delta\psi^*\left(\mathbf{k}\right)\right] \\ &+ \frac{g\rho_0}{\left(2\pi\right)^{3/2}}\int d\mathbf{k}_1\int d\mathbf{k}_2[\delta\left(\mathbf{k}-\mathbf{k}_1-\mathbf{k}_2\right)\delta\psi\left(\mathbf{k}_1\right)\delta\psi\left(\mathbf{k}_2\right) \\ &+ 2\delta\left(\mathbf{k}+\mathbf{k}_1-\mathbf{k}_2\right)\delta\psi^*\left(\mathbf{k}_1\right)\delta\psi\left(\mathbf{k}_2\right)]. \end{aligned} \tag{3.33}$$

At this point, the Bogoliubov transformation again is quite useful. It can be cast in the following form

$$\delta\psi\left(\mathbf{k}\right) = \frac{1}{2\sqrt{\rho_0}}\left(i\frac{\sqrt{\omega(k)}}{k} + \frac{k}{\sqrt{\omega(k)}}\right)a\left(\mathbf{k}\right) - \frac{1}{2\sqrt{\rho_0}}\left(i\frac{\sqrt{\omega(k)}}{k} - \frac{k}{\sqrt{\omega(k)}}\right)a^*\left(-\mathbf{k}\right), \tag{3.34}$$

convenient to analyze plane-wave solutions and their nonlinear corrections.[80,82] The function $\omega(k) = \sqrt{\frac{k^2}{2m}\left(\frac{k^2}{2m} + 2\mu\right)}$ is the dispersion relation for the linear problem (2.45). In this way,

the equation of motion for $a(\mathbf{k})$ can be obtained, and is given by

$$\begin{aligned} i\hbar\frac{da\,(\mathbf{k})}{dt} &= \omega(k)a\,(\mathbf{k}) \\ &+ \int d\mathbf{k}_1 \int d\mathbf{k}_2 V\,(\mathbf{k};\mathbf{k}_1,\mathbf{k}_2)\,[\delta\,(\mathbf{k}-\mathbf{k}_1-\mathbf{k}_2)\,a\,(\mathbf{k}_1)\,a\,(\mathbf{k}_2) \\ &+ 2\delta\,(\mathbf{k}+\mathbf{k}_1-\mathbf{k}_2)\,a^*\,(\mathbf{k}_1)\,a\,(\mathbf{k}_2)], \end{aligned} \tag{3.35}$$

where the quantity $V(\dots)$ is the interaction coefficient and depends on the interaction parameter g.

From the solution of (3.35) one can write the occupation number $n(\mathbf{k}) = |a(\mathbf{k})|^2$. Thus the total energy (which is mainly kinetic in weak interacting case) can be calculated from

$$E_{\text{tot}} = \int d^3k\,\omega(k)\,n(\mathbf{k}) = \int_0^\infty dk\,E(k), \tag{3.36}$$

where $E(k)$ is the one-dimensional energy spectrum.

The V-dependent terms inside the integral in Eq. (3.35) describe the *three-wave interactions*. The first term corresponds to the decay of two waves into one ($k_1 + k_2 \to k$) while the second term corresponds to the opposite process ($k + k_2 \to k_1$). According to the statistical theory of out-of-equilibrium waves,[80,81] such three-wave processes allow the existence of a steady state characterized by a direct energy cascade. Indeed the power-law distribution associated with the energy spectrum of the steady-state turbulent system can be entirely determined from the scaling properties of the dispersion relation and the interaction coefficient. For the particular case of long wavelength, i.e. phonon-like dispersion [$\omega(k) \approx ck$] and the BEC background is considerably strong ($\mu \gg \hbar^2k^2/2m$), the interaction coefficient scales as $V(k_1,k_2,k_3) \sim \sqrt{k_1k_2k_3}$. As a consequence, the energy spectrum displays the power-law behavior

$$E(k) \sim k^{-3/2}, \tag{3.37}$$

which is known as a Kolmogorov-Zakharov type of spectrum, due to its direct analogy with Kolmogorov type of spectra for classical hydrodynamic turbulence[80] – they both correspond to stationary cascade solutions, arising due to the existence of conserved quantities. This particular scaling is known as Zakharov-Sagdeev power-law.[83]

Associated with this Kolmogorov type of spectrum, one can obtain the density spectrum. At this point, for the particular case of strong condensate, the few analytical results in the literature seem contradictory. Following the WWT formalism, Fujimoto et al.[79] find that

$$n(k) \sim k^{-7/2}, \tag{3.38}$$

concluding that the scaling

$$n(k) \sim k^{-3/2}, \tag{3.39}$$

obtained by Proment et al.,[84] was incorrect.

In a recent experiment, Navon et al. find $n(k) \sim k^{-7/2}$ for an excited BEC in a box-like potential, while claiming that the expected scaling is $n(k) \sim k^{-3}$ [as opposed to (3.38)] for a sound-wave cascade, referencing analytical results from Zakharov.[81] However, the k^{-3} is a very particular case of Zakharov's discussion on Kolmogorov (scale-invariant isotropic) turbulence [see Eq. (9.22) in Nazarenko's review book[80]], in which the interaction coefficient is a particular homogeneous function that satisfies $V(\lambda k_1, \lambda\beta k_2, \lambda\beta k_3) = \lambda^\beta V(k_1, k_2, k_3)$ with $\beta = 0$ (β is known as the homogeneity degree). This is clearly not satisfied for the above-considered Zakharov-Sagdeev case. An early experiment by our group has obtained the scaling $n(k) \sim k^{-2.9}$ for experiments on excited harmonically trapped BECs.[85] Therefore, the mechanisms and a complete understanding of the statistical properties of waves and vortices (and how they affect each other) can be considered as an open problem.

3.9.2 Kelvin waves: waves on a vortex line

Another WT process that can occur in BEC is associated with the vibratory motion of vortex lines and vortex loops, the so-called Kelvin waves. The first WT theory for this system was formulated by Kozik and Svistunov.[86] In such a formulation, the relevant interaction term involves 6-wave processes. Two different cascade processes can simultaneously occur within a WT system led by N-wave interactions,[80] with N being an even number. A direct energy cascade is present, where the energy density in Fourier space $[\omega(k)n(k)]$ flows from large to small length scales. In addition to this, there can also be an inverse *wave action* $n(k)$ cascade. Such dual cascades have close analogies with the energy/enstrophy dual cascade in hydrodynamic turbulence.

In the Kozik-Svistunov theory, the dispersion relation, neglecting logarithm factors, is $\omega(k) \sim k^2$, which leads to the direct energy cascade spectrum

$$E(k) \sim k^{-7/5}, \tag{3.40}$$

while the inverse wave action spectrum is given by[86]

$$E(k) \sim k^{-1}. \tag{3.41}$$

The above results follow from a three-wave approach. It is worth mentioning that the Kelvin-waves excitation spectrum was also studied in the formalism of four-wave turbulence[87] and shown to exhibit a spectrum

$$E(k) \sim k^{-5/3}, \tag{3.42}$$

which should in fact replace Eq. (3.40), which may explain some confusion on the appearance of Kolmogorov scaling in numerical simulations of the GPE in small systems (see Sec. 5.3).

As mentioned before, rapidly rotating Kelvin waves of very short wavelength are created by wave interactions (a process called the Kelvin wave cascade[54,88]), which, if their

wavelength is short enough, emit phonons; the sink of turbulent kinetic energy is acoustic rather than viscous.

4 TWO-DIMENSIONAL TURBULENCE

In this chapter we present our results on simulations of a highly multicharged (giant) quantum vortex decaying in a two-dimensional (2D) harmonically trapped BEC.

In Sec. 4.1, one finds attached the publication where we detail a protocol to explore a giant vortex dynamical instability in order to generate a polarized turbulent scenario. This system is then used to investigate the validity of the phenomenological decay rate equation [Eq. (3.31)] for the number of vortices. An appropriate modification to Eq. (3.31) is thus proposed, after verifying that it does not capture the behavior of our polarized system. An important lead to this modification was that vortices (in this harmonically trapped system) annihilate through a four-body (instead of two-body) process.

In the subsequent Sec. 4.2, we provide supplementary material to the paper describing in more detail the initial state preparation, comparing one of the methods used to alternative two-dimensional numerical solution, where axial symmetry is imposed in the GPE. We then show that, in the absence of any perturbing potential, the giant vortex solution decays driven by a quadrupolar unstable mode.

Finally, in Sec. 4.3 we describe an application prospect to the study of such a giant vortex decay in 2D BECs. By considering few naive phenomenological dissipative models we observe considerably distinct after-split dynamics for each model. Our preliminary results suggest that this system could be used to confront different, more realistic, finite-temperature models predictions.

4.1 Paper: Controlled polarization of 2DQT in atomic BEC

PHYSICAL REVIEW A **93**, 033651 (2016)

Controlled polarization of two-dimensional quantum turbulence in atomic Bose-Einstein condensates

A. Cidrim,[1,2] F. E. A. dos Santos,[3] L. Galantucci,[2] V. S. Bagnato,[1] and C. F. Barenghi[2]

[1]*Instituto de Física de São Carlos, Universidade de São Paulo, Caixa Postal 369, 13560-970 São Carlos, São Paulo, Brazil*

[2]*JQC (Joint Quantum Centre Durham-Newcastle) and School of Mathematics and Statistics, Newcastle University, Newcastle upon Tyne, NE1 7RU, United Kingdom*

[3]*Departamento de Física, Universidade Federal de São Carlos, 13565-905, São Carlos, SP, Brazil*

(Received 11 July 2015; revised manuscript received 18 January 2016; published 30 March 2016)

We propose a scheme for generating two-dimensional turbulence in harmonically trapped atomic condensates with the novelty of controlling the polarization (net rotation) of the turbulence. Our scheme is based on an initial giant (multicharged) vortex which induces a large-scale circular flow. Two thin obstacles, created by blue-detuned laser beams, speed up the decay of the giant vortex into many singly quantized vortices of the same circulation; at the same time, vortex-antivortex pairs are created by the decaying circular flow past the obstacles. Rotation of the obstacles against the circular flow controls the relative proportion of positive and negative vortices, from the limit of strongly anisotropic turbulence (almost all vortices having the same sign) to that of isotropic turbulence (equal number of vortices and antivortices). Using this scheme, we numerically study the decay of two-dimensional quantum turbulence as a function of the polarization. Finally, we present a model for the decay rate of the vortex number which fits our numerical experiment curves, with the novelty of taking into account polarization time dependence.

DOI: 10.1103/PhysRevA.93.033651

I. INTRODUCTION

The study of quantum turbulence is heavily motivated by liquid helium (^{4}He and ^{3}He) experiments [1,2]. A striking discovery has been that, under appropriate forcing, quasiclassical behavior arises displaying statistical properties characteristic of ordinary turbulence; an example is the celebrated Kolmogorov $-\frac{5}{3}$ scaling of the energy spectrum [3] which suggests the existence of a classical energy cascade from large to small length scales. Under other conditions, a different kind of turbulence (called "ultraquantum turbulence" or "Vinen turbulence") has also been found [4,5], characterized by random tangles of vortices without large-scale, energy-containing flow structures. Quantum turbulence experiments are also performed in atomic Bose-Einstein condensates [6–9]; the relative small size of these condensates (compared to flows of liquid helium or of ordinary fluids) limits the study of scaling laws but offers opportunities to study minimal processes that also take place in larger systems (e.g., vortex interactions, vortex reconnections, vortex clustering) with greater experimental controllability and more direct visualization than in liquid helium.

Atomic condensates are also ideal systems to study two-dimensional (2D) turbulence [10], a problem with important applications to oceans, planetary atmospheres, and astrophysics. In classical systems, reduced dimensionality may arise from strong anisotropy, stratification, or rotation (via the Taylor-Proudman theorem). From the physicist's point of view, the dynamics of 2D turbulence is very different from three dimensional (3D) [11]. The existence (besides the kinetic energy) of a second inviscid quadratic invariant, the enstrophy, implies that a downscale enstrophy transfer is accompanied by an upscale energy cascade; in other words, in 2D turbulent flows the energy flows from small to large length scales rather than vice versa as in 3D turbulence. With the possible exception of soap films [12], 2D flows which can be created in the laboratory are only approximations. However, using suitable trapping potentials, atomic condensates can be easily shaped so that vortex dynamics is 2D rather than 3D. Unlike liquid helium, in atomic condensates 2D quantum vortices can be directly imaged, and, unlike classical systems, the motion of such 2D vortices is not hindered by viscous effects or friction with the substrate.

Several works have explored the generation of turbulence in 2D condensates. The 2D energy spectrum and scaling laws have been computed in numerical simulations [13–15], and the problem of what should be the quantum analog of the classical enstrophy has been raised. In Ref. [9], vortices were nucleated by small-scale stirring of a laser spoon, after which a persistent current was verified both experimentally and through numerical simulations, suggesting transfer of incompressible kinetic energy from small to large length scales. Emergence of large-scale order from vortex turbulence was also observed [16] as predicted by the "vortex gas" theory of Onsager. A similar setup was used to explore vortex shedding and annihilation processes in both experiments [17,18] and simulations [19]. The effect of stirring laser beams with different shapes or along different paths was investigated in Refs. [20–23]. However, in all cases cited, vortices have always been generated in such a way that the number of positive and negative vortices is approximately the same; in other words, all vortex configurations which have been investigated had approximately zero polarization. Since irrotational flow is a hallmark property of superfluidity, the polarization of the vortex configuration (i.e., the relative proportion of positive and negative vortices) plays the role of net rotational angular velocity Ω of a classical fluid, so it is important to explore its effects on the properties of turbulence.

In this work, we propose a scheme for generating 2D quantum turbulence in atomic condensates. Our scheme, which is based on a giant vortex as the initial state, is control over polarization of the turbulence, which can be interpreted as the

classical rotation of the entire flow. One of the most important properties of turbulence is its decay because the growth of the turbulence or its character in a steady state may depend on how it is forced, whereas the decay is an intrinsic property of the dynamics. We shall report the decay of 2D quantum turbulence as a function of the polarization.

II. GIANT VORTEX AND SMALL PINS

Multicharged vortices with circulations as large as 60 quanta have already been produced in condensates using dynamical methods, as consequences of rapid rotations of the confining trap [24]. Another route to achieve these highly excited states is using phase-engineering techniques, such as those described in Refs. [25–28]. In these cases, quanta of angular momentum are added to the condensate by adiabatically inverting the direction of the magnetic bias field which composes the usual Ioffe-Pritchard magnetic trap. To date, only charges below 10 quanta were produced using their proposed setups. However, an improvement on the method, known as the "vortex pump," has been described in Refs. [29–31]. In practical terms, a hexapole magnetic field is superposed to the Ioffe-Pritchard magnetic trap, allowing vorticity to be cyclically pumped into the condensate, thus generating giant vortices. Progress in this direction has been made in recent experiments with synthetic magnetic monopoles [32].

A giant vortex at the center of a harmonically trapped condensate can be described by a single-particle wave function of the form $\psi(\mathbf{r}) = f(r)e^{i\kappa\phi}$, where $f(r)$ is the wave function's amplitude, $\mathbf{r} = (r,\phi,z)$ is the position in cylindrical coordinates, and a large winding number κ corresponds to a large angular momentum. Such giant vortices are dynamically unstable [30,33], and split into singly quantized ($\kappa = 1$) vortices. Being parallel to one another, these singly quantized vortices impose a strongly azimuthal flow to the condensate. During the following evolution, some vortices of the opposite polarity may be generated by occasional large-amplitude density waves, but these events are rare, and do not change the main property of the flow resulting from the decay of a giant vortex configuration: the strong polarization of the vorticity (almost all vortices have the same sign).

The scheme that we propose uses blue-detuned lasers [18] to perturb this initial state with two diametrically opposite laser beams, creating thin obstacles (which we refer to as pins) with width σ of the order of magnitude of the healing length ξ (two pins are enough to homogenize the vortex distribution). The pins perturb the initial giant vortex, accelerating its decay; they also deflect the large azimuthal flow, generating vortex-antivortex pairs [19,34–36]. To control the effect of the pins, we move them at constant angular velocity ω in the direction opposite to the main azimuthal flow.

III. MODEL

The dynamics of our system is dictated by the 2D Gross-Pitaevskii equation (GPE). We introduce dimensionless variables based on the trapping potential of frequency ω_0, measuring times, distances, and energies in units of $\omega_0^{-1}, \sqrt{\hbar/m\omega_0}$, and $\hbar\omega_0$, respectively, where m is the mass of one atom and $\hbar$ is the reduced Planck's constant. The resulting dimensionless GPE is

$$i\frac{\partial\psi}{\partial t} = \left(-\frac{1}{2}\nabla^2 + V + C|\psi|^2 - \mu\right)\psi, \qquad (1)$$

where the time-dependent wave function $\psi(\mathbf{r},t)$ is normalized so that $\int|\psi|^2 d^2r = 1$. The external potential is $V(\mathbf{r},t) = V_{\rm trap}(\mathbf{r}) + V_{\rm pins}(\mathbf{r},t)$, where $V_{\rm trap}(\mathbf{r}) = (x^2+y^2)/2$ and $V_{\rm pins}(\mathbf{r},t) = V_+(\mathbf{r},t) + V_-(\mathbf{r},t)$ represent, respectively, the trapping potential which confines the condensates and the pins which perturb the initial giant vortex. The terms $V_\pm(\mathbf{r},t) = V_0\exp\{-|\mathbf{r}-\mathbf{r}_\pm(t)|^2/2\sigma^2\}$ with $\mathbf{r}_\pm(t) = [\pm x_0\cos(\omega t), y_0\sin(\omega t)]$ are diametrically opposite, thin, Gaussian potentials of width $\sigma = \xi$ which rotate clockwise (against the flow of the initially imposed giant vortex) at constant angular velocity ω. The quantity $C = 2\sqrt{2\pi}N(a/a_z)$ parametrizes the two-body collisions between the atoms, where N is the total number of atoms, a the scattering length, and a_z the axial harmonic oscillator's length; we choose $C = 17\,300$. The chemical potential μ is introduced to guarantee normalization of the wave function, and the amplitude of the pins is $V_0 \approx 1.43\mu$. In homogeneous systems ($V = 0$) the healing length is found by balancing kinetic and interaction energies terms in the GPE. In a harmonically trapped condensate, the healing length can be defined with reference to the density at the center of the trapped condensate in the absence of any vortex or hole. In our dimensionless units, we obtain $\xi \approx 0.13$, and $r_{\rm TF} \approx 74\xi$ for the Thomas-Fermi radius.

Our choice of dimensionless parameters corresponds to typical [17,18] experiments with ^{23}Na condensates (scattering length $a = 2.75$ nm, atom mass $m = 3.82\times10^{-26}$ kg) with $N = 1.3\times10^6$ atoms, radial and axial trapping frequencies $\omega_0 = 2\pi\times 9$ Hz and $\omega_z = 2\pi\times 400$ Hz, radial and axial harmonic oscillator's lengths $a_0 = \sqrt{\hbar/m\omega_0} \approx 7.1$ μm and $a_z = \sqrt{\hbar/m\omega_z} \approx 1.0$ μm, for which the dimensional healing length is $\xi = 0.13a_0 \approx 0.9$ μm; the laser beam would then have a Gaussian $1/e^2$ radius of $w_0 = 2\sigma \approx 1.8$ μm. Blue-detuned Gaussian laser beams have been used as pins in a series of experiments with highly oblate BECs [18,23,37]. Particularly in [37], a laser beam of width $w_0 \approx 2$ μm was used to stir a 2D ^{87}Rb condensate, similarly to what we propose, maintaining a circular motion with the help of piezodriven mirrors.

In order to define our initial state, a circulation of 37 quanta (i.e., winding number $\kappa = 37$) is initially imprinted around the center of the Thomas-Fermi profile, thus imposing an initial counterclockwise circular flow. Changing t into $-it$ in Eq. (1), we shortly evolve the state for $t = 0.09$ in imaginary-time description, guaranteeing a fixed phase of $2\pi\kappa$ in the center of the condensate and adjusting the density to the presence of the pins. We then compute the evolution in real time.

By substituting $t \to (1-i\gamma)t$ in Eq. (1), we are left with a phenomenological dissipative GPE (dGPE), where γ is a dissipation constant which models the interaction of the condensate with the surrounding thermal cloud. This equation can be used to investigate the effect of finite temperature in our system. With this aim, we also run simulations with the same initial states using dGPE instead of GPE. We choose $\gamma = 3.0\times10^{-4}$, a typical value of dissipative parameter [38–40], particularly chosen for the experimentally realistic case found

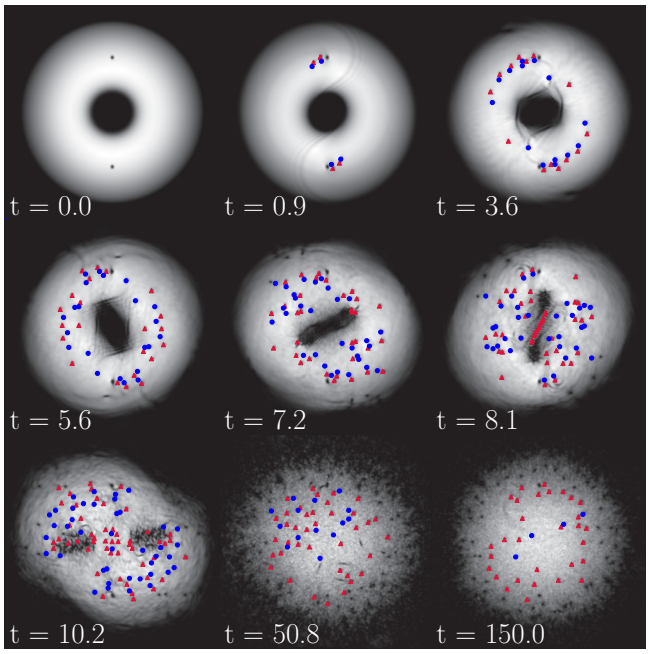

FIG. 1. Density plots of the condensate at different times t for $\omega = 0$ (nonrotating obstacles). Regions of large and low density are displayed in white and black, respectively. Red triangles and blue circles identify positive-charged and negative-charged vortices, respectively. The giant vortex decays by injecting a large number of singly quantized (positive) vortices into the condensate, while the pins generate vortex pairs, as can be clearly seen at time $t = 0.9$.

in current experiments [17,19]. Summarizing beforehand, we find the same overall behavior for both dissipationless and this specific dissipative case.

All numeric simulations are performed in the 2D domain $-25 \leqslant x, y \leqslant 25$ on a 512×512 grid using the fourth-order Runge-Kutta method in Fourier space with the help of XMDS [41].

IV. RESULTS

A. Creating polarized flow

We simulate the real-time evolution of the system for different values of the pins' angular velocity: $\omega = 0, \pi/16, \pi/8, \pi/6$, and $\pi/4$. A series of snapshots for the case of $\omega = 0$ is shown in Fig. 1 to exemplify a typical run. The initial large hole at the center of the figure is the core of the giant vortex. The two small holes (north and south of the giant hole) are the two stationary pins. The critical velocity v_c for the creation of a vortex-antivortex pair depends on the barrier's shape [19,42] and also on inhomogeneities of the system [18]. Typically, $v_c/c \sim 0.1$–0.4 for infinitely high cylindrical barriers, where c is the local speed of sound. Since our barriers (the pins) are either stationary or rotate against the main flow, vortex shedding is a dissipative mechanism which slows down the superfluid's azimuthal flow and removes angular momentum.

Aside from generating vortices of opposite sign, the pins act as a perturbation to the giant vortex and accelerate its decay process; for example, a wave front which perturbs the core of the giant vortex is visible at time $t = 0.9$ in Fig. 1. The decay of the giant vortex takes place via deformation of the core, which becomes elliptical before vanishing, and injecting a large number of positive, singly quantized vortices into the condensate. At the same time, vortex-antivortex pairs are created by the flow past the pins. This process continues until the large azimuthal flow is lower than the critical velocity v_c; at that point, the giant vortex has disappeared, and the pins are practically unable to generate further vortices. Therefore, after this slowdown and due to their small sizes, the pins are practically irrelevant to the vortex dynamics (apart from occasional creation of pairs in the fast rotating case, $\omega = \pi/4$). In spite of that, in order to study the vortex number decay, we simply remove them at $t = 82$ and allow for longer simulations.

We perform a phase-unwrapping procedure and, by detecting windings of $\pm 2\pi$ around small closed paths (plaquettes) on the phase profile [20], we are able to count the numbers N^+ and N^- of positive and negative singly quantized vortices in the system (anticlockwise and clockwise circulation, respectively). This vortex detection algorithm uses a density-cut criterion ($\sim$0.75 of $|\psi|^2$'s mean value) to avoid detection of ghost vortices. Given the initial giant vortex (which is multicharged and therefore not detected by our vortex-detecting algorithm), depending on the value of ω, there can be an imbalance of N^+ and N^- throughout the evolution. Vortices can be expelled from the condensate due to their mutual interaction, spiral out of the condensate because of dissipation, or undergo vortex-pair annihilation processes. In our particular finite-temperature simulation, we verify that the chosen experimentally realistic value of the dissipation parameter γ is small enough that, on the time scale analyzed (and compared to the dissipationless simulations), dissipation-induced spiraling out of individual vortices is less significant than vortex interactions or annihilations.

After the decay of the initial giant vortex, the imbalance of positive and negative vortices is measured by the polarization

$$P = \frac{(N^+ - N^-)}{(N^+ + N^-)} \tag{2}$$

which takes maximum or minimum values ($P = \pm 1$) if all vortices have positive or negative sign. Figure 2 shows the time evolution of the total number of vortices $N_{\rm tot}(t) = N^+ + N^-$ and of the polarization $P(t)$ under influence of the obstacles (present throughout the whole evolution) with angular velocity ω. Figure 2(a) shows that the maximum value of $N_{\rm tot}(t)$ increases with ω. It is apparent that, by choosing ω, we can control the polarization. We use this tunable mechanism to create initial vortex distributions (without the pins) as shown in Fig. 3, which plots $N_{\rm tot}(t)$ and $P(t)$ for initial states taken from instant $t = 82$ of Fig. 2. Clearly, by tuning ω we can produce a condensate free of external holes (the giant vortex or the obstacles) with approximately the desired vortex polarization.

By numerically detecting each vortex and its trajectory, we determine $N_{\rm tot}$ at each time step. By subtraction from the initial total vortex number $N_0 = N_{\rm tot}(0)$, we can infer the number of vortices which have drifted out of the condensate and the number of vortices which have disappeared in annihilation events, colliding with vortices of opposite sign. We find that such vortex-antivortex annihilation events generate density

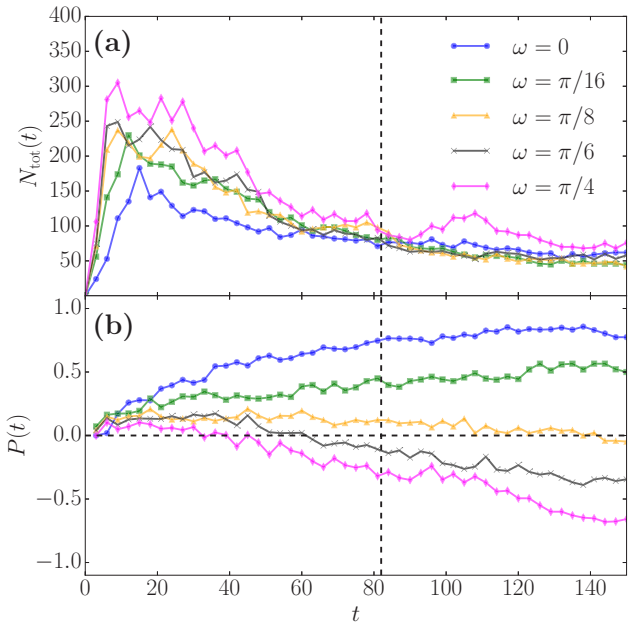

FIG. 2. (a) Total number of vortices N_{tot} vs time t; (b) polarization P vs time t. The vertical dashed line marks the time ($t = 82$) we use to make initial states for longer simulation without the pins. The curves are distributed in increasing value of ω from bottom to top, for the top plot, and conversely, for the bottom plot. In (a), at $t \approx 8$, from bottom to top, the curves refer, respectively, to $\omega = 0$, $\pi/16$, $\pi/8$, $\pi/6$, and $\pi/4$. In (b), from top to bottom, the curves refer, respectively, to the same latter series of increasing values of ω.

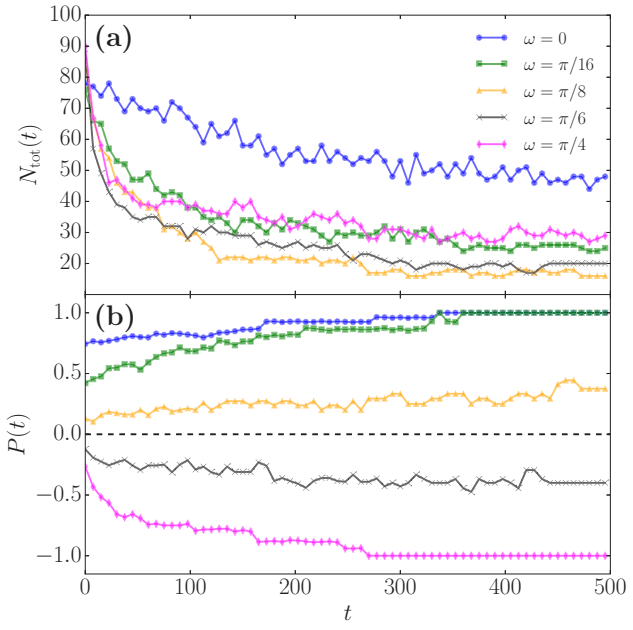

FIG. 3. (a) Total number of vortices N_{tot}; (b) polarization P vs time t, from initial states created at $t = 82$ in the previous stirring process (Fig. 2), labeled by the angular velocities which generated them. The pins are removed and we evolve those states longer in time to study the vortex number decay. In (a), at $t \approx 150$, from bottom to top, the curves refer, respectively, to $\omega = 0$, $\pi/4$, $\pi/16$, $\pi/6$, and $\pi/8$. In (b), from top to bottom, the curves are labeled as in Fig. 2(b).

waves, as already reported [19,43,44], turning incompressible energy into compressible energy. The reverse mechanism is also possible [45] and in our 2D case takes the form of vortex-antivortex creation events, which we observe. Creation events occur when the motion of the vortices induces a sufficiently deep density wave, or when a large amplitude wave approaches the edge of the condensate where the local speed of sound c is less than in the central region. We have also observed annihilation events immediately followed by creation events: this sequence happens when a vortex collides with an antivortex, producing a large sound wave, which almost immediately generates a new vortex-antivortex pair, due to the changing value of the local ratio v_c/c; this effect happens near the condensate's edge.

B. Polarized turbulence decay

Starting from $t > 82$ (when we remove the pins and start a new simulation), we examine whether there is a simple law for turbulence decay in 2D condensates. We remark that, consistently with previous work [17,19], in the time scales under investigation we do not observe a tendency to form large-scale clusters of vortices of the same sign, an effect called the inverse energy cascade in fluid dynamics and the negative temperature in the case of the Onsager gas of vortex points; the reason, as explained in a recent study [46], is the harmonic shape of the trapping potential. It has been suggested [17,19] that the decay rate of the total number of vortices is not exponential but can be phenomenologically described by the logistic equation

$$\frac{dN_{tot}}{dt} = -\Gamma_1 N_{tot} - \Gamma_2 N_{tot}^2, \tag{3}$$

where the linear term refers to vortex drifting out of the condensate, the nonlinear term arises from vortex-antivortex annihilation events, and the coefficients Γ_1 and Γ_2 are rates to be determined. We find that the solution of the logistic equation fits our decays for $t > 82$ (after pins removal) fairly well. However, in most cases which we examined, the fitting parameter Γ_1 is negative, corresponding to positive growth. Clearly, after the pins are removed, no vortex generation is expected (apart from occasional creation of vortex-antivortex pairs as mentioned above); therefore a naive association of the linear term of the logistic equation with vortex drifting out of the condensate does not seem appropriate.

In alternative to the logistic model of Eq. (3), we propose a model which captures some essential physics of the complex vortex interaction, although only in an idealized way. First, we model the rate of drift of vortices out of the condensate [attributed to the linear term of Eq. (3) in [17,19]]. Consider a positive vortex near the edge of the condensate. In the first approximation, its trajectory is a random zigzag caused by the other vortices (see Fig. 4). The azimuthal velocity component of the vortex v_θ will be biased by its sign and, hence, the (opposite) sign of its image with respect to the boundary of the condensate (in the present case of a positive vortex, the interaction with its negative image will give to v_θ an anticlockwise contribution). This azimuthal flow, however, gives no contribution to the vortex drift out of the condensate: what matters to the rate of vortex decay is only the radial

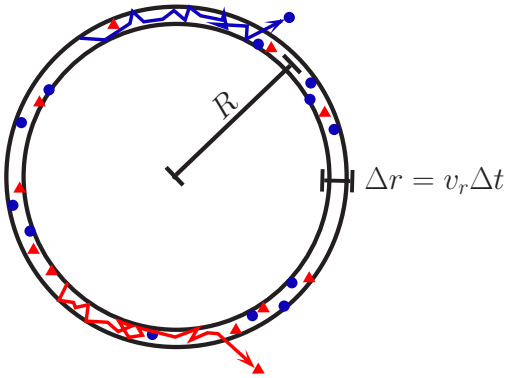

FIG. 4. Schematic trajectories of vortices in a thin annulus of thickness $\Delta r = v_r \Delta t$ near the edge of a condensate of radius R. Vortices (red triangles) and antivortices (blue dots) describe erratic paths (arrowed lines) due to interaction with other vortices. Collisions, mainly with same-signed vortices, drive vortices out of the condensate.

component v_r which will depend on the velocity induced by the surrounding vortices $\mathbf{v}_i$. In this simple model, $\mathbf{v}_i$ can be thought as the velocity induced by the nearest vortex located (if we consider a random vortex distribution) at the typical average inter-vortex distance $\ell \approx n^{-1/2}$, where $n = N/(\pi R^2)$ is the number of vortices per unit area (in 2D) or the length of vortex line per unit volume (in 3D) and N is the number of vortices in the condensate of radius R.[1]

[1]This scaling is well known in the superfluid helium literature, and has been numerically verified by D. Kivotides, Y. A. Sergeev, and C. F. Barenghi, Phys. Fluids **20**, 055105 (2008).

The magnitude of the induced velocity $\mathbf{v}_i$ will, hence, be approximately $v_i \approx \kappa/(2\pi\ell) = \kappa N^{1/2}/(2\pi^{3/2}R)$ (where $\kappa = \pm 1$ is the circulation in our units). The resulting radial velocity of the vortex v_r is therefore given by the expression $v_r \approx \beta v_i \approx \beta\kappa N^{1/2}/(2\pi^{3/2}R)$, where $|\beta| \leqslant 1$ depends on the direction of $\mathbf{v}_i$ and thus on the sign and the relative angular position of the nearest vortex.

Since collisions which take vortices out of the condensate are mainly with vortices of the same (positive) sign, we only use N^+ to estimate ℓ in this term, accounting for the polarization. In this idealized model, the number of positive vortices ΔN^+ expelled from the condensate in the (small) time Δt will therefore be proportional to the number of positive vortices N_a^+ lying in the small circular annulus of width $\Delta r = v_i \Delta t$ and area $\Delta A = 2\pi R \Delta r$, next to the edge of the condensate: these are the only positive vortices which can potentially travel a radial distance greater than their separation gap from the boundary of the condensate. Hence, assuming a uniform vortex distribution we have $\Delta N^+ \propto N_a^+ \approx N^+ \Delta A/(\pi R^2) = \kappa N^{+3/2} \Delta t/(\pi^{3/2} R^2)$. Taking the limit for small Δt, we conclude that positive vortices drift out of the condensate as $dN^+/dt \propto (N^+)^{3/2}$; similarly, $dN^-/dt \propto (N^-)^{3/2}$ for negative vortices.

We turn now the attention to the nonlinear term of Eq. (3), and remark that polarization must be included in the description. In Ref. [17], the authors added the nonlinear term on the intuitive assumption that annihilation rate depends on the number of vortex dipoles (composed of a positive and a negative vortex) which can be formed, which is of order $\propto N^2$ in a zero-polarized system. Following a similar reasoning, in a polarized system the annihilation rate should then be of order $\propto N^+ N^-$, as fewer vortex-dipole pairs are formed if $P \neq 0$

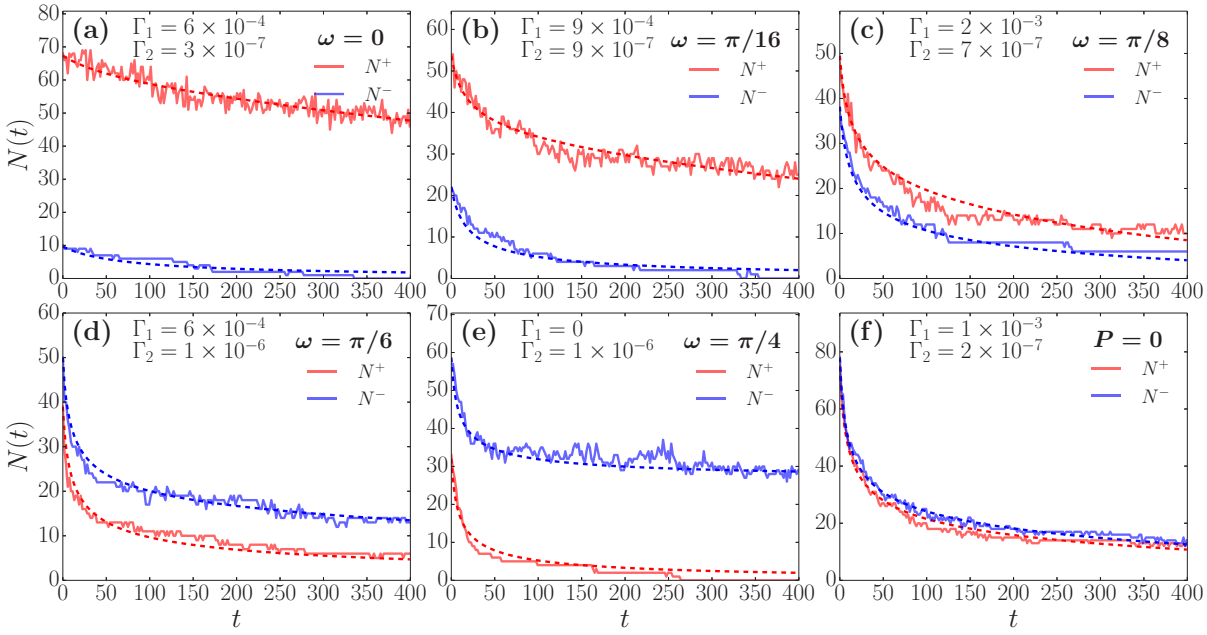

FIG. 5. Positive and negative vortex numbers N^+ and N^- decay as a function of time t for cases (a) $\omega = 0$; (b) $\omega = \pi/16$; (c) $\omega = \pi/8$; (d) $\omega = \pi/6$; (e) $\omega = \pi/4$; and (f) phase imprinted $P = 0$. The dashed lines are the respective fits for the numerical data (full lines) with the fitting parameters Γ_1 and Γ_2 appearing at top part of each plot. For plots (a), (b), and (c), the top and bottom curves are related to the positive and negative vortex numbers, respectively; for plots (d), (e), and (f), curves are in the opposite order.

(this consideration implicitly allows for any time dependence of the polarization).

We conclude that, in alternative to Eq. (3), a more physically realistic (although still rather idealized) model is

$$\frac{dN^+}{dt} = -\Gamma_1(N^+)^{3/2} - \Gamma_2(N^+N^-)^2,$$
$$\frac{dN^-}{dt} = -\Gamma_1(N^-)^{3/2} - \Gamma_2(N^+N^-)^2. \quad (4)$$

Summing up Eqs. (4), the total number of vortices $N_{tot} = N^+ + N^-$ decays nontrivially as a function of polarization $P = P(t)$ according to

$$\frac{dN_{\rm tot}}{dt} = -\Gamma_1 f(t) N_{\rm tot}^{3/2} - \Gamma_2 g(t) N_{\rm tot}^4, \quad (5)$$

where the time-dependent polarization $P(t)$ appears in the functions

$$f(t) \equiv [(1+P)/2]^{3/2} + [(1-P)/2]^{3/2}, \quad (6)$$

$$g(t) \equiv (1-P^2)^2/8. \quad (7)$$

Notice that in our model the rates of drift and annihilation have, respectively, dependence $N_{\rm tot}^{3/2}$ and $N_{\rm tot}^4$ [rather than $N_{\rm tot}$ and $N_{\rm tot}^2$ of Eq. (3)]. The fit to the data is slightly better, and both coefficients Γ_1 and Γ_2 are positive (see Fig. 5), consistently with the interpretation of the two terms of the equation. Above all, our model is not arbitrary, but attempts to capture some of the physics of vortex interaction.

The same $N_{\rm tot}^4$ scaling for the annihilation rate was justified heuristically in the context of a quenched 2D homogeneous system in Ref. [47]. Recently, in Ref. [46], the $N_{\rm tot}^4$ scaling was also associated with a four-body process in simulations of trapped systems, in agreement with our observations. The general behavior is as follows: initially, a vortex dipole interacts with a third, catalyst vortex (or antivortex), turning into a rarefaction wave which the authors of Ref. [46] called a *vortexonium* in analogy with the positronium (the neutral bound state of an electron an a positron). The vortexonium travels through the condensate until it encounters a fourth vortex (or antivortex), which acts as a second catalyst. The four-body annihilation process is completed when the collision of the vortexonium with the fourth vortex converts the vortexonium irreversibly into sound. Figure 6 illustrates the process, showing zoomed-in images of a typical vortex-pair annihilation time sequence from our simulations. In this particular case, the third and fourth bodies are catalyst vortex and antivortex, respectively [see Figs. 6(c) and 6(f)]. It is important to notice that the process of vortex unbind that we have previously discussed often frustrates the last step of this process (i.e., the interaction with the second catalyst vortex) and the annihilation does not happen: although the vortexonium is formed, the local speed of sound may quickly change and split the dipole back again.

Vortex decay curves as a function of the polarization are shown in Fig. 5. We can identify cases (b) and (e) ($\omega = \pi/16$ and $\omega = \pi/4$), (c) and (d) ($\omega = \pi/8$ and $\omega = \pi/6$), respectively, as counterparts with the opposite polarization: the decay curves are similar in behavior, with mirror-symmetric polarization. The main difference between a curve and its counterpart is the steeper number decay at initial times for (c) and (e). We found that the number of vortices lost due to annihilations is always considerably less than due to drift. Drift out of the condensate is strongly induced by vortex interactions: the values of the dissipation parameter γ which we used are too small to make vortices to spiral out of the condensate in the time scales studied. Therefore, both linear and nonlinear terms in Eq. (5) have origins in vortex interactions. Case (e) ($\omega = \pi/4$) illustrates well the need for a steeper than quadratic term in the rate equation since it characterizes a purely nonlinear decay (i.e., $\Gamma_1 = 0$).

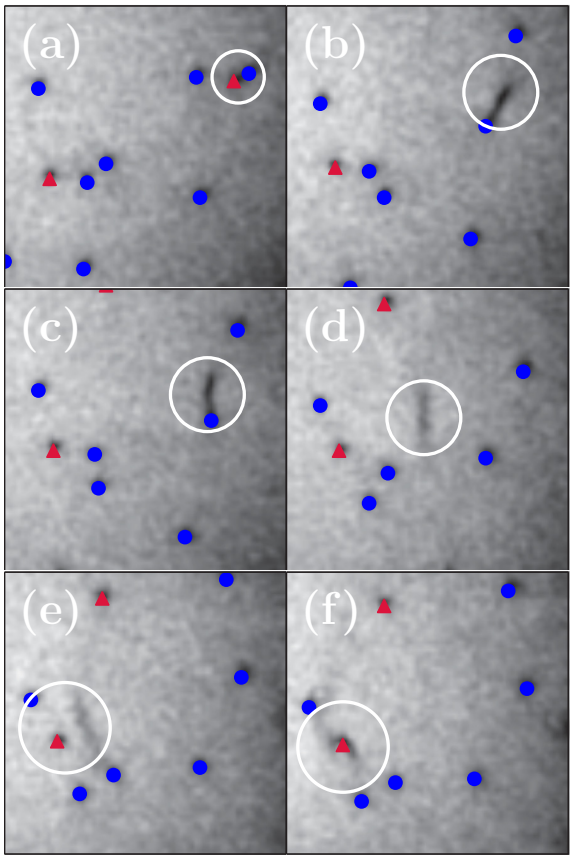

FIG. 6. Vortex annihilation through a four-body process. The white circles highlight the time sequence, which shows that (a) a vortex dipole is formed; (b) the dipole turns into a solitary wave (vortexonium) by interacting with a catalyst vortex; (c) the solitary wave deflects the catalyst vortex; (d) it travels to a higher density region, becoming a grayer, rarefaction pulse; (e) the pulse is about to collide with an anti-vortex; and (f) the annihilation process is complete after the collision, where the pulse is irreversibly converted into sound.

Finally, in order to compare models from Eqs. (3) with (5) we performed numerical experiments in which, rather than creating vorticity with the giant vortex pins set up here proposed, we simply numerically imprint a given initial number of vortices uniformly at random positions onto the same harmonically trapped condensate. We obtain essentially the following results: the polarization approximately retains its initial value $P = 0$ [see Fig. 5(f)], and a reasonable fit is obtained using Eq. (3). As opposed to the polarized cases, we find non-negative rates. However, we see in the comparison

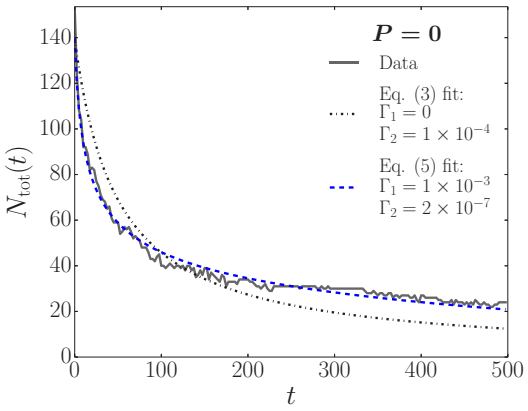

FIG. 7. Total number of vortices $N_{\rm tot}$ vs time t for the case where an unpolarized $P = 0$ vortex distribution was created through phase imprinting, in order to compare fits given by Eq. (3) (black dotted-dashed line) and Eq. (5) (blue dashed line).

shown in Fig. 4 that Eq. (5) fits the curve better than Eq. (3), clearly showing that the $\propto N^4$ scaling is a better fit than $\propto N^2$. Similarly to the polarized cases, drift is the main mechanism of vortex loss. Equation (3) has modeled well the decays studied by [17,19], which differs from our $P = 0$ case not in polarization but rather in the initial number of vortices ($\sim$60 as opposed to our $\sim$140) (see Fig. 7). Therefore, we attribute the departure from the quadratic decay (which is consistent with the "ultraquantum" decay observed [4,5] in superfluid helium, where the system's finiteness was not an issue) to vortex mutual interaction in a confined region. The finite-size system probably imposes a limit to the number of vortices which can be accommodated in the condensate.

In summary, for both polarized case and the particular unpolarized case where the vortex density is high, our rate equation (5) successfully describes the evolution of the total number of vortices.

V. CONCLUSION

We have presented a scheme for generating 2D quantum turbulence in atomic condensates which allows control over the polarization of the flow, equivalent to the net rotation of a turbulent ordinary fluid. Using this experimentally feasible scheme, we have examined the decay of the turbulence and the vortex interactions (vortex-antivortex creation and annihilation) which take place in the condensate. We have modeled the decay of the number of vortices using a rate equation that takes into account the time-dependent polarization. The rate equation (5) is physically more justified and gives a better fit to the numerical experiments than the logistic equation proposed by [17]; in particular, its two terms have clearly distinct physical meaning in terms of drift and annihilation. It also agrees with the recent finding of Ref. [46] in suggesting that vortex annihilation is a four-vortex process. The rate equation is therefore a better starting point to interpret the decay of 2D quantum turbulence in further experiments and simulations in which turbulence is generated in different ways, which will help understanding the scatter of the values of Γ_1 and Γ_2.

ACKNOWLEDGMENTS

We thank G. W. Stagg and A. J. Groszek for useful discussions, and W. J. Kwon and Y. Shin for insightful suggestion on the phenomenological model, particularly for proposing the inclusion of polarization in the vortex number rate equation as a nonlinear term $\propto N^+N^-$. This research was financially supported by CAPES (PDSE Proc. No. BEX 9637/14-1), CNPq, and FAPESP. L.G.'s work is supported by Fonds National de la Recherche, Luxembourg, Grant No. 7745104. The Núcleo de Apoio a Óptica e Fotônica (NAPOF-USP) is acknowledged for computational resources. This work made use of the facilities of N8 HPC Centre of Excellence, provided and funded by the N8 consortium and EPSRC (Grant No. EP/K000225/1).

[1] L. Skrbek and K. R. Sreenivasan, Phys. Fluids **24**, 011301 (2012).
[2] C. F. Barenghi, L. Skrbek, and K. R. Sreenivasan, Proc. Natl. Acad. Sci. USA, Suppl. **111**, 4647 (2014).
[3] C. F. Barenghi, V. S. L'vov, and P.-E. Roche, Proc. Natl. Acad. Sci. USA, Suppl. **111**, 4683 (2014).
[4] P. M. Walmsley and A. I. Golov, Phys. Rev. Lett. **100**, 245301 (2008).
[5] A. W. Baggaley, C. F. Barenghi, and Y. A. Sergeev, Phys. Rev. B **85**, 060501 (2012).
[6] M. C. Tsatsos, P. E. S. Tavares, A. Cidrim, A. R. Fritsch, M. A. Caracanhas, F. E. A. dos Santos, C. F. Barenghi, and V. S. Bagnato, Physics Reports **622**, 1 (2016).
[7] E. A. L. Henn, J. A. Seman, G. Roati, K. M. F. Magalhães, and V. S. Bagnato, Phys. Rev. Lett. **103**, 045301 (2009).
[8] E. A. L. Henn, J. A. Seman, G. Roati, K. M. F. Magalhães, and V. S. Bagnato, J. Low Temp. Phys. **158**, 435 (2009).
[9] T. W. Neely, A. S. Bradley, E. C. Samson, S. J. Rooney, E. M. Wright, K. J. H. Law, R. Carretero-González, P. G. Kevrekidis, M. J. Davis, and B. P. Anderson, Phys. Rev. Lett. **111**, 235301 (2013).
[10] A. C. White, B. P. Anderson, and V. S. Bagnato, Proc. Natl. Acad. Sci. USA, Suppl. **111**, 4719 (2014).
[11] R. H. Kraichnan and D. Montgomery, Rep. Prog. Phys. **43** 547 (1980).
[12] M. Rivera, P. Vorobieff, and R. E. Ecke, Phys. Rev. Lett. **81**, 1417 (1998).
[13] R. Numasato, M. Tsubota, and V. S. L'vov, Phys. Rev. A **81**, 063630 (2010).
[14] N. G. Parker and C. S. Adams, Phys. Rev. Lett. **95**, 145301 (2005).
[15] B. Nowak, D. Sexty, and T. Gasenzer, Phys. Rev. B **84**, 020506 (2011).
[16] T. Simula, M. J. Davis, and K. Helmerson, Phys. Rev. Lett. **113**, 165302 (2014).
[17] W. J. Kwon, G. Moon, J. Y. Choi, S. W. Seo, and Y.-i. Shin, Phys. Rev. A **90**, 063627 (2014).
[18] W. J. Kwon, G. Moon, S. W. Seo, and Y. Shin, Phys. Rev. A **91**, 053615 (2015).

[19] G. W. Stagg, A. J. Allen, N. G. Parker, and C. F. Barenghi, Phys. Rev. A **91**, 013612 (2015).
[20] A. C. White, C. F. Barenghi, and N. P. Proukakis, Phys. Rev. A **86**, 013635 (2012).
[21] M. T. Reeves, B. P. Anderson, and A. S. Bradley, Phys. Rev. A **86**, 053621 (2012).
[22] A. C. White, N. P. Proukakis, and C. F. Barenghi, J. Phys.: Conf. Ser. **544**, 012021 (2014).
[23] T. W. Neely, E. C. Samson, A. S. Bradley, M. J. Davis, and B. P. Anderson, Phys. Rev. Lett. **104**, 160401 (2010).
[24] P. Engels, I. Coddington, P. C. Haljan, V. Schweikhard, and E. A. Cornell, Phys. Rev. Lett. **90**, 170405 (2003).
[25] A. E. Leanhardt, A. Görlitz, A. P. Chikkatur, D. Kielpinski, Y. Shin, D. E. Pritchard, and W. Ketterle, Phys. Rev. Lett. **89**, 190403 (2002).
[26] M. Nakahara, T. Isoshima, and K. Machida, Phys. B (Amsterdam) **288**, 17 (2000).
[27] T. Isoshima, M. Okano, H. Yasuda, K. Kasa, J. A. M. Huhtamäki, M. Kumakura, and Y. Takahashi, Phys. Rev. Lett. **99**, 200403 (2007).
[28] M. Möttönen, N. Matsumoto, M. Nakahara, and T. Ohmi, J. Phys.: Condens. Matter **14**, 13481 (2002).
[29] M. Möttönen, V. Pietilä, and S. M. M. Virtanen, Phys. Rev. Lett. **99**, 250406 (2007).
[30] P. Kuopanportti and M. Möttönen, J. Low Temp. Phys. **161**, 561 (2010).
[31] P. Kuopanportti, B. P. Anderson, and M. Möttönen, Phys. Rev. A **87**, 033623 (2013).
[32] M. W. Ray, E. Ruokokoski, S. Kandel, M. Möttönen, and D. S. Hall, Nature (London) **505**, 657 (2014).
[33] P. Kuopanportti and M. Möttönen, Phys. Rev. A **81**, 033627 (2010).
[34] T. Frisch, Y. Pomeau, and S. Rica, Phys. Rev. Lett. **69**, 1644 (1992).
[35] T. Winiecki, J. F. McCann, and C. S. Adams, Europhys. Lett. **48**, 475 (1999).
[36] N. G. Berloff and P. H. Roberts, J. Phys. A: Math. Gen. **33**, 4025 (2000).
[37] R. Desbuquois, L. Chomaz, T. Yefsah, J. Léonard, J. Beugnon, C. Weitenberg, and J. Dalibard, Nat. Phys. **8**, 645 (2012).
[38] S. Choi, S. A. Morgan, and K. Burnett, Phys. Rev. A **57**, 4057 (1998).
[39] M. Tsubota, K. Kasamatsu, and M. Ueda, Phys. Rev. A **65**, 023603 (2002).
[40] A. S. Bradley and B. P. Anderson, Phys. Rev. X **2**, 041001 (2012).
[41] G. R. Dennis, J. J. Hope, and M. T. Johnsson, Comput. Phys. Commun. **184**, 201 (2013).
[42] F. Pinsker and N. G. Berloff, Phys. Rev. A **89**, 053605 (2014).
[43] M. Leadbeater, T. Winiecki, D. C. Samuels, C. F. Barenghi, and C. S. Adams, Phys. Rev. Lett. **86**, 1410 (2001).
[44] N. G. Parker, N. P. Proukakis, C. F. Barenghi, and C. S. Adams, Phys. Rev. Lett. **92**, 160403 (2004).
[45] N. G. Berloff and C. F. Barenghi, Phys. Rev. Lett. **93**, 090401 (2004).
[46] A. J. Groszek, T. P. Simula, D. M. Paganin, and K. Helmerson, arXiv:1511.06552 [Phys. Rev. A (to be published)].
[47] J. Schole, B. Nowak, and T. Gasenzer, Phys. Rev. A **86**, 013624 (2012).

4.2 Supplementary material

As previously discussed, a multicharged vortex at the center of a harmonically trapped condensate can be described by a wave-function of the form $\psi(\mathbf{r}) = f(r)e^{i\kappa\phi}$, where $f(r)$ is the wave-function's amplitude, $\mathbf{r} = (r, \phi, z)$ is the position in cylindrical coordinates, and a large winding number κ ($\gtrsim 10$) corresponds to the giant angular momentum. This is a stationary (in this case, a metastable) solution of the time-dependent GPE, meaning that $\psi(\mathbf{r}, t) = \psi(\mathbf{r})e^{-i\mu t}$. Therefore, the time-independent GPE can be cast in cylindrical coordinates as follows

$$\mu f(r) = -\frac{1}{2}\left(\frac{1}{r}\frac{\partial}{\partial r}r\frac{\partial}{\partial r} + \frac{\partial^2}{\partial^2 z} + \frac{\kappa^2}{r^2}\right) f(r) + \frac{r^2}{2}f(r) + Cf(r)\left|f(r)\right|^2. \tag{4.1}$$

The above equation can be identified as a type of nonlinear Bessel differential equation, whose solution converges to the exact amplitude of the stationary state, with the centrifugal term $\propto \kappa^2$. It can also be solved spectrally, however instead of the Fourier transform, the derivatives are solved with the help of Hankel transform (see Appendix A).

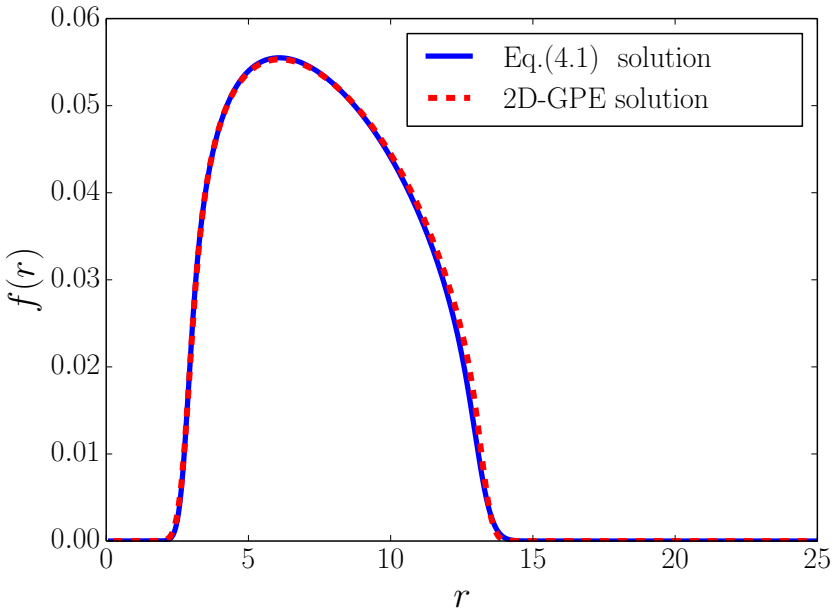

Figure 10 – Amplitude comparison between our approximate initial state solution using short imaginary-time evolution with the full 2D Gross-Pitaevkii equation (dashed line) and the correspondent numerical stationary solution of GPE in polar symmetry (continuous line), as given by Eq. (4.1).
Source: By the author.

In our publication we obtain the solution through an equivalent procedure (see comparison in Fig. 10). We assume that the initial state is approximately given by the Ansatz

$$\psi(\mathbf{r}) = \psi_{\mathrm{TF}}(\mathbf{r})(x + iy)^{\kappa}, \tag{4.2}$$

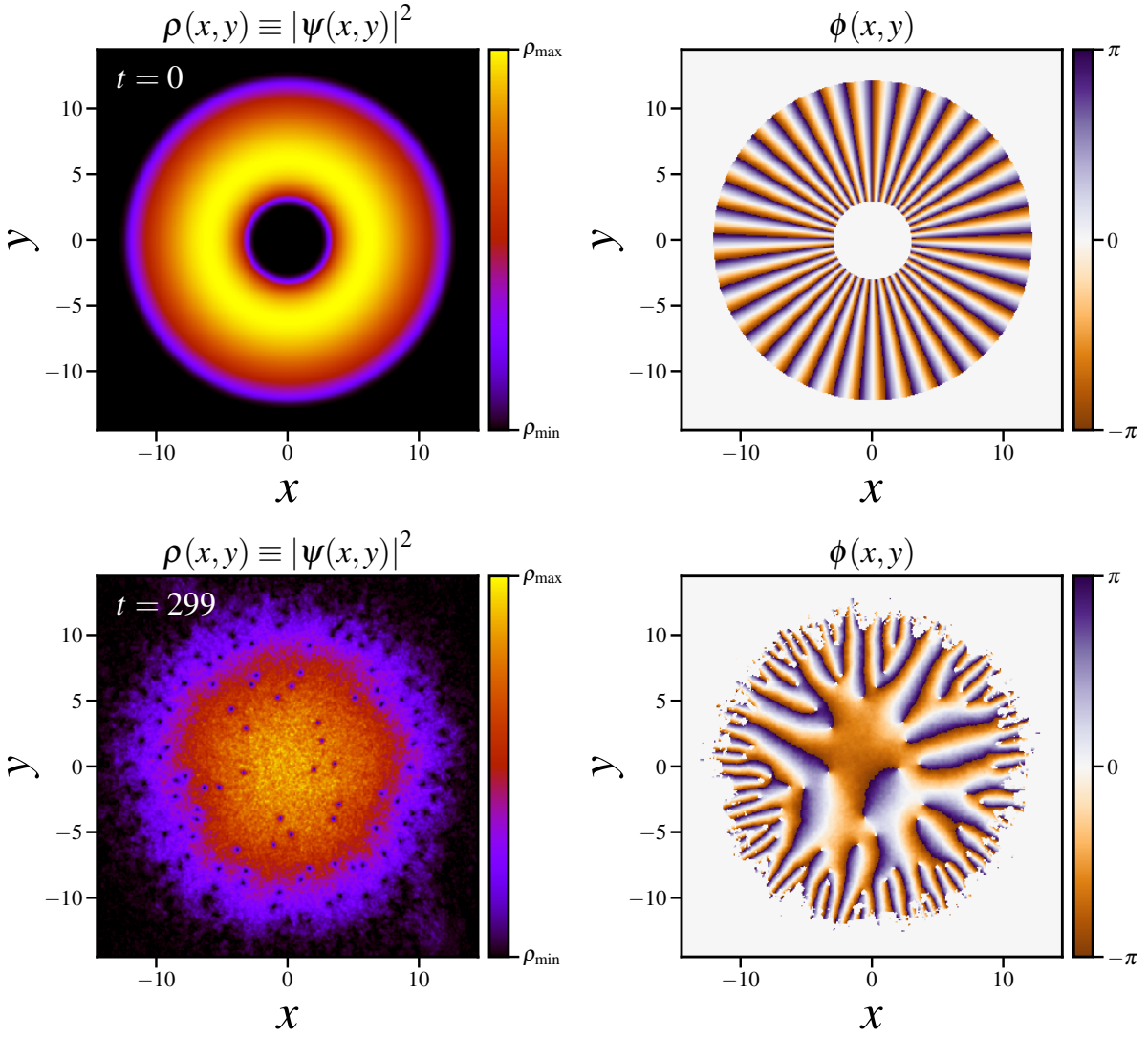

Figure 11 – Density and phase (left and right) of the giant vortex initial state (top) and later in the after-split evolution (bottom).
Source: By the author.

where $\psi_{\mathrm{TF}}(\mathbf{r})$ is the vortex-free Thomas-Fermi solution. We then relax (4.2) for a short imaginary-time ($t = 0.09$), while verifying the reshaping of the giant vortex core while the initially imposed phase ($\kappa = 37$) is unchanged (see Fig. 11). This procedure approximates the solution to a real axially symmetric stationary state with κ quanta of angular momentum. Since the phase is not imposed iteratively in each time step, a longer imaginary time evolution of the GPE in Cartesian coordinates would eventually leave us with a vortex-free cloud (the solution is not an energy global minimum). To ensure our solution is reasonable, we have compared it with the corresponding stationary state of (4.1), as can be seen in Fig. 10. We see that the short-relaxation method coincides extremely well with the numerical Bessel solution, indicating that, although setting an arbitrary relaxation

time, we have quickly converged to the desired local minimum of energy.

4.2.1 How does our unperturbed giant vortex decay?

As we have discussed in Sec 2.7, the most unstable Bogoliubov mode (the one whose eigenfrequency has the largest imaginary part) is typically the one that drives the decay, and its symmetry can still be verified right after the splitting process. With our particular set of parameters the quadrupole (a mode with two-fold symmetry, $l_q = 2$) is the driving mode, as can be verified through the giant vortex core oscillation (see Fig. 12). After oscillating in quadrupolar mode the vortex core undergoes an extreme squeezing process, destroying the giant coherent structure, which then becomes a line of singly-charged vortices.

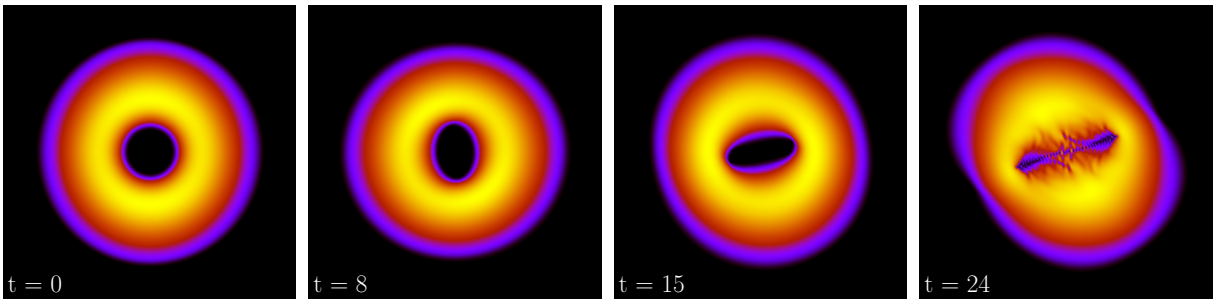

(a) Giant vortex initial state.

(b) Quadrupolar oscillation (led by Bogoliubov unstable mode $l_q = 2$).

(c) Quadrupolar oscillation strongly squeezes giant vortex core.

(d) The core breaks into a queue of singly-quantized vortices.

Figure 12 – Quadrupolar oscillation of the 37-charged vortex core. Notice the approximate two-fold symmetry throughout the entire process.
Source: By the author.

Interestingly, although this system (free of obstacles) is strongly polarized, we still observe the generation of anti-vortices in the after-split dynamics (see Appendix C for details on the vortex counting algorithm used, and see Sec. 5.2.1 for an alternative method). This starts with the splitting process itself, which generates deep density variations and vortex dipoles can be observed being scattered from this region of large fluctuations [see Fig. 12(d)]. Some of the pairs are promptly annihilated, particularly if they stay close to a vortex cluster. Others appear at late stages, when some deep sound waves travel longer distances and undergo an unbinding process due to the trap-induced inhomogeneity (as described at the end of Sec. IV-A of the attached publication). For sufficiently long times, all dipoles disappear and the system relaxes to an Abrikosov vortex lattice.

4.3 Prospects: effects of dissipation

In Sec. 4.1 we have considered dissipation phenomenologically (by including the parameter $\gamma = 3.0 \times 10^{-4}$ in the GPE), which turned out not to have much influence

on the vortex number decay, for the particular cases considered. Nevertheless, we are interested in understanding how dissipation could affect the decay process of the giant vortex (in the absence of external perturbing potentials). Therefore, in this section we describe simulations of the same giant vortex decaying, though under the influence of different (naive) phenomenological dissipative models. We verify that the vortex splits in clusters of singly-charged vortices and their spatial distribution is intimately related to the dissipative model used. The following preliminary analysis may serve as a prospect: using the giant-vortex decay process as a testbed for finite-temperature models. Other numerical experiments have been used before with similar purpose. Jackson et al.,[89] for instance, have investigated the spiral-path of an escaping singly-charged vortex in a trapped BEC in the light of well-known finite-temperature models, testing their accuracy in describing real-life experiments. With similar motivation in mind, it is also worthwhile to point out that, although the giant-vortex split process has already been studied in the literature,[35,40] the complicated after-decay dynamics is still under-explored.

4.3.1 Dissipative models

Our simple modeling lies again on the replacement $t \to (1-i\gamma)t$ in order to obtain a dissipative version of the GPE (see Sec.2.8). However, we now allow for spatial dependence of parameter $\gamma \to \gamma(\mathbf{r})$. We consider three different cases:

- **(1)** $\gamma(\mathbf{r}) = \gamma_0$;
- **(2)** $\gamma(\mathbf{r}) = \gamma_0\theta(r - r_{\rm cut})$: $\theta(x)$ is the Heaviside function and $r_{\rm cut} \equiv 0.7R_{\rm TF}$;
- **(3)** $\gamma(\mathbf{r}) = \gamma_0\left[1 - \frac{\rho(\mathbf{r})}{\rho_{\rm max}}\right]$: where $\rho(\mathbf{r}) \equiv |\psi(\mathbf{r})|^2$ and $\rho_{\rm max} = \max\{\rho(\mathbf{r})\}$;

where in all cases, we choose $\gamma_0 \approx 1 \times 10^{-3}$.

The parameter γ tries to phenomenologically mimic the presence of a thermal cloud. Thus it is reasonable to assume that, in a more realistic model, γ must have a spatial dependence that resembles the approximate density distribution of thermal atoms. Finite temperature models such as the stochastic Gross-Pitaevskii (SGP) and Zaremba-Nikuni-Griffin (ZNG) models attempt to model the thermal atoms distribution and dynamics.[41] Although divergent in some of their predictions, these models agree on the fact that the thermal cloud generally occupies the regions where the BEC density is low (due to repulsive interaction of particles[90]). Case (1) is the simplest, with no spatial dependence at all. Case (2) and (3) attempts to naively account for the probable thermal atoms distribution. For case (2), γ is a fixed Heaviside function of the radius, which tries to consider the average effect of a static surrounding thermal cloud. Case (3) may be considered the most realistic, while attempting to account for some dynamics of the overlapping thermal atoms (creating a sort of "inverted" image of the condensate density).

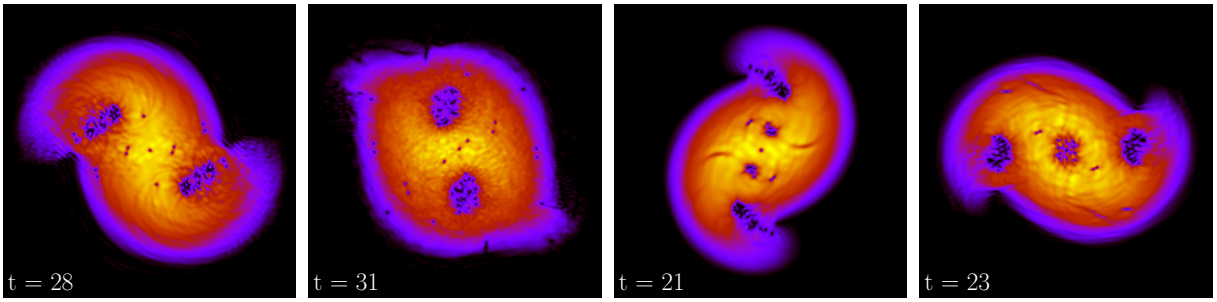

(a) Dissipationless. (b) Case **(1)**. (c) Case **(2)**. (d) Case **(3)**.

Figure 13 – Different cluster injection for the various dissipative models.
Source: By the author.

Numerical simulations for this part were performed for a domain of $-25 \leq x, y \leq 25$ in a grid of 1024×1024 using the 4th order Runge-Kutta method for integration with the help of spectral methods in Fourier space.

4.3.2 Dissipative effects on decay

We verify that the giant vortex decays undergoing the instability process depicted in Fig. 12 for the dissipationless case, independently of the dissipative model adopted. This means that the quadrupole is still the unstable leading mode which drives the vortex splitting. That corroborates previous results in similar systems,[40] which suggest that the decay process itself (its symmetry) is robust against the nature of initial perturbations (although its onset time may vary).

However, the different dissipative models strongly affect the after-decay dynamics. The line of singly-charged vortices [see Fig. 12(d)] that appears right after the splitting is an unstable configuration. Firstly because of the density inhomogeneity, which makes the precession velocity of an off-centered vortex to be locally dependent. This effect, alongside vortices mutual interaction, forces the line to break into clusters. Secondly, the general effect of dissipation on vortices is to make them spiral out of the condensate. Since we may now have spatial inhomogeneity in the dissipative parameter γ, this also means that vortices "feel" a local drag due to thermal effects (depending on their position inside the cloud). Therefore, the final arrangement of the clusters is a reflex of their interaction with the thermal cloud and should contain the information of its spatial distribution in the BEC.

We can look at how the angular momentum $l_z \equiv L_z/(N\hbar)$ is removed from the BEC due to dissipation, where

$$L_z = i\hbar \int\int dxdy\, \psi^*(x,y) \left(x\frac{\partial}{\partial y} - y\frac{\partial}{\partial x} \right) \psi(x,y) \tag{4.3}$$

is the total angular momentum for the 2D system. Its time evolution is shown in Fig. 14. In trapped systems, angular momentum is present not only in quantized vortices, but

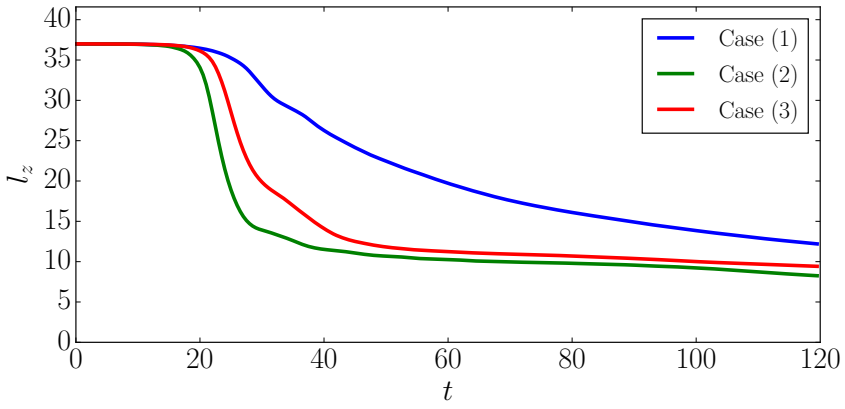

Figure 14 – Time evolution of the angular momentum per particle for the different dissipative cases.
Source: By the author.

also in collective modes.[17] These modes are damped by dissipation and contribute to the decline of l_z, as well. However vortices have a dominant effect, and the steep decrease in angular momentum is mostly due to the quick loss of vorticity and vortex migration to the border of the condensate.

In the beginning, for all cases, the coherent flow imposed by the giant vortex sets each particle to have the initial quanta of $l_z = 37$. Case (1) exhibits a more gradual decrease of angular momentum, which can be explained by Fig. 13(b), where we see the clusters of vortices close to the center of the trap. These clusters are larger when compared to the dissipationless case, Fig. 13(a), which indicates vortex spreading due to dissipation effect. We also see that the shape of the cloud is less deformed, which is an evidence that angular momentum was removed from collective modes. In cases (2) and (3), Figs. 13(c) and (d), respectively, we see that vortices are already agglutinated close to the condensate border, which justifies the more sudden drop of l_z. Thus, in these two cases, spatial inhomogeneity of dissipation plays an essential role.

4.3.3 Vortex clusters: statistical analysis

We see that the arrangement of vortex clusters is a direct result of the finite-temperature phenomenology. One can go beyond the visual aspect of these clusters and try to extract statistical features that can be quantified and eventually measured in real-life experiments. A possible quantifier is Besag's function[91](also related to Ripley's function[92]), which is essentially a second order statistical measure of how much agglutinated a certain set of points is in space. In other words, it measures how far the set is from a homogeneous, random distribution. In our case, the Besag's function is defined by

$$B(r/r_c) \equiv \sqrt{\frac{1}{N^2}\sum_{i=0}^{N}\sum_{j=0}^{N} f_{ij}(r/r_c)} - r/r_c, \tag{4.4}$$

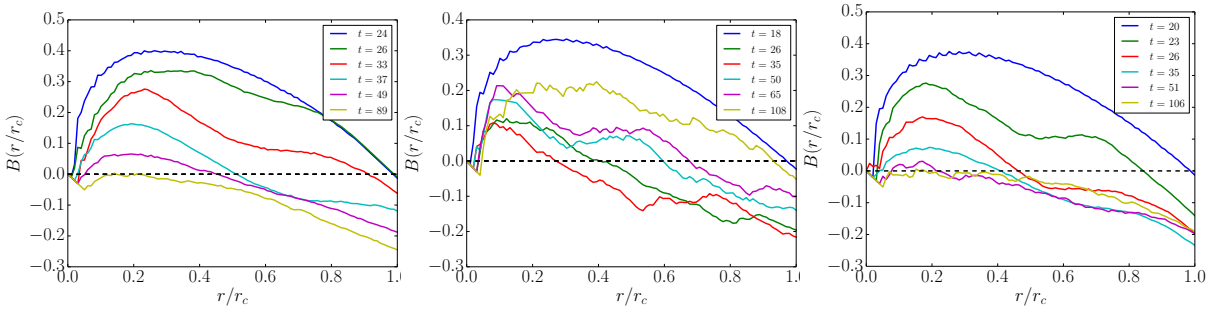

(a) Case (1). (b) Case (2). (c) Case (3).

Figure 15 – Time evolution of Besag's function showing quantitatively the clustering behavior. Source: By the author.

where the sum is made over all the N like-signed vortices. The normalizing distance $r_c \equiv \sqrt{A/\pi}$ is the typical condensate radius, where A is the area inside which the condensate density is larger than 5% of its peak value, and for each vortex pair (i, j) with relative position r_{ij} the function

$$f_{ij}(r/r_c) = \begin{cases} 1, & \text{if } r_{ij} < r \text{ and } i \neq j, \\ 0, & \text{if } r_{ij} > r \text{ or } i = j. \end{cases} \tag{4.5}$$

Therefore, from definition (4.4), B assumes values between -1 and 1, representing

$$B(r/r_c) = \begin{cases} 1, & \text{if vortices are } \textbf{clustered}, \\ 0, & \text{if vortices are } \textbf{randomized}, \\ -1, & \text{if vortices are } \textbf{dispersed}. \end{cases} \tag{4.6}$$

A positive peak in Besag's function at a point $r/r_c = a$ indicates the presence of clustering with a typical cluster dimension a. A randomized system is a uniformly distributed set of points. A disperse arrangement simply designates a set of points that is scattered over a wide area (comparable to the system's size).

For initial times, in all cases we see that $B(r/r_c)$ assumes positive values for practically all condensate extension r_c. This represents a large clustered structure, in this case being the above-mentioned line of vortices that appear immediately after the vortex split.

Consistently with Fig. 13, as time passes B decreases, indicating vortex dispersion for cases (1) and (3) and evidencing the randomized distribution for later times. In case (2) [Fig. 15(b)], however, smaller clusters ($r/r_c \lesssim 0.3$) are initially formed and are long-lived, if compared with the other cases. At $t \approx 40$, B grows to positive values for larger scales, suggesting that clustering increases. In fact, this is confirmed visually in the simulations, where we verify smaller clusters merging and forming larger structures for the rest of time evolution. One may notice that some curves of Fig. 15(b) are more wiggly than the other

two. This is related to smaller number of vortices for case (2) in the after-split ($N^+ \sim 20$) when compared to case (1) ($N^+ \sim 60$) and case (3) ($N^+ \sim 40$). In other words, the smaller the number of like-signed vortices N the stronger the discrete nature of the double sum in Eq. (4.4).

Studying the behavior of the Besag's function in this context can thus provide hints on the distribution (and dynamics) of the thermal cloud. It is a useful quantity in practical terms, since vortices can be nowadays easily resolved in typical 2D experiments. In summary, the complicated dynamics arising from the splitting of a giant vortex can be quantitatively useful for probing different dissipative models.

5 THREE-DIMENSIONAL TURBULENCE

In this chapter we present our numerical results on decaying multicharged quantum vortices in realistic three-dimensional (3D) harmonically trapped BECs.

In Sec. 5.1, we attach the corresponding publication, where we initially study the decay of a quadruply-charged vortex, identifying a twisted unwinding of the multicharged vortex. (This simulation was performed to describe an experiment currently under investigation in our group.[93]) We subsequently propose a protocol to study vortex turbulence, comprising of imprinting two anti-parallel, doubly-charged vortices. They undergo a twisted-unwinding process while favoring vortex reconnections, due to their proximity to one another and their self-induced velocity field. The turbulence arising from this setting is then characterized and shown to be connected to a known regime known as Vinen turbulence, first observed in superfluid Helium experiments.

In Sec. 5.2, we provide supplementary material to the publication, where we describe the numerical procedure and concept behind the identification of the vortices in the simulations (particularly the evaluation of the total vortex length density L). Additionally, we show the Fourier study of the condensate's radial oscillations, providing the typical collective-mode's frequencies.

Finally, in Sec. 5.3, we present a prospective study of the density momentum distribution $n(k)$ for the turbulent system that was proposed in the attached publication. We compare the preliminary results with further simulations of homogeneous systems. The obtained spectrum scalings are contrasted with known theoretical predictions and the few available experimental results in the literature.

5.1 Paper: Vinen turbulence via the decay of multicharged vortices

PHYSICAL REVIEW A **96**, 023617 (2017)

Vinen turbulence via the decay of multicharged vortices in trapped atomic Bose-Einstein condensates

A. Cidrim,[1,*] A. C. White,[2] A. J. Allen,[3] V. S. Bagnato,[1] and C. F. Barenghi[3]

[1]*Instituto de Física de São Carlos, Universidade de São Paulo, C.P. 369, 13560-970 São Carlos, SP, Brazil*

[2]*Quantum Systems Unit, Okinawa Institute of Science and Technology, Okinawa 904-0495, Japan*

[3]*Joint Quantum Centre (JQC) Durham-Newcastle, School of Mathematics and Statistics, Newcastle University, Newcastle upon Tyne NE1 7RU, United Kingdom*

(Received 22 April 2017; published 21 August 2017)

We investigate a procedure to generate turbulence in a trapped Bose-Einstein condensate which takes advantage of the decay of multicharged vortices to reduce surface oscillations. We show that the resulting singly charged vortices twist around each other, intertwined in the shape of helical Kelvin waves, which collide and undergo vortex reconnections, creating a disordered vortex state. By examining the velocity statistics, the energy spectrum, the correlation functions, and the temporal decay and comparing these properties with the properties of classical turbulence and observations in superfluid helium, we conclude that this disordered vortex state can be identified with the Vinen regime of turbulence which has been discovered in the context of superfluid helium.

DOI: 10.1103/PhysRevA.96.023617

I. MOTIVATION

The singular nature of quantized vorticity (concentrated along vortex lines) and the absence of viscosity make superfluids remarkably different from classical fluids. Nevertheless, recent studies [1] have revealed that superfluid helium, when suitably stirred, shares an important property with classical turbulence: the same Kolmogorov energy spectrum [2], describing a distribution of kinetic energy over the length scales which signifies an energy cascade from large length scales to small length scales. This finding suggests that the turbulence of quantized vortices (quantum turbulence) may represent the 'skeleton' of classical turbulence [3].

A puzzle arises, however: experiments [4,5] show that, besides *Kolmogorov* (or quasiclassical) *turbulence*, there is another regime in which turbulent superfluid helium lacks the Kolmogorov spectrum: *Vinen turbulence* (also known as the 'ultraquantum regime'). In their experiments with superfluid helium, Walmsley and Golov [4] were able to generate both regimes by controlling injections of vortex rings in their system. When monitoring the temporal decay of the vortex line density $L(t)$, they observed that short injections of vortex rings produced a regime in which $L(t) \sim t^{-1}$, as opposed to long injections, which displayed the scaling $L(t) \sim t^{-3/2}$. Numerical simulations [6] of this experiment revealed that Vinen turbulence [decaying as $L(t) \sim t^{-1}$] has a spectrum $E(k)$ which peaks at intermediate length scales and behaves as $E(k) \sim k^{-1}$ for large k in the hydrodynamical range $k < 2\pi/\ell$ (where ℓ is the average intervortex distance); on the contrary, Kolmogorov turbulence [decaying as $L(t) \sim t^{-3/2}$] has a spectrum $E(k)$ which peaks at the largest length scales and behaves as $E(k) \sim k^{-5/3}$ for large k.

It is now understood that Vinen's pioneering experiments [7] on counterflow heat transfer in superfluid helium also generated Vinen turbulence. This was demonstrated by numerical models of counterflow turbulence [8] driven by a uniform normal fluid which produced a superfluid energy spectrum peaking at mesoscales with the expected $E(k) \sim k^{-1}$ tail at large k. Additionally, the $L(t) \sim t^{-1}$ vortex line density decay was also observed, which is the large-t decaying solution of the equation $dL/dt \sim -L^2$ proposed by Vinen on simple physical arguments to model a randomlike flow. Moreover, a recent work [9] examining the properties of turbulence following the thermal quench of a Bose gas has found that topological defects created by the Kibble-Zurek mechanism evolve into a turbulent vortex tangle [10] which eventually decays into a vortex-free state. During the decay, which has the form $L(t) \sim t^{-1}$, the energy spectrum is concentrated at intermediate wave numbers and scales as $E(k) \sim k^{-1}$, and the velocity correlation functions drop to a few percent over the distance ℓ. The thermal quench is therefore a third clear example of Vinen turbulence. It has been argued [5] that, physically, Vinen turbulence differs from Kolmogorov turbulence because it lacks the energy cascade from large to small eddies which is characteristic of classical turbulence. At the moment, it is not clear whether this distinction between Vinen turbulence and Kolmogorov turbulence, first proposed by Volovik [11], is unique to superfluids. It is in principle possible that the former regime can appear only in systems with discrete vorticity, ruling out its presence in classical fluids (in which vorticity is a continuous quantity).

Given this context, it is clear that trapped atomic Bose-Einstein condensates (BECs) are ideal systems to tackle this puzzle and to eventually serve as a test bed for a crossover between Vinen and Kolmogorov turbulence. This is because, unlike helium, the physical properties of BECs (e.g., the strength of atomic interactions, the density, the vortex core radius) can be controlled. Moreover, individual quantized vortices are more easily nucleated, manipulated [12,13], and observed [14–16] in BECs than in helium.

The second motivation behind our work is that the study of three-dimensional (3D) turbulence in BECs [17] is held back

*andrecidrim@gmail.com

by the lack of a standard method to excite turbulence in a reproducible way, so that experiments and numerical simulations can be compared with each other and any generality of results can be more easily recognized. In classical turbulence, standard benchmarks are flows driven along channels or stirred by propellers, flows around well-defined obstacles (e.g. cylinders, spheres, steps), and wind tunnel flows past grids. Similar techniques are used for superfluid helium [18,19], which is mechanically or thermally driven along channels or stirred by oscillating wires, grids, forks, propellers, and spheres. Vortices and turbulence in BECs have been generated, either numerically or experimentally, by moving a laser beam across the BEC [15,20–26], by shaking [27] or stirring the trap, rotating it around two perpendicular axes [28], by phase imprinting staggered vortices [29], or by thermally quenching the system (Kibble-Zurek mechanism) [30–33]. This variety of techniques and the arbitrarily chosen values of physical parameters mean that comparisons are difficult. Moreover, the disadvantage of some of these techniques is that they tend to induce large surface oscillations or even fragmentation [34] of the condensate, which complicates the interpretation of results and the comparison with classical turbulence.

The aim of this report is to propose a technique to induce turbulence in BECs based on the decay of multicharged vortices (a more controlled and less forceful technique than the above-mentioned methods) and to characterize the turbulence which is produced. For this purpose, we compare two disordered vortex states, which we call "anisotropic" and "quasi-isotropic" for simplicity, resulting from the decay of a single $j = 4$ charged vortex and from the decay of two antiparallel $j = 2$ vortices, respectively. We reveal a connection between BEC turbulence and the Vinen turbulent regime discovered in superfluid helium.

II. MULTICHARGED VORTICES

In a superfluid, the circulation around a vortex line is an integer multiple ($j = 1,2,\dots$) of the quantum of circulation [35] $\kappa = h/m$, that is, $\oint_C \mathbf{v}\cdot d\ell = j\kappa$, where C is a closed path around the vortex line, h is Planck's constant, and m the atomic mass. The velocity field around an isolated vortex line is therefore constrained to the form $v = j\kappa/(2\pi r)$, where r is the distance to the vortex axis. This property is in marked contrast to classical fluids, where the velocity of rotation about an axis (e.g., swirls, tornadoes, galaxies) has arbitrary strength and radial dependence.

The angular momentum and the energy of an isolated vortex in a homogeneous superfluid grow, respectively, with j and j^2 [35]. Therefore, for the same angular momentum, multicharged ($j > 1$) vortices carry more energy and, in the presence of thermal dissipative mechanisms, tend to decay into singly charged vortices [36–39]. Besides the energy instability, there is also a dynamical instability [40–42], which would destabilize a multicharged vortex. The time scale of these effects has been investigated [36,38,39,41,43–46]. The technique of topological phase imprinting [47] has allowed the controlled generation of multicharged vortices [36,38,45,48] in atomic condensates. The decay of a doubly quantized vortex into two singly quantized vortices has been studied [36,43,44] in a Na BEC. Quadruply charged quantized vortices are also theoretically predicted [49] to decay. Recent work has determined that the stability of such vortices is affected by the condensate's density [36] and size [44] and by the nature of the perturbations [49].

III. MODEL

We model the condensate's dynamics using the 3D Gross-Pitaevskii equation (GPE) [35] for a zero-temperature condensate,

$$i\hbar\frac{\partial\psi}{\partial t} = \left(-\frac{\hbar^2}{2m}\nabla^2 + U(\mathbf{r}) + g|\psi|^2\right)\psi, \qquad (1)$$

where $\psi(\mathbf{r},t)$ is the condensate's wave function, $\mathbf{r}$ the position, t the time, and

$$U(\mathbf{r}) = \frac{m}{2}\left(\omega_x^2x^2 + \omega_y^2y^2 + \omega_z^2z^2\right) = \frac{m}{2}(\omega_r r^2 + \omega_z z^2) \qquad (2)$$

the harmonic trapping potential. The parameter $g = 4\pi\hbar^2 a_s/m$ characterizes the strength of the interatomic interactions, where a_s is the s-wave scattering length. The normalization is $\int_V |\psi|^2 dV = N$, where V is the BEC's volume and N the number of atoms. We cast the GPE in dimensionless form using $\tau_{\rm HO} = \omega_r^{-1}$, $\ell_{\rm HO} = \sqrt{\hbar/m\omega_r}$, and $\hbar\omega_r$ as units of time, distance, and energy, respectively. The interatomic interaction parameter, $g(=8600)$, is chosen to describe a typical BEC with $N \approx 1\times10^5$ atoms of ^{87}Rb trapped harmonically in a cigar-shaped BEC with radial and axial frequencies such that $\omega_z/\omega_r = \lambda = 0.129$. It is of our particular interest to study properties of the condensate's velocity-field components, which are computed from the definition $\mathbf{v}(\mathbf{r}) = (\psi\nabla\psi^* - \psi^*\nabla\psi)/2i|\psi|^2$. The dimensionless GPE is solved numerically in the 3D domain $-10\ell_{\rm HO} \leqslant x,y \leqslant 10\ell_{\rm HO}$ and $-40\ell_{\rm HO} \leqslant z \leqslant 40\ell_{\rm HO}$ on a $128\times128\times512$ grid (keeping the same spatial discretization in the three directions) with time step $\Delta t = 10^{-3}$ using the fourth-order Runge-Kutta method with XMDS2 (eXtensible Multi-Dimensional Simulator 2) [50]. We have performed tests with different grid sizes and verified that our results are independent of the discretization.

IV. DECAY OF SINGLE QUADRUPLY CHARGED VORTEX

The shape of the singly charged vortex lines emerging from the decay of a multicharged vortex depends on where and when the decay starts. The singly charged lines may be straight or intertwined (as reported here), depending on the perturbation's symmetry and the local density homogeneity. If the perturbation is uniform and the density does not vary much in the z direction, every point on the vortex unwinds at the same rate, and straight singly charged vortex lines will emerge. However, if the density changes significantly along z, the unwinding takes place at different times and different positions, inducing intertwining, as discussed in [43].

The twisted vortex decay is shown in Fig. 1 and in the first movie in the Supplemental Material [51]. The main feature visible during the evolution is Kelvin waves. Kelvin waves consist of helical displacements of the vortex core axis and play an important role in quantum turbulence [18]; they have recently been experimentally identified in superfluid helium

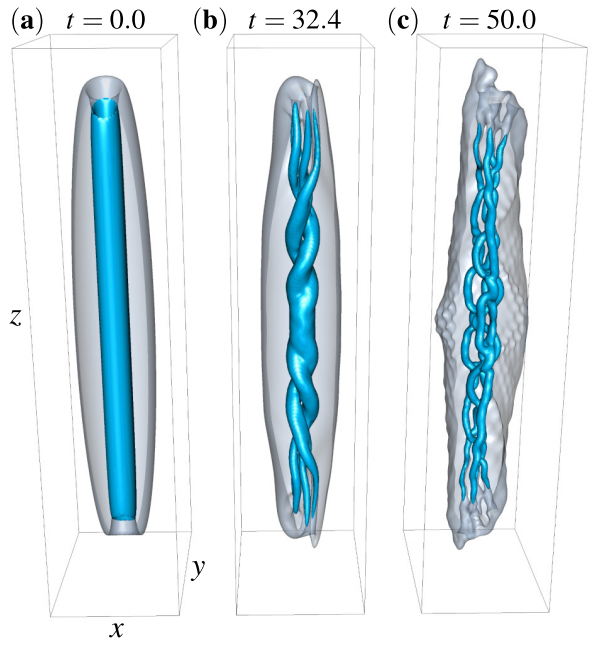

FIG. 1. Three-dimensional isodensity plots show the time (in units of $\tau_{\rm HO}$) evolution of an initial $j = 4$ multicharged vortex (a); note the twisted unwinding of the vortex (b), which finally decays into four singly charged ($j = 1$) vortices (c) in the disordered, anisotropic state. The density isosurfaces representing the condensate and the vortices are gray and blue, respectively. The 3D domain is displayed within the plot limits $-7\ell_{\rm HO} \leqslant x \leqslant 7\ell_{\rm HO}$, $-10\ell_{\rm HO} \leqslant y \leqslant 10\ell_{\rm HO}$, and $-30\ell_{\rm HO} \leqslant z \leqslant 30\ell_{\rm HO}$.

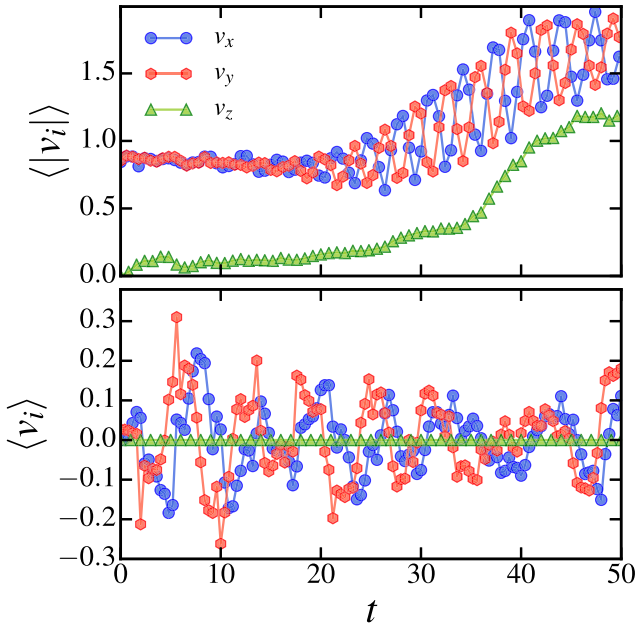

FIG. 2. Decay of a quadruply charged vortex (anisotropic state). Time evolution of average velocity components v_i and $|v_i|$ (in units of $\ell_{ho}/\tau_{\rm HO}$, where $i = x,y,z$) vs time (in units of $\tau_{\rm HO}$). The symbol $\langle \dots \rangle$ denotes the spatial average over the condensate.

[52] and their presence has been recognized in atomic condensates [53,54]. Considering Fig. 1, it is worth distinguishing the Kelvin waves which, in our case, emerge on parallel vortices from the decay of a multicharged vortex [41,44] in a confined geometry from the Kelvin waves generated by the Crow instability [55] on antiparallel vortices in a homogeneous condensate.

Despite its known dynamical instability, in the absence of large perturbations, a symmetric multicharged vortex can be a long-lived state in a harmonic trap. We have, for instance, simulated the time evolution for the quadruply charged vortex when symmetrically imprinted along the z direction (i.e., centered at the origin) up to $t = 150\tau_{\rm HO}$ without verifying its decay (observing instead the development of only low-amplitude collective modes). However, our numerical experiments suggest that the decay of the multicharged vortex can be sped up. Imposing uniformly distributed random fluctuations ($\leqslant$10% of $|\psi|$) on the initial $j = 4$ wave function does not significantly change the decay time scale, probably because the symmetry of the initial condition is not completely broken. A small displacement of the vortex core axis ($\approx 0.2\ell_{\rm HO}$) is more efficient, triggering the onset of twisted unwinding in about $14.0\tau_{\rm HO}$; a larger displacement ($\approx 0.5\ell_{\rm HO}$) reduces this time to $12.0\tau_{\rm HO}$. Among the other methods which we have investigated, the most efficient is to gently squeeze the harmonic potential in the xy plane by an amount $\omega_x/\omega_y = 0.9$ when preparing the initial state in imaginary time, then reset $\omega_x/\omega_y = 1$ when propagating the GPE in real time; the squeeze triggers the onset of decay in only $6.0\tau_{\rm HO}$. In the experiments, it is usually difficult to control perturbations well enough to reproducibly determine the time scale of decay.

Figure 2 shows the time evolution of the (spatially) averaged velocity components and their magnitudes during the decay. The x and y components display oscillations which become large for $t > 20\tau_{\rm HO}$, after the initial multicharged vortex has split. The z component behaves differently because all vortices are aligned in the z direction. The oscillations of the transverse velocity components v_x and v_y appear practically out of phase [see Fig. 2 (top)], and these suggest the existence of collective modes. In order to properly identify these modes we have evaluated the time evolution of the condensate's transverse widths w_x and w_y (found by adjusting Gaussian fits in the x and y directions over the z-integrated density). As shown in Fig. 3, the condensate exhibits a quadrupolar mode, in which w_x and w_y oscillate out of phase in time. After performing a Fourier analysis of these quadrupolar oscillations we verified the mode's frequency to be $\omega \sim \sqrt{2}\omega_r$, in agreement with theoretical predictions for a vortex-free cloud [56]. This mode is reminiscent of the unstable (quadrupolar) Bogoliubov mode that drives the decay of the initial multicharged vortex, as identified for analogous 2D [46] and 3D [42] trapped systems.

For simplicity of reference, we call the resulting disordered vortex configuration an 'anisotropic state'.

V. DECAY OF TWO ANTIPARALLEL DOUBLY CHARGED VORTICES

Now we exploit the twisted unwinding of a multicharged vortex as a convenient technique to generate turbulent vortex tangles which are relatively free of high-density perturbations. We start by numerically imprinting antiparallel, doubly

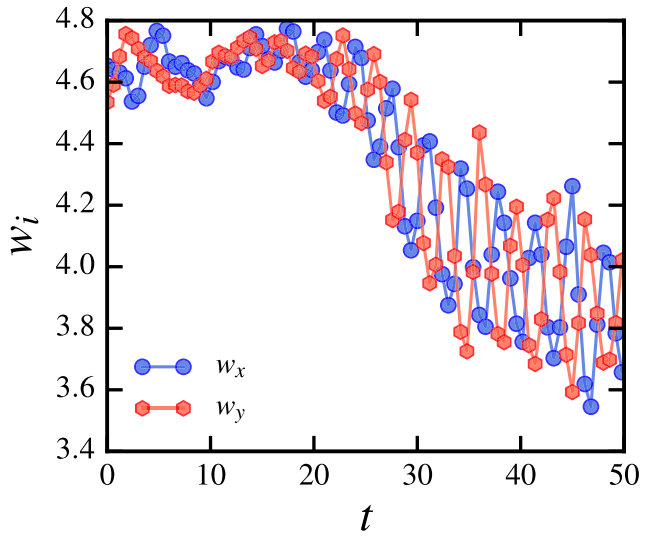

FIG. 3. Decay of quadruply charged vortex (anisotropic state). Time (in units of $\tau_{\rm HO}$) evolution of the condensate's width w_i (in units of $\ell_{\rm HO}$).

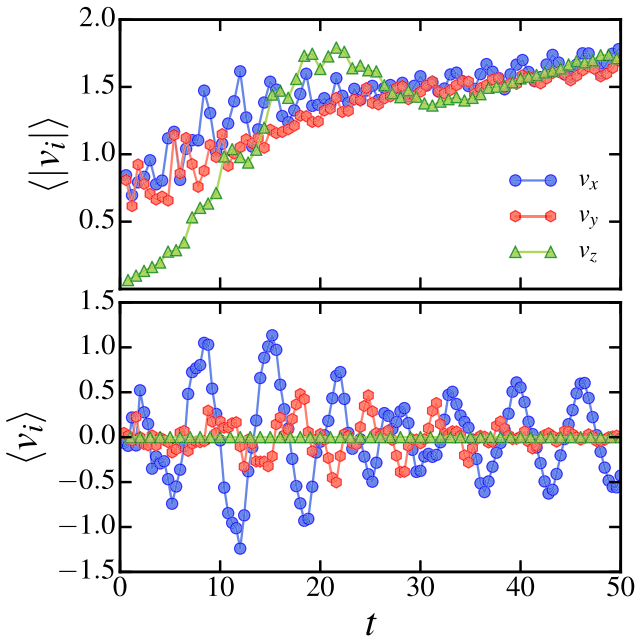

FIG. 5. Decay of antiparallel doubly charged vortices (quasi-isotropic state). Time evolution of velocity components as in Fig. 2.

charged vortices as the initial state. One vortex is centered at position $(x,y) = (1.8\ell_{\rm HO}, 1.5\ell_{\rm HO})$ and the other at $(x,y) = (1.0\ell_{\rm HO}, -1.3\ell_{\rm HO})$, as shown in Fig. 4(a). We have performed several simulations, with different initial positions for the vortex pair. When the system was prepared in a symmetric initial state, the vortex pair annihilation was too quick, and less vortex tangling was observed. Since our aim was to induce more vortex tangling (therefore stretching the turbulence time window), the values we present are the results of an optimized choice, which breaks the symmetry by imposing a noncentered initial state. During the evolution, the vortices unwind, twist, move slightly forward due to the self-induced velocity field, and then reconnect, generating a turbulent state with only moderate density oscillations, as shown in Fig. 4(b).

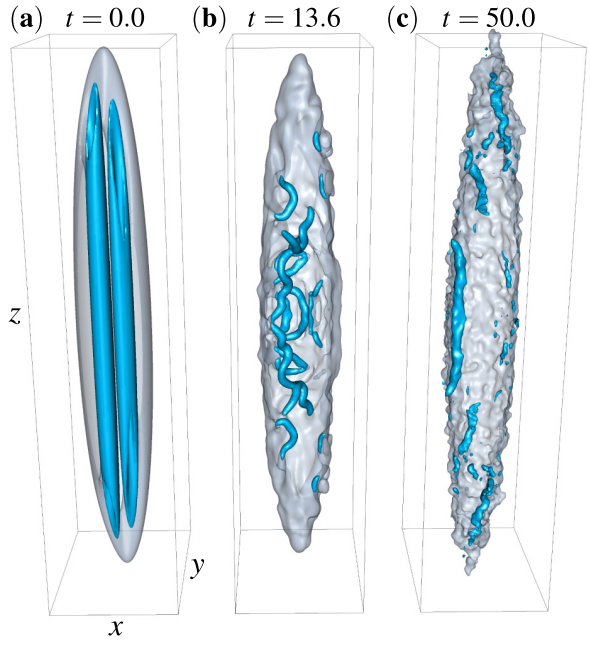

FIG. 4. Isodensity plots showing the evolution (with time t in units of $\tau_{\rm HO}$) of two initial doubly charged ($j = 2$) antiparallel vortices at $t = 0\tau_{\rm HO}$ (a) into the turbulent quasi-isotropic state at $t = 13.6\tau_{\rm HO}$ (b), which has finally decayed at $t = 50\tau_{\rm HO}$ (c). The 3D domain is displayed within the plot limits $-7\ell_{\rm HO} \leqslant x \leqslant 7\ell_{\rm HO}$, $-10\ell_{\rm HO} \leqslant y \leqslant 10\ell_{\rm HO}$, and $-30\ell_{\rm HO} \leqslant z \leqslant 30\ell_{\rm HO}$.

We analyze the turbulent state in terms of the spatial averages of the velocity components. At the beginning of the decay, we find $\langle|v_y|\rangle/\langle|v_x|\rangle \approx 1$ and (as expected, as vortices are initially aligned in the z direction) $\langle|v_z|\rangle/\langle|v_x|\rangle \approx 0$. Figure 5 (top) shows that, as time proceeds, the vortex configuration becomes almost isotropic; indeed at $t = 10\tau_{\rm HO}$ we have $\langle|v_y|\rangle/\langle|v_x|\rangle \approx 1.00$ and $\langle|v_z|\rangle/\langle|v_x|\rangle \approx 0.77$. For simplicity of reference, we call the resulting disordered vortex configuration a 'quasi-isotropic state'.

As opposed to the anisotropic case, the oscillations of the transverse velocity components v_x and v_y appear almost completely in phase for this quasi-isotropic case [compare Fig. 2 (top) and Fig. 5 (top)], and these also suggest the existence of collective modes. We have evaluated the time evolution of the condensate's transverse widths for this scenario as well. Figure 6 shows that after $t \approx 10\tau_{\rm HO}$ there is a small ($\sim 0.2\ell_{\rm HO}$) in-phase oscillation of the widths (as opposed to the larger oscillations for the anisotropic case in Fig. 3). This can be identified as a breathing mode and (again, through a Fourier analysis) it was found to exhibit a characteristic frequency of $\omega \sim 2\omega_r$, also in agreement with theoretical predictions for a vortex-free cloud [56]; this value is expected to hold even for rapidly rotating trapped systems [57]. These results, alongside a visual comparison of Figs. 1 and 4, show that the outer surface of the condensate is actually slightly less disturbed in the quasi-isotropic case. Our turbulent condensate [Fig. 4(b)] is clearly less 'wobbly' than condensates made

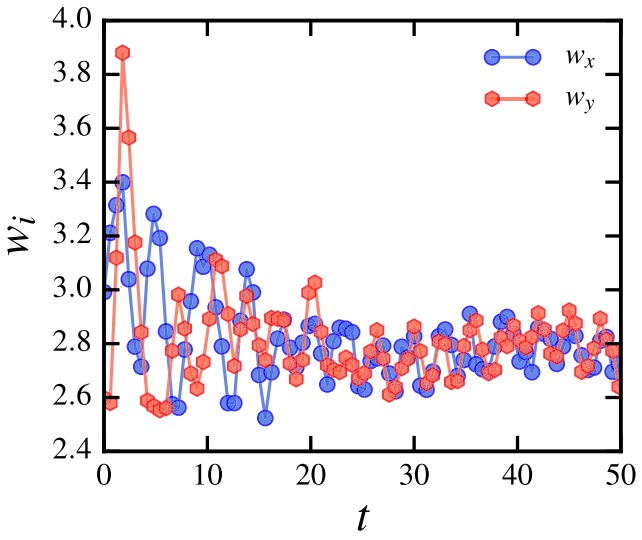

FIG. 6. Decay of antiparallel doubly charged vortices (quasi-isotropic state). Time evolution of the condensate's width.

turbulent via other stirring methods, as in, notably, Refs. [29], [58], and [34]. (See the Appendix for a quantitative discussion of the surface oscillations of the condensate.)

We proceed and analyze the distribution of values of the turbulent velocity components (Fig. 7). We find that the probability density functions (PDFs, or normalized histograms) display the typical power-law scaling $\mathrm{PDF}(v_i) \sim v_i^{\alpha_i}$

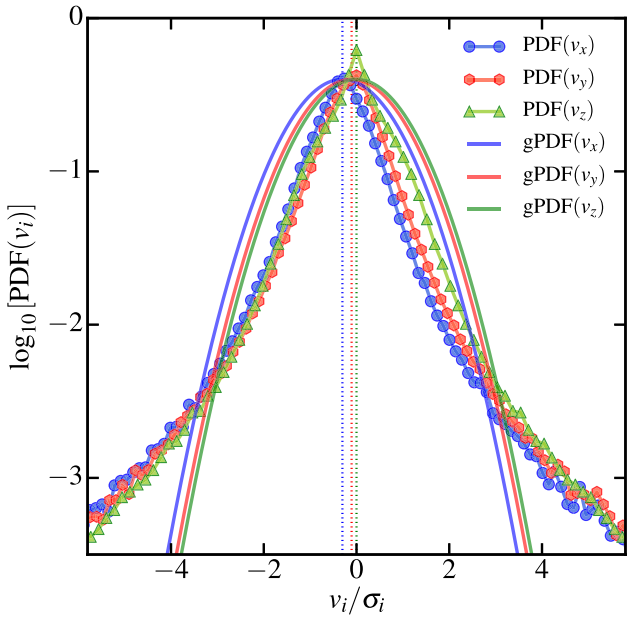

FIG. 7. Decay of antiparallel doubly charged vortices (quasi-isotropic state). PDFs of velocity components v_i ($i = x$, $i = y$, and $i = z$ corresponding to blue, red, and green symbols, respectively) plotted vs v_i/σ_i (where σ_i are the corresponding standard deviations) at $t = 12.6\tau_{\mathrm{HO}}$. For reference, solid curves are Gaussian fits (gPDFs) with standard deviations $\sigma_x = 1.8$, $\sigma_y = 1.7$, and $\sigma_z = 1.4$, and mean values (plotted as vertical lines near the origin) $\mu_x = -0.3$, $\mu_y = -0.1$, and $\mu_z = 0.0$.

($i = x,y,z$), where $\alpha_x \approx -2.97$, $\alpha_y \approx -2.95$, $\alpha_z \approx -3.20$, in agreement with findings in larger condensates [29]. Such power-law scaling, characteristic of quantum turbulence and observed in helium experiments [59], is in contrast to Gaussian PDFs, which are typical of classical turbulence. The difference between power-law and Gaussian statistics is important at high velocities (power-law PDFs have larger values in the tails) and arises from the quantization of vorticity [which creates very high velocities for $r \to 0$, as $v = \kappa/(2\pi r)$]. For the sake of comparison, Fig. 7 also displays Gaussian fits [60].

VI. IDENTIFICATION OF THE TURBULENCE

The two disordered vortex states, anisotropic and quasi-isotropic, produced, respectively, by the decay of a single quadruply charged vortex (Sec. IV) and by the decay of two antiparallel doubly charged vortices (Sec. V), are clearly different. In the anisotropic state, all vortex lines are aligned in the same direction, and the net nonzero angular momentum constrains the flow. In the quasi-isotropic state, the oscillations of the average transverse velocity components $\langle v_i \rangle$ are three times larger, suggesting the presence of high-velocity events (vortex reconnections between Kelvin waves growing on opposite-oriented vortices), which are the hallmarks of turbulence. Moreover, in the quasi-isotropic state, the zero angular momentum of the initial configuration allows a redistribution of the velocity field, making the amplitudes of the three velocity components almost equal; indeed, after the initial vortex has split ($t \approx 10\tau_{\mathrm{HO}}$), the axial velocity, $\langle |v_z| \rangle \approx 0.9\ell_{\mathrm{HO}}/\tau_{\mathrm{HO}}$, is not much lower than the transverse velocity, $\langle |v_x| \rangle \approx 1.2\ell_{\mathrm{HO}}/\tau_{\mathrm{HO}}$ and $\langle |v_y| \rangle \approx 1.1\ell_{\mathrm{HO}}/\tau_{\mathrm{HO}}$. On the contrary, in the anisotropic state, at the same stage ($t \approx 10\tau_{\mathrm{HO}}$), the axial velocity component is much smaller than the transverse components. In other words, the velocity field which results from the decay of the antiparallel doubly charged vortex state is indeed almost isotropic.

Since there is not yet a precise definition of turbulence, in principle both disordered states investigated here could be considered somewhat 'turbulent'. However, at this early stage of investigation, we want to make conceptual connections to the simple isotropic cases known in the literature (in particular, the Kolmogorov and Vinen regimes of turbulence). Therefore hereafter we concentrate on the quasi-isotropic state.

The next question is whether the quasi-isotropic state is turbulent in the sense of classical turbulence or in comparison with turbulent superfluid helium. To find the answer, we turn to the workhorse of statistical physics: the correlation function.

The quantity which measures the degree of randomness of a turbulent flow is the (normalized) longitudinal correlation functions [9,61], defined by

$$f_i(r) = \frac{\langle v_i(\mathbf{x} + r\hat{\mathbf{e}}_i) v_i(\mathbf{x}) \rangle}{\langle v_i(\mathbf{x})^2 \rangle}, \tag{3}$$

where the symbol $\langle \ldots \rangle$ denotes an average over the position vector $\mathbf{x} = (x,y,z)$, and $\hat{\mathbf{e}}_i$ is the unit vector in the corresponding Cartesian direction. The distance r is limited by the size of the BEC, approximately the transverse and axial Thomas-Fermi radii, $d_{\mathrm{TF}} = 4.2\ell_{\mathrm{HO}}$ and $D_{\mathrm{TF}} = 32.6\ell_{\mathrm{HO}}$, respectively. From the longitudinal correlation function one

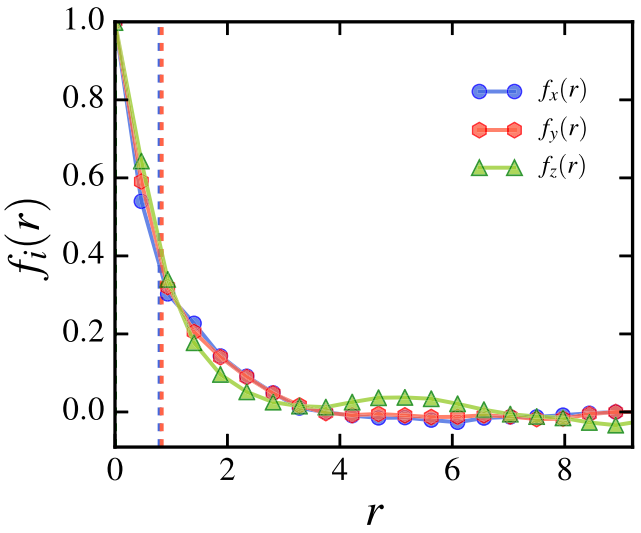

FIG. 8. Decay of antiparallel doubly charged vortices (quasi-isotropic state). Longitudinal correlation functions $f_i(r)$ $(i = x, y, z)$ vs r (in units of $\ell_{\rm HO}$) at $t = 13\tau_{\rm HO}$. Dashed vertical lines indicate the length ℓ_c over which the velocity field is highly correlated, as defined in Eq. (4).

obtains the integral length scale

$$\ell_c = \int_0^\infty f_i(r)dr. \tag{4}$$

In fluid dynamics, ℓ_c represents the size of the large eddies. In our case, ℓ_c is the length scale over which the velocity field is highly correlated. Figure 8 shows that the correlation functions drop to only $\approx$10% at distances of the order of the average separation between the vortex lines, $\ell \approx 6.1\ell_{\rm HO}$; the last quantity is estimated as $\ell \approx L^{-1/2}$ from the measurement of the vortex line density L (the vortex length per unit volume). Physically, this lack of correlation means that the vortex lines are randomly oriented with respect to each other. The analysis of the correlation function therefore suggests that the turbulent velocity field arising from the decay of antiparallel doubly charged vortices is essentially a random flow.

This result implies that the distribution of the kinetic energy over the length scales, or energy spectrum $E(k)$ (where the wave number k represents the inverse length scale), should be very different from the celebrated Kolmogorov scaling, $E(k) \sim k^{-5/3}$, which is observed in classical turbulence and implies a particular structure of the flow. The importance of the Kolmogorov scaling is that it is the signature of a nonlinear cascade mechanism which transfers energy from large length scales to small length scales. Besides classical turbulence, the Kolmogorov scaling has been observed in helium experiments [62,63] when the turbulence is generated by grids in wind tunnels or by counter-rotating propellers. Numerical simulations [64] revealed that the Kolmogorov scaling is associated with the presence of large-scale polarization (bundles) of vortex lines which become locally parallel to each other; the bundles locally create a net average rotation over length scales larger than ℓ, thus building up energy at wave numbers $k < k_\ell = 2\pi/\ell$ (the hydrodynamical range).

To compute the energy spectrum $E(k)$ of our turbulent condensate, we use a standard procedure [65] to extract

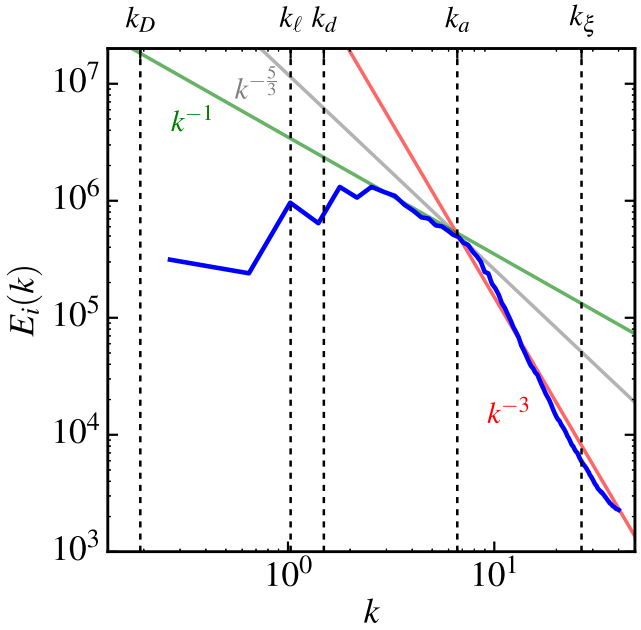

FIG. 9. Decay of two antiparallel doubly charged vortices (quasi-isotropic state). Incompressible kinetic energy spectrum $E_i(k)$ (arbitrary units) vs wave number k (in units of $\ell_{\rm HO}^{-1}$) at $t = 12.8\tau_{\rm HO}$. Vertical lines mark the wave numbers corresponding to the healing length $\xi = 0.24\ell_{\rm HO}$, the vortex core size $a = 0.96\ell_{\rm HO}$, the average distance between vortex lines $\ell = 6.10\ell_{\rm HO}$, and the radial and axial Thomas-Fermi radii $d_{\rm TF} = 4.21\ell_{\rm HO}$ and $D_{\rm TF} = 32.64\ell_{\rm HO}$. Red, gray, and green lines represent the power laws k^{-3}, $k^{-5/3}$, and k^{-1}, respectively.

the incompressible kinetic energy from the total energy, obtaining Fig. 9. To interpret the figure, we mark with vertical lines the wave numbers $k_\xi = 2\pi/\xi$, $k_a = 2\pi/a$, $k_\ell = 2\pi/\ell$, $k_d = 2\pi/d_{\rm TF}$, and $k_D = 2\pi/D_{\rm TF}$, corresponding to the healing length ξ, the vortex core radius a, the average vortex separation ℓ, and the radial and axial Thomas-Fermi radii $d_{\rm TF}$ and $D_{\rm TF}$, respectively. Figure 9 shows that the energy spectrum is not of the Kolmogorov type: under the classical Kolmogorov scenario, most of the energy would be contained in the largest eddies in the small-k region (the apparent deficit, estimated by extrapolating the $k^{-5/3}$ slope to the left, is more than two orders of magnitude). Instead of the $k^{-5/3}$ scaling, we observe the $E(k) \sim k^{-1}$ spectrum, which is characteristic of an isolated straight vortex line. This means that, at distances less than ℓ, the velocity field is dominated by the nearest vortex in the vicinity of the point of observation—the effects of all the other vortices in a random tangle canceling each other out. The range of k space where this scaling takes place is less than a decade because not much k space is available in a typical atomic condensate (unlike superfluid helium and classical fluids), but the scaling is clearly visible (the fact that $k_\ell < k_{\rm TF}$ simply means that, at this time in the decay, the vortex lines are spread throughout the condensate with typical distances ℓ larger than the radial dimension $d_{\rm TF}$; note that $\ell < D_{\rm TF}$, of course.) It is also noteworthy that the $E(k) \sim k^{-3}$ scaling which appears in the region $k_a < k < k_\xi$ is characteristic of the vortex core [66,67]. We conclude that Fig. 9 is consistent with the random flow interpretation which results from the analysis of the correlation functions.

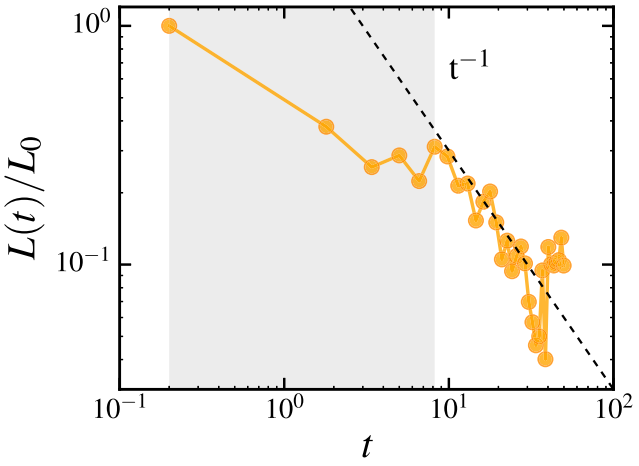

FIG. 10. Time evolution of the vortex line density (t in units of $\tau_{\rm HO}$). The shaded area corresponds to the time elapsed for the decay of the two antiparallel multiply charged vortices, $t \approx 8\tau_{\rm HO}$, after which we only see singly quantized vortices in the system in the quasi-isotropic state.

Besides the correlation function and the energy spectrum, further insight into the nature of our turbulence is acquired by measuring the temporal decay of the vortex line density $L(t)$. This decay is caused by sound radiated away by vortices as they accelerate about each other [68] or reconnect [69] with each other. Figure 10 shows that, at large t, the decay is consistent with the form $L(t) \sim t^{-1}$, as reported for a larger spherical condensates [29]; the decaying turbulence is shown in the second movie in the Supplemental Material [51].

Therefore the short correlation length, the lack of energy at small k, the $E(k) \sim k^{-1}$ scaling of the energy spectrum for large k in the hydrodynamical range, and the $L(t) \sim t^{-1}$ temporal behavior of the decay allow us to identify our quasi-isotropic vortex state as an example of the Vinen turbulent regime in a trapped system.

VII. CONCLUSION

In this work we have explored the decay of initially imprinted multicharged vortices as a method to generate turbulence in a trapped Bose-Einstein condensate, which is relatively free of large surface oscillations and fragmentation (see the Appendix). We have examined the decay of two multicharged vortex systems in a typical cigar-shaped, harmonically confined, atomic Bose-Einstein condensate. The first (a quadruply charged vortex) led to the disordered, anisotropic vortex state. The second (two antiparallel doubly charged vortices) generated helical Kelvin waves on oppositely oriented vortex lines which reconnected, creating a second disordered, quasi-isotropic vortex state. Looking for similarities to classical turbulence in its simplest possible forms—in particular, with the property of isotropy—we have concentrated our attention on the quasi-isotropic state and carefully considered in what sense it is turbulent.

This question is subtle. In classical physics, turbulence implies a large range of length scales which are all excited and interact nonlinearly. In classical fluids, the presence and the intensity of turbulence are inferred from the Reynolds number Re, which must be sufficiently large (typically few thousands, depending on the problem) for turbulence to exist. But the Reynolds number has two definitions. The first definition is

$$\mathrm{Re} = \frac{uD}{\nu}, \tag{5}$$

where D is the system's large length scale, i.e., the system's size or the size of the energy-containing eddies, u is the flow's velocity at that large scale, and ν is the kinematic viscosity; this definition follows directly from the Navier-Stokes equation and measures the ratio of the magnitudes of inertial and viscous forces acting on a fluid parcel. The definition makes apparent why large-scale (e.g., geophysical) flows are always turbulent and why microfluids flows are not (indeed, with microfluids one has to rely on chaos, not turbulence, to achieve any desired mixing). The second definition assumes Kolmogorov theory and is

$$\mathrm{Re} = \left(\frac{D}{\eta}\right)^{4/3}, \tag{6}$$

where η is the length scale of viscous dissipation. This definition measures the degree of separation between the large length scale (at which energy is typically injected) and the small length scale (at which energy is dissipated). In the context of condensates, the two definitions clash with each other: The first definition implies that Re is infinite (because the viscosity is zero), and the second that Re is not much larger than unity (because the size of a typical condensate is larger, but not orders of magnitude larger, than the healing length, which can be considered the length scale at which acoustic dissipation of kinetic energy occurs). Although interesting work is in progress to identify a definition of Reynolds number suitable for a superfluid system (for example, exploring dynamical similarities [70]), to answer the question which we asked, at this stage, we have to leave the Reynolds number and proceed in other ways.

We have therefore carefully examined the properties of the disordered, quasi-isotropic state in terms of velocity statistics, energy spectrum, correlation function, and temporal decay and compared them to the properties of classical turbulence and of turbulent superfluid helium. Clearly, the quasi-isotropic state does not compare well with the properties of classical turbulence. Despite the limited range of length scales available in a small BEC, we conclude that, in the decay of the two antiparallel doubly charged vortices, the quasi-isotropy of our disordered state, the short correlation length, the properties of the energy spectrum, and the temporal behavior of the vortex decay identify our disordered, quasi-isotropic vortex state as an example of the Vinen turbulent regime first discovered in superfluid helium at low temperatures, which is interpreted as a state of turbulence without an energy cascade.

The nature of the disorder, or turbulence, in the anisotropic case generated by the decay of the single quadruply charged vortex will be the subject of future investigations: one should vary the amount of polarization and study fluctuations of the velocity field over the mean rotating flow. There are no numerical studies yet of such turbulence in trapped Bose systems, and (because of the role played by boundaries in the spin-down of viscous flows) no immediate classical analogies, so this case is less straightforward to analyze; spin-down dynamics experiments in superfluid helium [71–73] should be the main reference systems.

In summary, our scheme describes a controllable system to investigate different regimes of quantum turbulence in trapped atomic condensates, where isotropy could be a tunable parameter (depending on the initial configuration of multicharged vortices). This control, alongside the versatility of experiments with condensates, could shed light on fundamental aspects of turbulence. Future work will, for instance, address the next natural question: Can the classical Kolmogorov regime be achieved in much larger condensates under suitable forcing at the largest length scale, as suggested by some numerical simulations [28], thus identifying the crossover between Vinen and Kolmogorov turbulence?

Finally, an important question which must be addressed by further work is whether Vinen turbulence is unique to superfluids or can be generated also in classical fluids. If the definying property of Vinen turbulence is, as it seems [5], the absence of a Kolmogorov energy cascade, the line of inquiry should start with studies of turbulent flows in wind tunnels with fractal (rather than uniform) grids, which suggest the absence of an energy cascade [74].

Data supporting this publication is openly available under an 'Open Data Commons Open Database License'. Additional metadata are available in Ref. [76]. Please contact Newcastle Research Data Service at rdm@ncl.ac.uk for access instructions.

ACKNOWLEDGMENTS

We acknowledge financial support from CAPES (PDSE Proc. No. BEX 9637/14-1), CNPq, FAPESP (program CEPID), EPSRC Grant No. EP/I019413/1, and JSPS Grant No. KAKENHI-16K05461. This research was developed making use of the computational resources (Euler cluster) of the Center for Mathematical Sciences Applied to Industry (Centro de Ciências Matemáticas Aplicadas à Indústria; CeMEAI) financed by FAPESP.

APPENDIX: CHARACTERIZING SURFACE OSCILLATIONS

In order to quantify our claim that the generation of turbulence via the decay of multicharged vortices reduces large surface oscillations of the condensate and prevents fragmentation, we introduce the following *isoperimetric quotient* [75] as a measure of the condensate's surface oscillations, or "wobbliness":

$$Q \equiv \frac{4\pi A}{P^2}, \tag{A1}$$

where P is the perimeter of a closed curve C, and A the area enclosed by it. This quantity intuitively quantifies the departure from circularity. Q equals its maximum value 1 for a perfect circle and reaches smaller values for greater surface oscillations of C.

For the time evolution of our quasi-isotropic case, we define a curve C representing the edge of the condensate for a transverse cross section. An average over 40 adjacent cross sections (separated by the numerical spatial resolution) from a thin, horizontal stripe around the center of the axial z axis (equivalent to less than a tenth of the condensate z direction extension) was necessary to avoid numerical issues in the definition of the condensate edge. See examples shown in Figs. 11(a) and 11(b) for the (green) curve C, compared to the radial Thomas-Fermi (magenta) circumference, for the initial state and a turbulent instant, respectively.

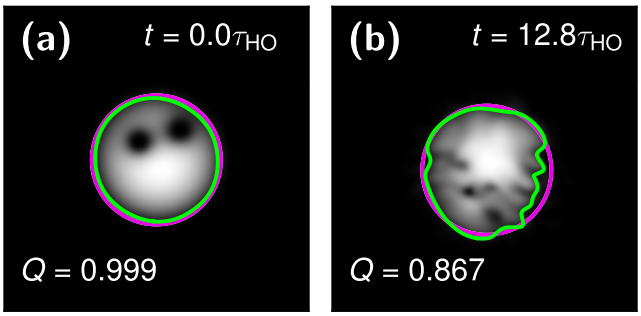

FIG. 11. Transverse cross section of the condensate in the quasi-isotropic case. The green curve defines the condensate edge C compared to the magenta curve, representing the radial Thomas-Fermi circumference for (a) the initial state and (b) at a turbulent instant. The circularity of both edges is given by Q as defined in Eq. (A1).

In Fig. 12, we see the values of Q for the entire evolution. For the sake of comparison, we apply the same analysis to images taken from simulations [58] of a combined shaking and rotation of the trap that has been successfully used to generate quantum turbulence in BECs [27]. In particular, applying the criterion to images from Fig. 3 in [58], at times of 15.54 and 15.92 ms, we find $Q = 0.401$ and $Q = 0.386$, respectively. Their described technique clearly excites high-amplitude modes, such as scissors modes and dipolar oscillations, including other large density fluctuations, which justify such low values of circularity, compared to the induction of turbulence from the decay of multicharged vortices. We conclude that for all instants, Q is much closer to 1 in our case, suggesting less perturbation of the condensate's surface. Not only does our method generate a less wobbly condensate, but also the center of mass of the cloud stays practically still, as opposed to the case in [58]. The absence of large oscillations of the center of mass in our scheme offers a practical advantage for experiments which make use of time-of-flight imaging. The less momentum the cloud's center of mass acquires, the easier to focus when taking the time-of-flight absorption image.

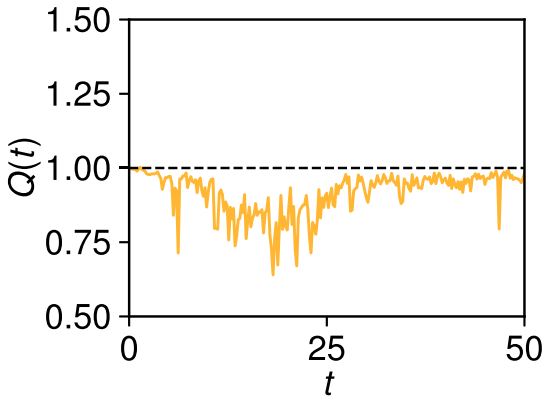

FIG. 12. Time evolution of the isoperimetric quotient (t in units of τ_{HO}).

[1] C. F. Barenghi, V. S. L'vov, and P.-E. Roche, Proc. Natl. Acad. Sci. USA **111**, 4683 (2014).
[2] U. Frisch, *Turbulence: The Legacy of A. N. Kolmogorov* (Cambridge University Press, Cambridge, UK, 1995).
[3] R. Hänninen and A. W. Baggaley, Proc. Natl. Acad. Sci. USA **111**, 4667 (2014).
[4] P. M. Walmsley and A. I. Golov, Phys. Rev. Lett. **100**, 245301 (2008).
[5] C. F. Barenghi, Y. A. Sergeev, and A. W. Baggaley, Sci. Rep. **6**, 35701 (2016).
[6] A. W. Baggaley, C. F. Barenghi, and Y. A. Sergeev, Phys. Rev. B **85**, 060501 (2012).
[7] W. Vinen, in *Proceedings of the Royal Society of London A: Mathematical, Physical and Engineering Sciences*, Vol. 240 (The Royal Society, London, 1957), pp. 114–127.
[8] A. W. Baggaley, L. K. Sherwin, C. F. Barenghi, and Y. A. Sergeev, Phys. Rev. B **86**, 104501 (2012).
[9] G. W. Stagg, N. G. Parker, and C. F. Barenghi, Phys. Rev. A **94**, 053632 (2016).
[10] N. G. Berloff and B. V. Svistunov, Phys. Rev. A **66**, 013603 (2002).
[11] G. E. Volovik, JETP Lett. **78**, 533 (2003).
[12] T. Aioi, T. Kadokura, T. Kishimoto, and H. Saito, Phys. Rev. X **1**, 021003 (2011).
[13] M. C. Davis, R. Carretero-González, Z. Shi, K. J. H. Law, P. G. Kevrekidis, and B. P. Anderson, Phys. Rev. A **80**, 023604 (2009).
[14] K. W. Madison, F. Chevy, W. Wohlleben, and J. Dalibard, Phys. Rev. Lett. **84**, 806 (2000).
[15] C. Raman, J. R. Abo-Shaeer, J. M. Vogels, K. Xu, and W. Ketterle, Phys. Rev. Lett. **87**, 210402 (2001).
[16] D. V. Freilich, D. M. Bianchi, A. M. Kaufman, T. K. Langin, and D. S. Hall, Science **329**, 1182 (2010).
[17] M. C. Tsatsos, P. E. Tavares, A. Cidrim, A. R. Fritsch, M. A. Caracanhas, F. E. A. dos Santos, C. F. Barenghi, and V. S. Bagnato, Phys. Rep. **622**, 1 (2016).
[18] C. F. Barenghi, L. Skrbek, and K. R. Sreenivasan, Proc. Natl. Acad. Sci. USA **111**, 4647 (2014).
[19] L. Skrbek and K. R. Sreenivasan, Phys. Fluids **24**, 011301 (2012).
[20] T. W. Neely, E. C. Samson, A. S. Bradley, M. J. Davis, and B. P. Anderson, Phys. Rev. Lett. **104**, 160401 (2010).
[21] A. C. White, C. F. Barenghi, and N. P. Proukakis, Phys. Rev. A **86**, 013635 (2012).
[22] A. C. White, N. P. Proukakis, and C. F. Barenghi, J. Phys.: Conf. Ser. **544**, 012021 (2014).
[23] W. J. Kwon, G. Moon, J. Y. Choi, S. W. Seo, and Y. I. Shin, Phys. Rev. A **90**, 063627 (2014).
[24] G. W. Stagg, A. J. Allen, N. G. Parker, and C. F. Barenghi, Phys. Rev. A **91**, 013612 (2015).
[25] A. J. Allen, N. G. Parker, N. P. Proukakis, and C. F. Barenghi, Phys. Rev. A **89**, 025602 (2014).
[26] A. Cidrim, F. E. A. dos Santos, L. Galantucci, V. S. Bagnato, and C. F. Barenghi, Phys. Rev. A **93**, 033651 (2016).
[27] E. A. L. Henn, J. A. Seman, G. Roati, K. M. F. Magalhães, and V. S. Bagnato, Phys. Rev. Lett. **103**, 045301 (2009).
[28] M. Kobayashi and M. Tsubota, Phys. Rev. A **76**, 045603 (2007).
[29] A. C. White, C. F. Barenghi, N. P. Proukakis, A. J. Youd, and D. H. Wacks, Phys. Rev. Lett. **104**, 075301 (2010).
[30] C. N. Weiler, T. W. Neely, D. R. Scherer, A. S. Bradley, M. J. Davis, and B. P. Anderson, Nature **455**, 948 (2008).
[31] L. Chomaz, L. Corman, T. Bienaimé, R. Desbuquois, C. Weitenberg, S. Nascimbène, J. Beugnon, and J. Dalibard, Nat. Commun. **6**, 6162 (2015).
[32] G. Lamporesi, S. Donadello, S. Serafini, F. Dalfovo, and G. Ferrari, Nat. Phys. **9**, 656 (2013).
[33] N. Navon, A. L. Gaunt, R. P. Smith, and Z. Hadzibabic, Science **347**, 167 (2015).
[34] N. G. Parker and C. S. Adams, Phys. Rev. Lett. **95**, 145301 (2005).
[35] C. Barenghi and N. Parker, *A Primer on Quantum Fluids*, Springer Briefs in Physics (Springer International, Cham, Switzerland, 2016).
[36] Y. Shin, M. Saba, M. Vengalattore, T. A. Pasquini, C. Sanner, A. E. Leanhardt, M. Prentiss, D. E. Pritchard, and W. Ketterle, Phys. Rev. Lett. **93**, 160406 (2004).
[37] M. Kumakura, T. Hirotani, M. Okano, Y. Takahashi, and T. Yabuzaki, Phys. Rev. A **73**, 063605 (2006).
[38] M. Okano, H. Yasuda, K. Kasa, M. Kumakura, and Y. Takahashi, J. Low Temp. Phys. **148**, 447 (2007).
[39] T. Isoshima, M. Okano, H. Yasuda, K. Kasa, J. A. M. Huhtamäki, M. Kumakura, and Y. Takahashi, Phys. Rev. Lett. **99**, 200403 (2007).
[40] H. Pu, C. K. Law, J. H. Eberly, and N. P. Bigelow, Phys. Rev. A **59**, 1533 (1999).
[41] M. Möttönen, T. Mizushima, T. Isoshima, M. M. Salomaa, and K. Machida, Phys. Rev. A **68**, 023611 (2003).
[42] J. A. M. Huhtamäki, M. Möttönen, and S. M. M. Virtanen, Phys. Rev. A **74**, 063619 (2006).
[43] J. A. M. Huhtamäki, M. Möttönen, T. Isoshima, V. Pietilä, and S. M. M. Virtanen, Phys. Rev. Lett. **97**, 110406 (2006).
[44] A. M. Mateo and V. Delgado, Phys. Rev. Lett. **97**, 180409 (2006).
[45] T. Kuwamoto, H. Usuda, S. Tojo, and T. Hirano, J. Phys. Soc. Jpn. **79**, 034004 (2010).
[46] P. Kuopanportti and M. Möttönen, Phys. Rev. A **81**, 033627 (2010).
[47] M. Nakahara, T. Isoshima, K. Machida, S.-i. Ogawa, and T. Ohmi, Physica B: Condens. Matter **284-288**, 17 (2000).
[48] A. E. Leanhardt, A. Görlitz, A. P. Chikkatur, D. Kielpinski, Y. Shin, D. E. Pritchard, and W. Ketterle, Phys. Rev. Lett. **89**, 190403 (2002).
[49] Y. Kawaguchi and T. Ohmi, Phys. Rev. A **70**, 043610 (2004).
[50] G. R. Dennis, J. J. Hope, and M. T. Johnsson, Comput. Phys. Commun. **184**, 201 (2013).
[51] See Supplemental Material at http://link.aps.org/supplemental/10.1103/PhysRevA.96.023617. Movie 1: real decay of a $j = 4$ multicharged vortex line. Movie 2: real decay of two antiparallel, doubly charged vortex lines.
[52] E. Fonda, D. P. Meichle, N. T. Ouellette, S. Hormoz, and D. P. Lathrop, Proc. Natl. Acad. Sci. USA **111**, 4707 (2014).
[53] V. Bretin, P. Rosenbusch, F. Chevy, G. V. Shlyapnikov, and J. Dalibard, Phys. Rev. Lett. **90**, 100403 (2003).
[54] N. L. Smith, W. H. Heathcote, J. M. Krueger, and C. J. Foot, Phys. Rev. Lett. **93**, 080406 (2004).
[55] T. P. Simula, Phys. Rev. A **84**, 021603 (2011).
[56] S. Stringari, Phys. Rev. Lett. **77**, 2360 (1996).
[57] G. Watanabe, Phys. Rev. A **73**, 013616 (2006).

[58] J. A. Seman, E. A. L. Henn, R. F. Shiozaki, G. Roati, F. J. Poveda-Cuevas, K. M. F. Magalhães, V. I. Yukalov, M. Tsubota, M. Kobayashi, K. Kasamatsu *et al.*, Laser Phys. Lett. **8**, 691 (2011).

[59] M. S. Paoletti, M. E. Fisher, K. R. Sreenivasan, and D. P. Lathrop, Phys. Rev. Lett. **101**, 154501 (2008).

[60] The definition is $\mathrm{gPDF}(v_i)=(2\pi\sigma_i^2)^{-1/2}\exp[-(v_i-\mu_i)^2/(2\sigma_i^2)]$, where μ_i and σ_i $(i=x,y,z)$ are the mean values and the standard deviations, respectively.

[61] P. Davidson, *Turbulence: An Introduction for Scientists and Engineers* (Oxford University Press, Oxford, UK, 2004).

[62] J. Maurer and P. Tabeling, Europhys. Lett. **43**, 29 (1998).

[63] J. Salort, C. Baudet, B. Castaing, B. Chabaud, F. Daviaud, T. Didelot, P. Diribarne, B. Dubrulle, Y. Gagne, F. Gauthier, A. Girard, B. Hébral, B. Rousset, P. Thibault, and P.-E. Roche, Phys. Fluids **22**, 125102 (2010).

[64] A. W. Baggaley, J. Laurie, and C. F. Barenghi, Phys. Rev. Lett. **109**, 205304 (2012).

[65] C. Nore, M. Abid, and M. E. Brachet, Phys. Rev. Lett. **78**, 3896 (1997).

[66] G. Krstulovic and M. Brachet, Phys. Rev. Lett. **105**, 129401 (2010).

[67] A. S. Bradley and B. P. Anderson, Phys. Rev. X **2**, 041001 (2012).

[68] M. Leadbeater, D. C. Samuels, C. F. Barenghi, and C. S. Adams, Phys. Rev. A **67**, 015601 (2003).

[69] M. Leadbeater, T. Winiecki, D. C. Samuels, C. F. Barenghi, and C. S. Adams, Phys. Rev. Lett. **86**, 1410 (2001).

[70] M. T. Reeves, T. P. Billam, B. P. Anderson, and A. S. Bradley, Phys. Rev. Lett. **114**, 155302 (2015).

[71] P. Walmsley, A. Golov, H. Hall, W. Vinen, and A. Levchenko, J. Low Temp. Phys. **153**, 127 (2008).

[72] J. Hosio, V. Eltsov, P. Heikkinen, R. Hänninen, M. Krusius, and V. L'vov, Nat. Commun. **4**, 1614 (2013).

[73] J. J. Hosio, V. B. Eltsov, M. Krusius, and J. T. Mäkinen, Phys. Rev. B **85**, 224526 (2012).

[74] N. Mazellier and J. C. Vassilicos, Phys. Fluids **22**, 075101 (2010).

[75] H. T. Croft, K. Falconer, and R. K. Guy, *Unsolved Problems in Geometry: Unsolved Problems in Intuitive Mathematics*, Vol. 2 (Springer Science & Business Media, Berlin, 2012).

[76] A. Cidrim, A. White, A. J. Allen, V. Bagnato, and C. Barenghi, Numerical data from mean-field simulations of a trapped atomic superfluid in a Vinen turbulent regime, Newcastle University, 2017, doi:10.17634/101785-6.

5.2 Supplementary material:

5.2.1 Highlighting vortices: pseudo-vorticity

We know from Eq. (2.52) that vorticity ($\nabla \times \mathbf{v}$) in quantum fluids is singular over a vortex line. This definition thus makes any analogy with vorticity in classical fluids very restrictive. A way to circumvent this pathological definition is to substitute it by the concept of *pseudo-vorticity*.[94,95] In this case, (pseudo-)vorticity is given by

$$\vec{\omega}_{\text{pseudo}} \equiv \nabla \times \mathbf{j}, \tag{5.1}$$

where $\mathbf{j} = \rho\mathbf{v}$, as discussed in Sec. 2.4.

In fact, a vortex is a line over which the condensate wavefunction goes to zero, implying that both ψ_{R} and ψ_{I} are also null. This means that the density ρ along a direction $\hat{\omega}$ that is defined to be parallel to the vortex line must not change. That is to say

$$\hat{\omega} \cdot \nabla\rho = 0, \tag{5.2}$$

and, in particular,

$$\hat{\omega} \cdot \nabla\psi_{\text{R}} = \hat{\omega} \cdot \nabla\psi_{\text{I}} = 0. \tag{5.3}$$

The above equation tells us that the orientation of a vortex line is always perpendicular to the spatial variations of ψ_{R} and ψ_{I}, which implies that $\hat{\omega}$ can only be given by

$$\hat{\omega}_{\text{pseudo}} \equiv \frac{\nabla\psi_{\text{R}} \times \nabla\psi_{\text{I}}}{|\nabla\psi_{\text{R}} \times \nabla\psi_{\text{I}}|}, \tag{5.4}$$

which is a unit vector whose direction defines the orientation of a vortex. Substituting the explicit form of $\mathbf{v}$ in (5.1) one can show that it is equivalent to (5.4).

In order to identify and highlight a vortex in our simulations, we have calculated the pseudo-vorticity and defined the isosurface that encloses a vortex-line with radius $r \sim \xi$ to approximately match the vortex core (see blue isosurface in Fig. 1 from publication). This allows us to calculate the important quantity of the total vortex line density L (as measured in Fig. 10 of the publication), since the total volume of the isosurface is equivalent to the total volume occupied by the vortices. This method is also a useful alternative to identify vortices in 2D. In the latter case, the direction of the pseudo-vorticity vector (either up or down) defines the vortex sign (positive or negative), while its magnitude's maximum value pin-points the center of the vortex core.

5.2.2 Fourier analysis: radial oscillations

In order to identify the radial oscillation frequencies in the publication, a Fourier decomposition was used to filter the main modes as shows Fig. 16. The top plots, (a) and (d), show the data (dots) for radial oscillations in the anisotropic and quasi-isotropic cases, respectively. The full lines are result of the filtered frequencies, as shows the respective bottom plots.

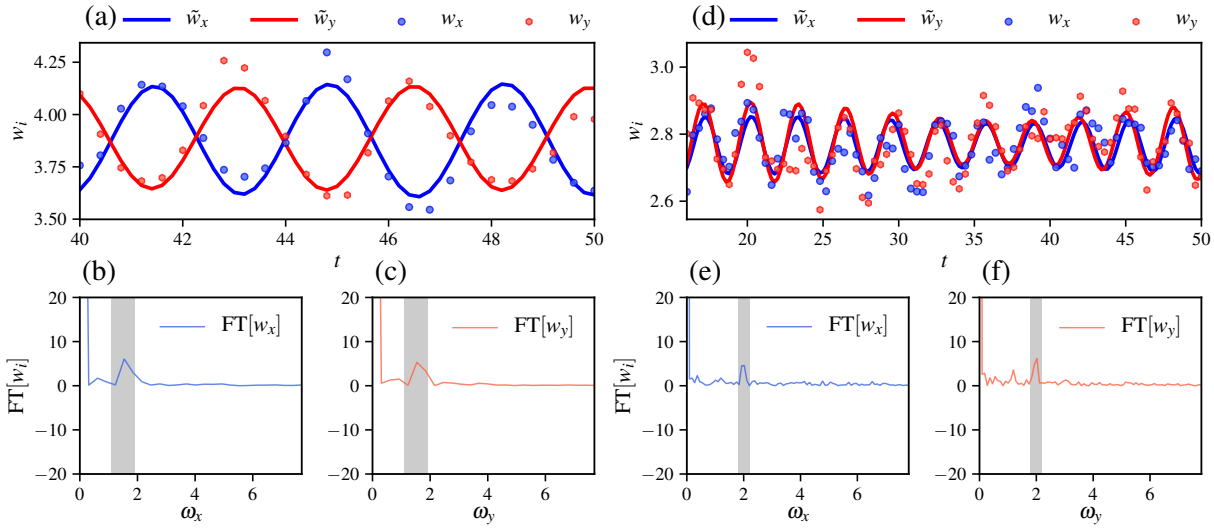

Figure 16 – **(a)**/**(b)** Radial oscillations for the anisotropic/quasi-isotropic case. Data (w_x and w_y) for earlier times are omitted in the plots, since large amplitude modes (see Figs. 3 and 6 in publication) are present and complicate visual comparison with the filtered results ($\tilde{w}_x$ and $\tilde{w}_y$). **(b)**/**(e)** and **(c)**/**(f)** show the Fourier decomposition of radial oscillations in x and y directions, where the gray area indicates the filtered region used to match frequencies in the top plots.
Source: By the author.

5.3 Prospect: scalings of density spectrum

Whilst there are extensive numerical studies on the scalings of the energy spectrum $E(k)$ in hydrodynamic quantum turbulence, little is known about the influence of vortices on the density spectrum $n(k)$ and the role played by other nonlinear structures. In a practical point of view, experiments with atomic BECs allow for a relatively easy access to the density spectrum $n(k)$, as opposed to $E(k)$. The former is a straightforward result of long time-of-flight (TOF) absorption images of expanding condensates,[85] and knowing its behavior may offer more insight on characteristics of the turbulence under investigation. In Sec. 3.9, for instance, we have briefly discussed the existence of wave-turbulence, which may (and typically do) coexist with hydrodynamic turbulence. We have also pointed out the still open problem of the appropriate scaling expected for the case of a strong condensate as a background for sound-waves (mentioning contradictory results in the literature). As a prospect for our numerical investigations, we present below the behavior of $n(k)$ for our trapped system, while comparing to analogous, homogeneous cases. Further development of this study can provide hints on which analytical approach (if any) is more appropriate to describe statistical properties of these realistic systems.

Similarly to what we have done with the energy spectrum, we evaluate the density momentum distribution of the quasi-isotropic regime described in the publication, obtaining a power-law behavior of $n(k) \sim k^{-3}$ at the apex of hydrodynamic turbulence ($t \sim 12.8$), as

shows Fig. 17. Our simulations were devised to match the real parameters of experiments performed in our group's laboratory.[85,93]

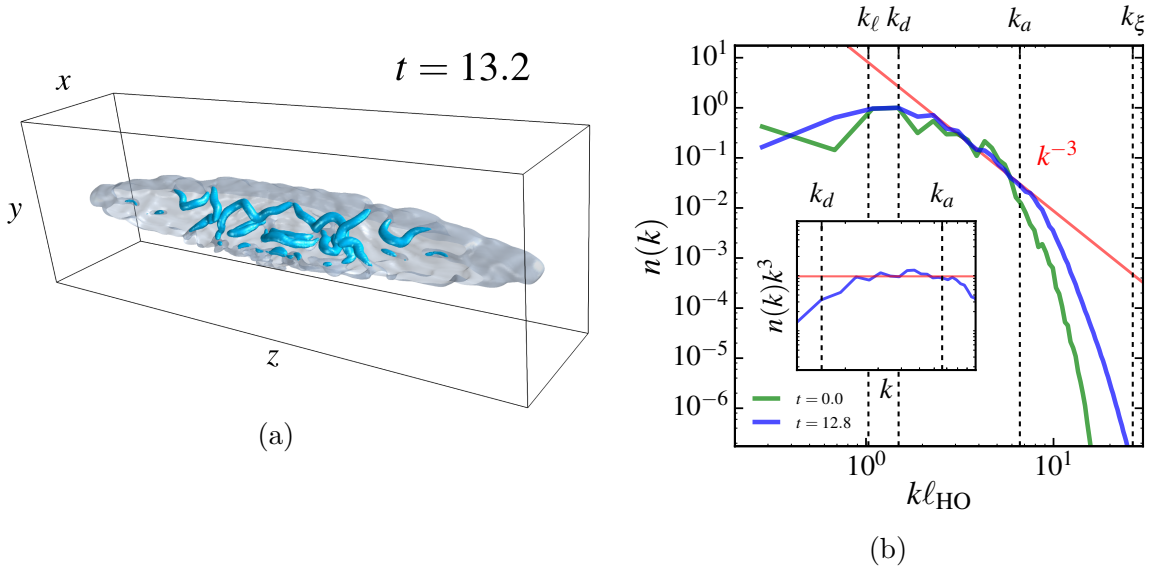

Figure 17 – **(a)** Vinen turbulence in a trapped system. **(b)** Corresponding density momentum distribution. We see the scaling of k^{-3} for almost a decade, as shows inset in a compensated plot of $n(k)$.
Source: By the author.

5.3.1 Comparing with homogeneous systems

In order to compare our results with more paradigmatic systems, we simulate two different homogeneous systems and compute the density spectrum, as well. For this matter, it is convenient to write the GPE in dimensionless, homogeneous form as follows

$$i\frac{\partial\psi}{\partial t} = \left[-\frac{1}{2}\nabla^2 + \left(|\psi|^2 - 1\right)\right]\psi, \tag{5.5}$$

where space, energy, and time are in the characteristic units of the healing length ξ, chemical potential μ, and $\hbar/\mu$, respectively. The dynamics is solved numerically in the 3D domain $-L \leq x, y, z \leq L$ with $L = 48\ \xi$ and grid size of 128^3 to ensure a spatial resolution of $0.75\ \xi$. The integration is performed using the 4th order Runge-Kutta method with a time-step $\Delta t = 10^{-3}$.

Stacking vortices – In this first case, the initial state is created by randomly stacking vortex lines in three perpendicular directions over a homogeneous background. The initial vortex distribution can be seen in Fig. 18(a). As expected, since no large scale flow is created, the incompressible kinetic energy spectrum is characterized by a k^{-1} scaling [see Fig. 18(b)], an example of Vinen regime of hydrodynamic turbulence. For the density spectrum, as in the trapped system, we also observe a scaling consistent with the k^{-3}, as seen in Fig. 18(c).

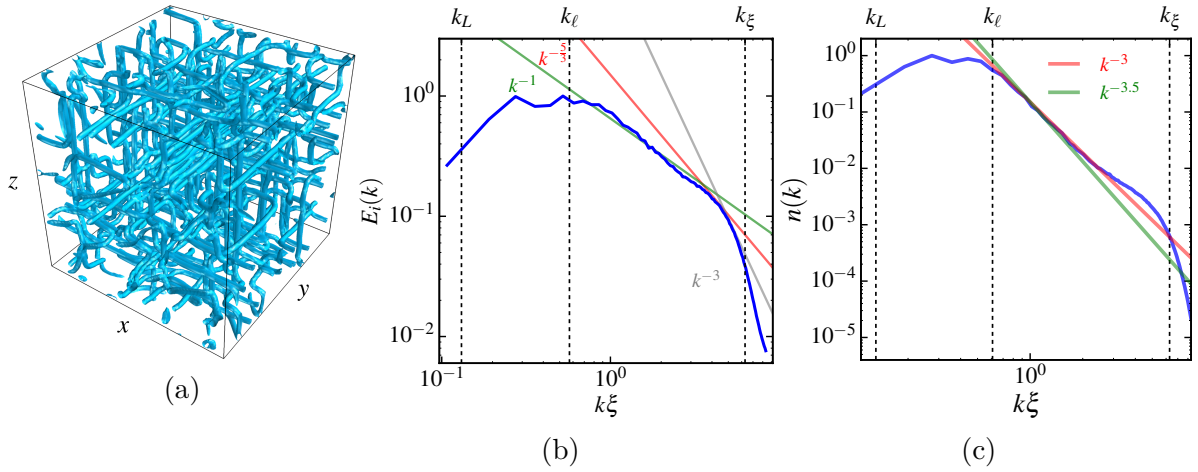

Figure 18 – Plots for the stacked vortices. **(a)** Turbulent flow created by stacking vortices in three perpendicular directions. **(b)** Incompressible kinetic energy spectrum follows a Vinen-like k^{-1} scaling. **(c)** Corresponding density momentum distribution for the homogeneous random-flow system.
Source: By the author.

Imprinting random vortex rings – In this second homogeneous case, the initial state is constructed by imprinting randomly distributed vortex rings (adapting the ring solutions proposed by Helm et al.[96]), which are allowed to have random radii (as large as $30\xi \sim L$), with both center and propagation direction arbitrarily oriented in all space. In Fig. 19 we see the initial vortex distribution and the corresponding spectra for later time in the evolution. We again observe the k^{-3} scaling for $n(k)$.

A Kolmogorov-like energy spectrum is observed for this second case [Fig. 19(b)], although one must beware of the scale-range over which the power-law $k^{-5/3}$ appears. Momenta $k \gtrsim k_\ell$ indicate spatial scales smaller or of the order of the typical inter-vortex distance, therefore not suggesting a proper quasi-classical limit. Although this system is homogeneous (much larger than the trapped case considered above) it still lacks energy in large scales, as shows the energy spectrum for $k < k_\ell$. The same limitation was observed for similar simulations of hydrodynamic turbulence of the homogeneous GPE,[97] once incorrectly claimed to be associated with the quasi-classical interpretation of quantum turbulence. While still debatable, the probable real reason behind this coincident scaling may instead be linked to strongly nonlinear Kelvin waves, as pointed out by Nazarenko.[80] This latter result was obtained under the formalism of four-wave turbulence[87] (as we have anticipated in the discussion of Eq. 3.42 and analogous Fig. 5).

5.3.2 Preliminary conclusions and open questions

We see that in all three cases $n(k) \sim k^{-3}$. Although we lack theoretical support to completely understand this behavior, it is reasonable to assume that wave-turbulence plays a major role. The analytical prediction provided by Fujimoto et al.[79] [Eq. (3.38)],

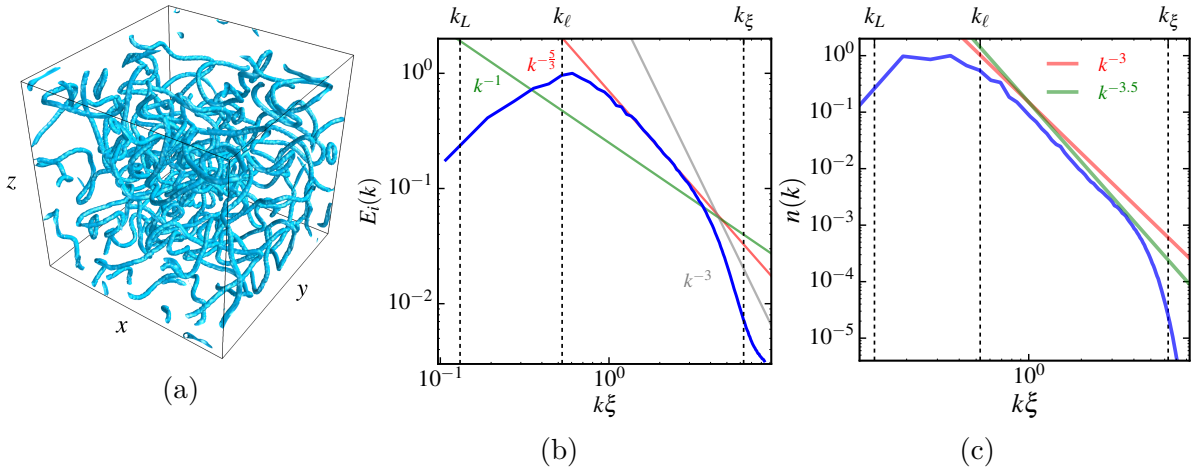

Figure 19 – Plots for the stacked vortices. **(a)** Turbulent flow created by randomly imprinting vortex rings. **(b)** Incompressible kinetic energy spectrum follows a Kolmogorov-like $k^{-5/3}$ scaling. **(c)** Corresponding density momentum distribution.
Source: By the author.

despite assuming weak interaction of waves and neglecting the effects of vortices, can provide some insight in the possible cascade involved in this scaling. When comparing to current experiments which have measured $n(k)$, this scaling agrees with the power-law observed for a trapped, turbulent BEC cloud (with similar dimensions) investigated in our group[85] [$n(k) \sim k^{-2.9}$] and resembles the scaling determined in recent experiment for a box-trapped BEC[98] [$n(k) \sim k^{-3.5}$].

This problem poses interesting questions and offers the opportunity to test idealized models. One aspect that can be analyzed is the limitation of weak-wave turbulence to explain the scaling observed. How does the presence of vortices and other stronger nonlinearities, for instance, change the predictions of the theory? Another particularity of our system lies on its finite size. The anisotropy influence on the spectrum (although expected for spatial scales larger than inter-vortex distances) may impose deviations from theoretical predictions, which are typically obtained under the assumption of homogeneity and isotropy. These open questions will be object of future investigations.

6 CONCLUSIONS AND PROSPECTS

In this thesis our main focus was to investigate hydrodynamic (or vortex) quantum turbulence in trapped atomic BECs. Although this field has seen great advances in the past decade, both theoretical and experimental, the characterization of the turbulence in such systems is often a challenge for the lack of analytical approaches. For this reason, we have first discussed here how to characterize quantum turbulence in this context, showing the limits of usual analogies with classical hydrodynamics and seminal interpretations of turbulence in superfluid Helium. As a general conclusion, due to their lack of available length scales, our investigated systems can only fit the ultraquantum (or Vinen) type of quantum turbulence. Given that, we explore numerically both two and three-dimensional turbulence, making use of dynamical instability of multicharged vortices as an onset for complex dynamics.

In 2D, we have proposed an experimentally feasible scheme that allows the control over vortex polarization in the harmonically trapped system.[73] This setup is then used to study how turbulence decays in such a scenario, through the phenomenological modeling of the vortex-number rate equation. Our proposed description allowed us to conclude that vortex annihilation in these trapped systems is a four-vortex process. Subsequently, we have also verified that different finite-temperature models may have distinct predictions regarding the decay of a 2D giant vortex. As can be expected, shortly after the giant-vortex splitting process, singly-charged vortices tend to cluster differently depending on the spatial profile of the phenomenological dissipation parameter. As a prospect, we have shown the possibility of experimentally exploring the giant-vortex decay dynamics as testbed for different finite temperature models.

Finally, in 3D, we have first provided a study on the decay of a quadruply-charged vortex, also in a harmonically trapped BEC.[75] Having this setting as a comparison point, we propose a quasi-isotropic turbulent system, starting from an initial state of two phase-imprinted, anti-parallel vortices. The vortex turbulence arisen from such configuration was shown to behave in the Vinen turbulent regime, after we characterized specific features of the decay, such as the energy spectrum $[E(k) \sim k^{-1}]$ and the time evolution of the vortex-line density $[L(t) \sim t^{-1}]$. Although these features have been frequently verified in the context of superfluid Helium turbulence, this is the first time these identification was done for realistic, trapped atomic BECs. As an extension to our investigations, we have also presented preliminary studies on the density distribution $n(k)$ in this 3D trapped system, which indicates the appearance of a power-law k^{-3} (despite the anisotropy). This is consistent with both wave-turbulence theory[80] and few existing experimental results.[85,98]

REFERENCES

1 FEYNMAN, R. P. Application of quantum mechanics to liquid helium. **Progress in Low Temperature Physics**, v. 1, n. 17, p. U53, 1955.

2 SKRBEK, L.; SREENIVASAN, K. R. Developed quantum turbulence and its decay. **Physics of Fluids**, v. 24, n. 1, p. 011301, 2012.

3 BARENGHI, C. F.; SKRBEK, L.; SREENIVASAN, K. R. Introduction to quantum turbulence. **Proceedings of the National Academy of Sciences of the United States of America**, v. 111, suppl. 1, p. 4647–52, 2014.

4 MAURER, J.; TABELING, P. Local investigation of superfluid turbulence. **Europhysics Letters**, v. 43, n. 1, p. 29–34, 1998.

5 HENN, E. et al. Emergence of turbulence in an oscillating Bose-Einstein condensate. **Physical Review Letters**, v. 103, n. 4, p. 045301, 2009.

6 HENN, E. A. L. et al. Generation of vortices and observation of quantum turbulence in an oscillating Bose-Einstein condensate. **Journal of Low Temperature Physics**, v. 158, n. 3-4, p. 435–442, 2009.

7 HENN, E. et al. Observation of vortex formation in an oscillating trapped Bose-Einstein condensate. **Physical Review A**, v. 79, n. 4, p. 043618, 2009.

8 SEMAN, J. et al. Route to turbulence in a trapped Bose-Einstein condensate. **Laser Physics Letters**, v. 8, n. 9, p. 691, 2011.

9 NEELY, T. W. et al. Characteristics of two-dimensional quantum turbulence in a compressible superfluid. **Physical Review Letters**, v. 111, n. 23, p. 235301, 2013.

10 KWON, W. J. et al. Relaxation of superfluid turbulence in highly oblate Bose-Einstein condensates. **Physical Review A**, v. 90, n. 6, p. 063627, 2014.

11 LEGGETT, A. J. **Quantum liquids:** Bose condensation and Cooper pairing in condensed-matter systems. Oxford: Oxford University Press, 2006.

12 SALINAS, S. **Introduction to statistical physics**. Berlin: Springer Science & Business Media, 2013.

13 BOSE, S. N. Plancks Gesetz und Lichtquantenhypothese (Planck's law and light quantum hypothesis). **Zeitschrift für Physik**, v. 26, n. 1, p. 178, 1924.

14 PENROSE, O.; ONSAGER, L. Bose-Einstein condensation and liquid helium. **Physical Review**, v. 104, n. 3, p. 576, 1956.

15 TSATSOS, M. C. et al. Quantum turbulence in trapped atomic Bose-Einstein condensates. **Physics Reports**, v. 622, p. 1, 2016. doi:10.1016/j.physrep.2016.02.003.

16 MERZBACHER, E. **Quantum mechanics**. New York: John Wiley & Sons, 1998.

17 PETHICK, C.; SMITH, H. **Bose-Einstein condensation in dilute gases**. Oxford: Oxford University Press, 2008.

18 GROSS, E. P. Structure of a quantized vortex in boson systems. **Nuovo Cimento**, v. 81, n. 3, p. 454, 1961.

19 PITAEVSKII, L. P. Vortex lines in an imperfect Bose gas. **Soviet Journal of Experimental and Theoretical Physics**, v. 13, n. 2, p. 445, 1961.

20 LONDON, F. On the Bose-Einstein condensation. **Physical Review**, v. 54, n. 11, p. 947, 1938.

21 TILLEY, D. R.; TILLEY, J. **Superfluidity and superconductivity**. Boca Raton: CRC Press, 1990.

22 LANDAU, L. Theory of the superfluidity of helium II. **Physical Review**, v. 60, n. 4, p. 356, 1941.

23 FETTER, A.; SVIDZINSKY, A. A. Vortices in a trapped dilute Bose-Einstein condensate. **Journal of Physics:** condensed matter, v. 13, n. 12, p. R135, 2001.

24 FETTER, A. Rotating trapped Bose-Einstein condensates. **Reviews of Modern Physics**, v. 81, n. 2, p. 647–691, 2009.

25 TISZA, L. Transport phenomena in helium II. **Nature**, v. 141, n. 3577, p. 913, 1938.

26 FRISCH, T.; POMEAU, Y.; RICA, S. Transition to dissipation in a model of superflow. **Physical Review Letters**, v. 69, n. 11, p. 1644–1647, 1992.

27 JACKSON, B.; MCCANN, J.; ADAMS, C. Vortex formation in dilute inhomogeneous Bose-Einstein condensates. **Physical Review Letters**, v. 80, n. 18, p. 3903, 1998.

28 BERLOFF, N. G.; ROBERTS, P. H. Motions in a Bose condensate: boundary-layer separation. **Journal of Physics A:** mathematical and general, v. 33, n. 22, p. 4025–4038, 2000.

29 WINIECKI, T. et al. Vortex shedding and drag in dilute Bose-Einstein condensates. **Journal of Physics B:** atomic, molecular and optical physics, v. 33, n. 19, p. 4069, 2000.

30 KWON, W. J. et al. Critical velocity for vortex shedding in a Bose-Einstein condensate. **Physical Review A**, v. 91, n. 5, p. 053615, 2015.

31 STAGG, G.; PARKER, N.; BARENGHI, C. Superfluid boundary layer. **Physical Review Letters**, v. 118, n. 13, p. 135301, 2017.

32 SANTOS, F. E. A. dos. Hydrodynamics of vortices in Bose-Einstein condensates: a defect-gauge field approach. **Physical Review A**, v. 94, n. 6, p. 063633, 2016.

33 ONSAGER, L. Statistical hydrodynamics. **Nuovo Cimento**, v. 6, p. 249, 1949. doi:10.1007/BF02780991.

34 BRETIN, V. et al. Fast rotation of a Bose-Einstein condensate. **Physical Review Letters**, v. 92, n. 5, p. 050403, 2004.

35 JOSSERAND, C. Stability of giant vortices in quantum liquids. **Chaos:** an interdisciplinary journal of nonlinear science, v. 14, n. 3, p. 875–81, 2004.

36 CASTIN, Y.; DUM, R. Bose-Einstein condensates with vortices in rotating traps. **European Physical Journal D**, v. 7, n. 3, p. 399, 1999.

37 ENGELS, P. et al. Observation of long-lived vortex aggregates in rapidly rotating Bose-Einstein condensates. **Physical Review Letters**, v. 90, n. 17, p. 170405, 2003.

38 SHIN, Y. et al. Optical weak link between two spatially separated Bose-Einstein condensates. **Physical Review Letters**, v. 95, n. 17, p. 170402, 2005.

39 KUOPANPORTTI, P.; MöTTöNEN, M. Splitting dynamics of giant vortices in dilute Bose-Einstein condensates. **Physical Review A**, v. 81, n. 3, p. 033627, 2010.

40 KUOPANPORTTI, P. et al. Core sizes and dynamical instabilities of giant vortices in dilute Bose-Einstein condensates. **Physical Review A**, v. 81, n. 2, p. 023603, 2010.

41 PROUKAKIS, N. P.; JACKSON, B. Finite-temperature models of Bose–Einstein condensation. **Journal of Physics B:** atomic, molecular and optical physics, v. 41, n. 20, p. 203002, 2008.

42 REYNOLDS, O. An experimental investigation of the circumstances which determine whether the motion of water shall be direct or sinuous, and of the law of resistance in parallel channels. **Philosophical Transactions of the Royal Society A**, v. 174, p. 935, 1883. doi:10.1098/rstl.1883.0029.

43 RICHARDSON, L. The supply of energy from and to atmospheric eddies. **Proceedings of the Royal Society of London A**, v. 97, n. 686, p. 354, 1920.

44 KOLMOGOROV, A. N. Local structures of turbulence in an incompressible fluid for very large Reynolds number. **Proceedings of the USSR Academy of Sciences**, v. 31, n. 4, p. 301, 1941.

45 RIVERA, M.; VOROBIEFF, P.; ECKE, R. E. Turbulence in flowing soap films: velocity, vorticity, and thickness fields. **Physical Review Letters**, v. 81, n. 7, p. 1417–1420, 1998.

46 KRAICHNAN, R. H. Inertial ranges in two-dimensional turbulence. **Physics of Fluids**, v. 10, n. 7, p. 1417, 1967.

47 _____. Inertial-range transfer in two- and three-dimensional turbulence identifying a superfluid Reynolds number via dynamical similarity. **Journal of Fluid Mechanics**, v. 47, n. 3, p. 525, 1971.

48 KRAICHNAN, R. H.; MONTGOMERY, D. Two-dimensional turbulence. **Reports on Progress in Physics**, v. 43, n. 5, p. 198, 1980.

49 BOFFETTA, G. Energy and enstrophy fluxes in the double cascade of two-dimensional turbulence. **Journal of Fluid Mechanics**, v. 589, p. 253, 2007. doi:10.1017/S0022112007008014.

50 FEYNMAN, R. P. **Perfectly reasonable deviations from the beaten track:** the letters of Richard P. Feynman. New York: Basic Books, 2008.

51 HALL, H. E.; VINEN, W. The rotation of liquid Helium II: experiments on the propagation of second sound in uniformly rotating Helium II. **Proceedings of the Royal Society of London**, v. 242, n. 1213, p. 204, 1956.

52 _____. The rotation of liquid Helium II: the theory of mutual friction in uniformly rotating Helium II. **Proceedings of the Royal Society of London**, v. 238, n. 1213, p. 215, 1956.

53 VINEN, W. Mutual friction in a heat current in liquid helium II: experiments on steady heat currents. **Proceedings of the Royal Society of London**, v. 240, n. 1220, p. 114–127, 1957.

54 BARENGHI, C. F.; L'VOV, V. S.; ROCHE, P.-E. Experimental, numerical, and analytical velocity spectra in turbulent quantum fluid. **Proceedings of the National Academy of Sciences**, v. 111, suppl. 1, p. 4683, 2014.

55 TSUBOTA, M. Quantum turbulence from superfluid helium to atomic Bose-Einstein condensates. **Contemporary Physics**, v. 50, n. 3, p. 463–475, 2009.

56 TSUBOTA, M.; KASAMATSU, K.; UEDA, M. Vortex lattice formation in a rotating Bose-Einstein condensate. **Physical Review A**, v. 65, n. 2, p. 023603, 2002.

57 BRADLEY, A. S.; ANDERSON, B. P. Energy spectra of vortex distributions in two-dimensional quantum turbulence. **Physical Review X**, v. 2, n. 4, p. 041001, 2012.

58 HORNG, T.-L. et al. Two-dimensional quantum turbulence in a nonuniform Bose-Einstein condensate. **Physical Review A**, v. 80, n. 2, p. 023618, 2009.

59 PETRASCHECK, D.; FOLK, R. Helmholtz decomposition theorem and blumenthal's extension by regularization. **Condensed Matter Physics**, v. 20, n. 1, p. 13002, 2017.

60 TSUBOTA, M. Quantum turbulence. **Journal of the Physical Society of Japan**, v. 77, n. 11, p. 111006, 2008.

61 SASA, N. et al. Energy spectra of quantum turbulence: large-scale simulation and modeling. **Physical Review B**, v. 84, n. 5, p. 054525, 2011.

62 BAGGALEY A, W.; LAURIE, J.; BARENGHI, C. F. Vortex-density fluctuations, energy spectra, and vortical regions in superfluid turbulence. **Physical Review Letters**, v. 109, n. 20, p. 205304, 2012.

63 WALMSLEY, P. M.; GOLOV, A. I. Quantum and quasiclassical types of superfluid turbulence. **Physical Review Letters**, v. 100, n. 24, p. 245301, 2008.

64 BAGGALEY, A.; BARENGHI, C.; SERGEEV, Y. Quasiclassical and ultraquantum decay of superfluid turbulence. **Physical Review B**, v. 85, n. 6, p. 060501, 2012.

65 BAGGALEY, A. W.; LAURIE, J.; BARENGHI, C. F. Vortex-density fluctuations, energy spectra, and vortical regions in superfluid turbulence. **Physical Review Letters**, v. 109, n. 20, p. 205304, 2012.

66 VINEN, W. Mutual friction in a heat current in liquid helium II: theory of the mutual friction. **Proceedings of the Royal Society of London**, v. 242, n. 1231, p. 493, 1957.

67 SIMULA, T.; DAVIS, M. J.; HELMERSON, K. Emergence of order from turbulence in an isolated planar superfluid. **Physical Review Letters**, v. 113, n. 16, p. 165302, 2014.

68 NUMASATO, R.; TSUBOTA, M.; L'VOV, V. S. Direct energy cascade in two-dimensional compressible quantum turbulence. **Physical Review A**, v. 81, n. 6, p. 063630, 2010.

69 NOWAK, B.; SEXTY, D.; GASENZER, T. Superfluid turbulence: nonthermal fixed point in an ultracold bose gas. **Physical Review B**, v. 84, n. 2, p. 020506, 2011.

70 WHITE, A. C.; ANDERSON, B. P.; BAGNATO, V. S. Vortices and turbulence in trapped atomic condensates. **Proceedings of the National Academy of Sciences of the United States of America**, v. 111, suppl. 1, p. 4719–26, 2014.

71 BILLAM, T. P.; REEVES, M. T.; BRADLEY, A. S. Spectral energy transport in two-dimensional quantum vortex dynamics. **Physical Review A**, v. 91, n. 2, p. 023615, 2015.

72 STAGG, G. W. et al. Generation and decay of two-dimensional quantum turbulence in a trapped Bose-Einstein condensate. **Physical Review A**, v. 91, n. 1, p. 013612, 2015.

73 CIDRIM, A. et al. Controlled polarization of two-dimensional quantum turbulence in atomic Bose-Einstein condensates. **Physical Review A**, v. 93, n. 3, p. 033651, 2016.

74 STAGG, G. W.; PARKER, N. G.; BARENGHI, C. F. Ultraquantum turbulence in a quenched homogeneous bose gas. **Physical Review A**, v. 94, n. 5, p. 053632, 2016.

75 CIDRIM, A. et al. Vinen turbulence via the decay of multicharged vortices in trapped atomic Bose-Einstein condensates. **Physical Review A**, v. 96, n. 2, p. 023617, 2017.

76 STAMPER-KURN, D. M. et al. Excitation of phonons in a Bose-Einstein condensate by light scattering. **Physical Review Letters**, v. 83, n. 15, p. 2876, 1999.

77 PARKER, N. G. et al. Soliton-sound interactions in quasi-one-dimensional Bose-Einstein condensates. **Physical Review Letters**, v. 90, n. 22, p. 220401, 2003.

78 LEADBEATER, M. et al. Sound emission due to superfluid vortex reconnections. **Physical Review Letters**, v. 86, n. 8, p. 1410, 2001.

79 FUJIMOTO, K.; TSUBOTA, M. Bogoliubov-wave turbulence in Bose-Einstein condensates. **Physical Review A**, v. 91, n. 5, p. 053620, 2015.

80 NAZARENKO, S. **Lecture notes in physics:** wave turbulence. Berlin: Springer, 2010.

81 ZAKHAROV, V. E.; L'VOV, V. S.; FALKOVICH, G. **Kolmogorov spectra of turbulence I**. Berlin: Springer, 1992.

82 ZAKHAROV, V. E.; NAZARENKO, S. V. Dynamics of the Bose-Einstein condensation. **Physica D:** nonlinear phenomena, v. 201, n. 3, p. 203–211, 2005.

83 PROMENT, D.; NAZARENKO, S.; ONORATO, M. Sustained turbulence in the three-dimensional Gross-Pitaevskii model. **Physica D:** nonlinear phenomena, v. 241, n. 3, p. 304–314, 2012.

84 _____. Quantum turbulence cascades in the Gross-Pitaevskii model. **Physical Review A**, v. 80, n. 5, p. 051603, 2009.

85 THOMPSON, K. J. et al. Evidence of power law behavior in the momentum distribution of a turbulent trapped Bose-Einstein condensate. **Laser Physics Letters**, v. 11, n. 1, p. 015501, 2014.

86 KOZIK, E. V.; SVISTUNOV, B. V. Kelvin-wave cascade and decay of superfluid turbulence. **Physical Review Letters**, v. 92, n. 3, p. 035301, 2004.

87 L'VOV, V. S.; NAZARENKO, S. Spectrum of Kelvin-wave turbulence in superfluids. **JETP Letters**, v. 91, n. 8, p. 428–434, 2010.

88 VINEN, W. F. Decay of superfluid turbulence at a very low temperature: the radiation of sound from a Kelvin wave on a quantized vortex. **Physical Review B**, v. 64, n. 13, p. 134520, 2001.

89 JACKSON, B. et al. Finite-temperature vortex dynamics in Bose-Einstein condensates. **Physical Review A**, v. 79, n. 5, p. 053615, 2009.

90 COCKBURN, S. P. et al. Fluctuating and dissipative dynamics of dark solitons in quasicondensates. **Physical Review A**, v. 84, n. 4, p. 043640, 2011.

91 WHITE, A. C.; BARENGHI, C. F.; PROUKAKIS, N. P. Creation and characterization of vortex clusters in atomic Bose-Einstein condensates. **Physical Review A**, v. 86, n. 1, p. 013635, 2012.

92 LAGACHE, T. et al. Analysis of the spatial organization of molecules with robust statistics. **Public Library of Science One**, v. 8, n. 12, p. e80914, 2013.

93 TELLES, G. et al. **Twisted unwinding of multi-charged quantum vortex and generation of turbulence in atomic Bose-Einstein condensates**. 2016. Available at: <https://arxiv.org/abs/1505.00616>. Access date: 18 Oct. 2017.

94 SERAFINI, S. et al. Vortex reconnections and rebounds in trapped atomic Bose-Einstein condensates. **Physical Review X**, v. 7, n. 2, p. 021031, 2017.

95 RORAI, C. et al. Approach and separation of quantised vortices with balanced cores. **Journal of Fluid Mechanics**, v. 808, p. 641–667, 2016. doi:10.1017/jfm.2016.638.

96 HELM, J. L.; BARENGHI, C. F.; YOUD, A. J. Slowing down of vortex rings in bose-einstein condensates. **Physical Review A**, v. 83, n. 4, p. 045601, 2011.

97 TSUBOTA, M. Turbulence in quantum fluids. **Journal of Statistical Mechanics**, v. 2014, n. 2, p. P02013, 2014.

98 NAVON, N. et al. Emergence of a turbulent cascade in a quantum gas. **Nature**, v. 539, n. 7627, p. 72–72, 2016.

99 PRESS, W. H. et al. **Numerical recipes:** the art of scientific computing. Cambridge: Cambridge University Press, 2007.

100 HIRSCH, C. **Numerical computation of internal and external flows:** the fundamentals of computational fluid dynamics. Oxford: Butterworth-Heinemann, 2007.

Appendix

APPENDIX A – NUMERICAL INTEGRATION

Here we describe our general numerical procedure to solve the evolution of a system described by the Gross-Pitaevskii equation (GPE). The GPE is a second order partial differential equation in spatial coordinates which can be efficiently solved numerically making use of Fast-Fourier transform methods. This allows the fast back-and-forth evaluation of large grids in spectral and spatial basis. Generically, we want to solve

$$\frac{\partial\psi(\mathbf{x},t)}{\partial t} = \mathcal{L}[\psi(\mathbf{x},t)] + f(\mathbf{x},t,\psi), \tag{A.1}$$

where $\mathcal{L}$ describes a time-independent linear operation (e.g. spatial derivatives) and f a generic operation over ψ.

The calculation is split in two parts: (1) terms involving spatial derivatives are calculated in Fourier space, in which a linear operation inside $\mathcal{L}[\psi]$ of the form of $\partial_i\psi(\mathbf{x})$ becomes a simple multiplication $ik_i\tilde{\psi}(\mathbf{k})$; and (2) the remaining terms of the evolution inside operation f, including e.g. nonlinearities on ψ, are calculated in coordinate space.

For the temporal integration we typically choose the 4th order Runge-Kutta method (RK4). Assuming Δt the time-step and $\psi_n = \psi(t_n)$ the wave-function at a discretized instant t_n, the RK4 recipe for the time integration is given by[99]

$$\psi_{n+1} = \psi_n + \frac{1}{6}k_1 + \frac{1}{3}k_2 + \frac{1}{3}k_3 + \frac{1}{6}k_4 + \mathcal{O}(\Delta t^5), \tag{A.2}$$

where

$$\begin{aligned} k_1 &= \Delta t \;\; g(t_n,\psi_n) \\ k_2 &= \Delta t \;\; g\left(t_n + \frac{1}{2}\Delta t, \psi_n + \frac{1}{2}k_1\right) \\ k_3 &= \Delta t \;\; g\left(t_n + \frac{1}{2}\Delta t, \psi_n + \frac{1}{2}k_2\right) \\ k_4 &= \Delta t \;\; g(t_n + \Delta t, \psi_n + k_3), \end{aligned} \tag{A.3}$$

and $g(t,\psi) \equiv \mathcal{L}[\psi(\mathbf{x},t)] + f(\mathbf{x},t,\psi)$.

The temporal Δt and spatial Δx discretization parameters are initially guessed by using Von-Neumann's criterion for linear diffusion equations,[100] which serves as a convergence guide. This condition only applies rigorously for linear problems, however it hints on reasonable values for some nonlinear equations. In our particular cases, it translates into the condition

$$\frac{\Delta t}{(\Delta x)^2} \leq 1, \tag{A.4}$$

which, when satisfied, has successfully guaranteed the convergence of all evolutions here considered.

APPENDIX B – IMAGINARY TIME-EVOLUTION

Before simulating the real-time dynamics, we prepare initial states $\psi(\mathbf{r}, t = 0)$ by relaxing a trial function of the type $\psi(\mathbf{r}) = A(\mathbf{r})e^{i\phi(\mathbf{r})}$ through an imaginary time evolution, by replacing $t \to -it$ in the GPE.

Let us assume that the non-linearity is small enough so that we can decompose the system in its linear expansion over eigenstates

$$\psi(\mathbf{r}, t) = \sum_i c_i(t)\gamma_i(\mathbf{r}). \tag{B.1}$$

Therefore, in a small time step Δt, we know that the state will change to

$$\psi(\mathbf{r}, t + \Delta t) = \sum_i c_i(t)\gamma_i(\mathbf{r})e^{i\epsilon_i \Delta t}, \tag{B.2}$$

therefore acquiring a phase factor $e^{-i\epsilon_i \Delta t}$, where ϵ_i is the eigen-energy for state i. If we replace $t \to -it$, we clearly see that the time evolution of the state's decomposition converges exponentially to a state with lowest energy (ground-state), with more energetic states having their amplitude damped by a factor $e^{-\epsilon_i \Delta t}$.

APPENDIX C – VORTEX COUNTING ALGORITHM

Here we present the general algorithm for the vortex counting, used to identify vortices in two-dimensional simulations. As we have already mentioned in the text, another option would be to calculate the two-dimensional pseudo-vorticity, as defined in Eq. (5.4).

Input: Two-dimensional wave-function ψ with cartesian dimensions $[\mathrm{d}_x, \mathrm{d}_y]$.
Output: vortices coordinates, $p_i = [x_i, y_i]$.

Algorithm:

1 - Extract the phase field from the wave-function by evaluating $\phi = \arctan\left(\frac{\mathrm{Im}\{\psi\}}{\mathrm{Re}\{\psi\}}\right)$.

2 - Artificial phase jumps must be corrected through a phase-unwrapping algorithm. This guarantees that the phase does not jump more than $\pm 2\pi$. The phase-unwrapping algorithm has standard routine implementations in several programming languages (particularly, Python and MATLAB).

3 - Calculate the phase difference around every plaquette of the numerical grid. This step is efficiently implemented by making use of two-dimensional convolution of the phase field with the filters f_1 and f_2, defined as

$$f_1 = \begin{pmatrix} 1 & -1 \\ -1 & 1 \end{pmatrix} \quad \text{and} \quad f_2 = \begin{pmatrix} -1 & 1 \\ 1 & -1 \end{pmatrix}.$$

4 - Vortices are thus identified as ± 1 if the phase around a plaquette jumps of $\pm 2\pi$, according to their circulation. The coordinate of a vortex i is thus stored as $p_i = [x_i, y_i]$.

5 - Ghost vortices are removed by imposing a mask which disregards phase jumps in regions where the condensate density is lower than 2% of the mean density $\left\langle |\psi|^2 \right\rangle$.

APPENDIX D – SEPARATING INCOMPRESSIBLE AND COMPRESSIBLE PARTS

Let us start by defining a density weighted velocity field of the form $\mathbf{w}(\mathbf{r},t) \equiv |\psi(\mathbf{r},t)|\,\mathbf{v}(\mathbf{r},t)$ in order to extract its incompressible/compressible components. As a consequence of Helmholtz theorem,[59] a vector field can be decomposed as a sum $\mathbf{w}(\mathbf{r},t) = \mathbf{w}_c(\mathbf{r},t) + \mathbf{w}_i(\mathbf{r},t)$ whose terms satisfy $\nabla \times \mathbf{w}_c = 0$ and $\nabla \cdot \mathbf{w}_i = 0$. Consider then the following vector identity

$$\nabla\left(\nabla \cdot \mathbf{w}\right) = \nabla^2 \mathbf{w} + \nabla \times \left(\nabla \times \mathbf{w}\right). \tag{D.1}$$

Since $\nabla \cdot \mathbf{w}_i = 0$, the above relation implies that

$$\nabla\left(\nabla \cdot \mathbf{w}\right) = \nabla\left(\nabla \cdot \mathbf{w_c}\right) + \nabla(\cancelto{0}{\nabla \cdot \mathbf{w_i}}) = \nabla^2 \mathbf{w}_c + \nabla \times (\cancelto{0}{\nabla \times \mathbf{w_c}}). \tag{D.2}$$

It is now useful to represent these identities in Fourier space (using Einstein's notation, i.e. repeated indices meaning implicit sum)

$$k_a k_b \tilde{w}^b = k^2 \tilde{w}_c^a, \tag{D.3}$$

where we have used the fact that $\partial_a \to i k_a$ and $\mathbf{w}(\mathbf{r},t) \to \tilde{\mathbf{w}}(\mathbf{k},t)$ in the transform space. Finally, since $\tilde{\mathbf{w}}(\mathbf{k},t) = \tilde{\mathbf{w}}_i(\mathbf{k},t) + \tilde{\mathbf{w}}_c(\mathbf{k},t)$, we can write

$$\tilde{w}_c^a = \frac{k_a}{k^2} k_b \tilde{w}^b, \tag{D.4}$$

and

$$\tilde{w}_i^a = \left(1 - \frac{k_a}{k^2}\right) k_b \tilde{w}^b, \tag{D.5}$$

which give us the explicit expressions in Fourier space of the compressible and incompressible components of $\mathbf{w}$, respectively.